NORTHWESTERN UNIVERSITY

# Understanding Control of the Shoulder after Stroke
# Towards Myoelectric Control of Vertical Support to Improve Reach

A DISSERTATION

SUBMITTED TO THE GRADUATE SCHOOL

IN PARTIAL FULFILLMENT OF THE REQUIREMENTS

For the degree

DOCTOR OF PHILOSOPHY

Field of Biomedical Engineering

By

Joseph Victor Kopke

EVANSTON, ILLINOIS

June 2021

# Abstract

Stroke affects millions of people each year and although modern medicine has improved chances of survival after stroke, it has not yet been able to affect a change in repairing damaged neural tissue leaving one to two thirds of survivors with chronic disability in their affected upper-extremity; specifically, hemiparesis, hypertonicity, loss of coordination, and spasticity. These impairments require survivors to adapt and compensate for the loss of function in their arm, wrist, and hand. These impairments also discourage many survivors and cause them to use their arm less and less leading to atrophy and limitations in range of motion.

One phenomenon which limits in-part both the rehabilitation process as well as the efficacy of mechanical intervention (exoskeletons or wearable assistive devices) is the abnormal synergy, in which greater proximal effort of the arm leads to increased tone and contraction in a patterned way throughout the arm, wrist, and hand. Lifting the arm against gravity often causes unintentional co-activation of elbow, wrist, and finger flexors. By reducing effort at the shoulder, this phenomenon is reduced thus enabling greater control and range of motion at these joints. Without arm support, individuals with stroke and any equipment they utilize must overcome these increased abnormal joint torques. With the advancement of exoskeletons, a powered device that supports humeral elevation is foreseeable but with that comes the requirement for a control system to control it.

This dissertation explores the possibility of using pattern recognition, a type of machine learning, to control vertical support at the shoulder after stroke thus reducing the effort required and consequently reducing the severity of presentation of the abnormal synergy. It is hoped that this work will contribute towards the realization of a control paradigm that will aid in the rehabilitation

and assistance of those surviving stroke. These chapters progress from a purely isometric single direction shoulder task (Chapter 2) to a quasi-static, quasi-dynamic dual-task (Chapters 3 and 4), to finally real-time control of vertical support using machine learning (Chapter 5). The nature of this work limits any strong conclusive statements but ultimately has shown the promise and efficacy of such a control system. Specifically, Chapter 5 shows that myoelectric based pattern recognition control enables survivors of stroke to control both vertical support force and vertical position well enough to place their arm in a target window and improve their forward reach ability by increasing joint excursion at the elbow and the shoulder.

Chapter 4 questions the presence of abnormal synergy within shoulder joint degrees of freedom. It concludes that a natural synergy exists between adduction/internal rotation based on normal muscle biomechanics that constrains shoulder movements "outside of synergy" such as adduction/external rotation or abduction/internal rotation. This is a deviation from the commonly accepted hypothesis that abduction or adduction drive causes patterned and obligatory torque coupling with external rotation and internal rotation respectively.

Ultimately these results have advanced our understanding of control of the shoulder after stroke and have demonstrated the feasibility and efficacy of using a myoelectric based control system to control vertical support in order to increase function. Further work is required to refine and optimize these techniques and possibly develop automated decision making systems to aid in rehabilitation.

# Acknowledgment

In the name of God, the All-Glorious

I would like to begin by acknowledging the existence and continued guidance, sustenance, and support of God, through Who all things are possible. I would like to acknowledge the native people whose land we live on and benefit from here in the Evanston and Chicago area, including the Ojibwe, Odawa, and Potawatomi, as well as the Miami, Ho-Chunk, Menominee, Sac, Fox, Kickapoo, and Illinois Nations. I would like to acknowledge I have grown up in a world with systemic problems, including systemic racism in which I have benefitted from.

I would also like to recognize the greatest thing I have learned has nothing to do with physical existence or science but rather spiritual existence. Specifically, Baha'u'llah Who is the Manifestation of God for our day, a Divine Educator, who brought us the remedy for the problems of our time, as each illness requires its own treatment. The problems of today require the recognition of the oneness of humanity. Racism, climate change, extremes of wealth and poverty, equality of women and men and of all people will be solved through the growth and development of our spiritual virtues and a transformation of our own selves, our community, and of all social institutions pivoting around this concept of the oneness of mankind. There is no magic bullet that will heal humanity instantly, but rather just like in science, it will happen through a series of steps taken purposefully after reflection and planning, done in a humble posture of learning, united with others in the pursuit of truth, betterment, and advancement.

Ultimately, communities throughout the world are learning to implement the scientific process to building and transforming themselves, uprooting age old prejudice and blossoming into vibrant,

virtuous, united communities. Just as racism is a system, it will take a system of education, capacity building, and transformation to dismantle it. Be patient, see the end in the beginning, and work together in ever expanding circles of friends committed to transformation, and never lose hope.

I would like to thank my friends who have helped me through this process, fellow travelers on the path of life, Kojo Clarke, Mark Hoggarth, Anita “Nayo” Hill, Amir Vahabi, Sarah Hilu Iverson, and Haleh Karbasforoushan. I would like to thank all the students in the dual-degree program who understand all too well the nature of our journey here at Northwestern.

I would like to thank the extreme kindness, friendliness, and helpfulness exuded by all the staff that I have had the opportunity to interact with at both PTHMS and CBM including Bessie Cofield, Pam Easton, Evangeline “Vangie” Walker, Kisha Nelson, Brad Holubar, Laura Haugh-Scheidt, and Andrea Moore. Without them, we would all be lost!

I would like to thank Dr.’s Jules Dewald and Ana Maria Acosta whose patience, generosity, and unbridled support for me and all of the dual-degree students has made all the difference. They never fail to see us as future leaders of our fields, seeing us greater than we are. Thank you for believing in us.

I would like to recognize and thank my committee for their support, guidance, and encouragement.

Finally, I would like to thank my two advisors, Dr.’s Levi Hargrove and Mike Ellis, for so generously giving up their time and effort in support of my pursuits; for their unique perspectives and insights, for their patience, encouragement, and generosity of spirit. No matter how bad I thought I was doing, or how uncertain I was as to if I wanted to continue, they were there

supporting me to make the best decision for me and my reality. Having the freedom to wander, get lost, and find my way at least a few times has been helpful to my growth as an individual and as a scientist. I have come so far yet I have so much further to go, so much more to learn.

I would like to thank my wonderful parents, Vic and Sally Kopke for their unconditional love throughout my life. They raised me in a way that allowed me to recognize Baha'u'llah, to strive for excellence, and with a pretty solid moral compass.

I am happy to be on this continued journey with my steadfast, strong, kind, and loving wife, Katie and my two children Aidan and Ava. They love and support me through all of life's twists, turns, ups and downs. We are in it together, praise God. The world may not need more PhD's as much as it needs people committed to contributing to the spiritual (as well as the material) development of the world so we shall see what doors open and confirmations are received in my attempt to be of some service to the world of humanity.

God is the All-Glorious

# Table of Contents

# List of Figures

# List of Tables

**Chapter 2**



**Chapter 3**



**Chapter 4**



**Chapter 5**



**Appendix A**

# Chapter 1: Introduction

Stroke affects millions of people worldwide each year with a significant portion (30-60%) retaining chronic upper-extremity impairments for the remainder of their lives. These impairments include weakness, increased tone, spasticity, loss of fine motor control, and loss of coordination and independent joint control. Stroke is the interruption of blood flow to the brain resulting in neuronal death and although modern medicine has increased survival rates of stroke, it has yet been able to effect a reduction in its incidence. Unfortunately, the human nervous system has little to no ability to repair itself after insult, leaving researchers to look for ways to minimize impairments and maximize function and quality of life for survivors of stroke.

In the early 1950's Thomas Twitchell documented the recovery of 121 patients with stroke noting commonalities and patterns.[1] Since then the field of stroke recovery has expanded exponentially with current guidance directing intense, task specific, and repetitive practice.[2] Although some progress has been made to enable increased independence and accomplishment of activities of daily living after stroke, impairments remain.[2,3] In fact, six months after stroke, about 65 percent of patients cannot incorporate the affected hand into their usual activities.[4] The persistence of these chronic impairments in addition to the advancement in robotics and exoskeletons have enabled researchers to explore, in new ways, the impairments and possible technologies to rehabilitate or to assist individuals after stroke.

Since the late 1980's and early 1990's around the time of the development of the MIT-MANUS, research devoted to the use of robotics to understand impairments of neurologic injury and provide interventions to improve function rapidly expanded.[5] Technological abilities have expanded but

long term meaningful improvement after stroke remains elusive as robotic therapy has not proven more effective than traditional therapy.[6] At best it has effected small but significant changes due to pure repetition and intensity that it offers.[7] Although robotics has not yet been able to effect great improvements in outcomes, it has offered insight into underlying impairments and offers a way to facilitate increased function via assistance.

Twitchell described two abnormal patterns which commonly occur after stroke: a flexion synergy and an extension synergy. Specifically, the flexion synergy is described as unintentional movement of joints throughout the limb into a flexion pattern at the shoulder, elbow, wrist, and fingers. Conversely, the extension pattern was described as unintentional movement of the limb into extension at the shoulder, elbow, wrist, and fingers. These have since been elucidated quantitatively using isometric and robotic setups for both the upper- and lower- extremities. One critical finding is that the expression of these synergies is proportional to the amount of neural drive, or simply the amount of effort being used in attempt to move.

By reducing the amount of effort at the shoulder, the unintentional co-activation of elbow, wrist, and finger muscles is reduced, improving reach and coordination. Using robotics, the amount of effort can easily and precisely be controlled by controlling the amount of load or support at the shoulder. Supporting the shoulder has proven to be an effective way of reducing abnormal co-activation at the elbow, wrist, and fingers, improving reach area and distance as well as improving determination of intent of hand movements.

These results have implications to the realm of assistive robotics. Devices targeting the elbow, wrist, and hand add weight to the arm, and thus increase the amount of shoulder effort required to

lift it. These devices then need to overcome or overpower, in addition to any forces, the increased presentation of the abnormal synergy at those joints. Although supporting the shoulder does not directly result in improved dexterity of the fingers, it does reduce the intensity of these abnormal co-activation patterns and subsequently the abnormal joint torques that result from shoulder effort. This has direct implication to the devices designed to aid the wrist and hand as they will have to overcome less resistance due to unintentional muscle activity and can better detect what the user is trying to do.

Determining the intent of someone without neurological injury is relatively straight forward. But aberrant forces and muscle signal patterns due to the presentation of the abnormal synergy make it more difficult to discern what the user is truly trying to do. If underlying muscle activity is causing joint forces and movement that is not intended, how can true user intention be detected or inferred? In either case, force or EMG data can be used alongside machine learning techniques such as pattern recognition to decipher what a person is intending to do. Many groups continue focused lines research on what algorithms and what features result in the highest classification accuracy. That is not the intent of this work. This work uses linear discriminant analysis based pattern recognition as a starting point as it has proven computationally efficient and effective in the population with amputation to control powered prostheses.

Of course many other machine learning classifying techniques exist and have proven as or even more accurate than an LDA based classifier. Additionally, many other features exist that may enable improved pattern recognition but we focus on the Hudgin's feature set (mean absolute value, number of zero crossing, number of slope sign changes, and waveform length) combined

with $6^{th}$ order autoregressive features. The Hudgin's features have been tested and used extensively. The aforementioned techniques and features have been used for individuals post-stroke in attempt to rehabilitate or assist the elbow, wrist, and hand.

Chapter 2 begins my exploration of using muscle signals as a possible control signal to control a future device designed to support the shoulder and assist it to move the arm against gravity. It aimed to answer the question, can pattern recognition of muscle signals correctly discriminate between eight intended motions? Maximal isometric voluntary contractions and corresponding joint torques were used as it was assumed this was the worst case scenario in which the abnormal synergy would be maximally present. This work was published in its present form in JNER…

Chapter 3 explores some findings springing from Chapter 2. Mainly, it attempted to determine if some of the classification errors found in Chapter 2 were the result of the design of the experiment or due to the abnormal synergy. Specifically, it used a robotic device ($ACT^{3D}$) in a novel way to test the motions that were commonly confused in Chapter 2. This was accomplished using the $ACT^{3D}$ robotic setup combined with a dual-task requiring different amounts of shoulder abduction and adduction effort simultaneously with maximal isometric internal and external rotation. This chapter was published in its present form in TNSRE.

Chapter 4 expounds on some of the joint torque data acquired in the same study as Chapter 3. The aim of this chapter is to understand how control of the shoulder compares between the paretic, the non-paretic, and the control shoulder in a dual-task of the shoulder. This was accomplished using the same setup on the $ACT^{3D}$ as in Chapter 3 with a dual-task requiring different amounts of shoulder abduction and adduction effort simultaneously with maximal isometric internal and

external rotation. This chapter has implications into the design requirements of a future device and if internal and external rotation must or should be controlled. This chapter has been submitted for publication in its present form.

Chapter 5 moves from understanding the possibilities and consequences of stroke towards real-time assistance using a robotic device by applying what has been learned in the previous chapters. An embedded controller, using the same machine learning techniques as Chapters 2 and 3, was used to control the vertical position and the vertical force applied to the users arm. The user was required to move their arm into a vertical target window and then reach out straight in front of them as far as possible. This chapter has also been submitted for publication in its present form.

Chapter 6 discusses the results of the previous chapters and their implications to the field as a whole. Although there is significant work to be done, this line of research followed a path by taking the next logical step as best as we could discern, and has resulted in a promising outlook of future possibilities.

# Chapter 2. Pattern Recognition of Isometric Shoulder Tasks after Stroke

Kopke JV, Hargrove LJ, Ellis MD. Applying LDA-based pattern recognition to predict isometric shoulder and elbow torque generation in individuals with chronic stroke with moderate to severe motor impairment. J Neuroeng Rehabil. 2019;16

## 2.1 Abstract

**Background**

Abnormal synergy is a major stroke-related movement impairment that presents as an unintentional contraction of muscles throughout a limb. The flexion synergy, consisting of involuntary flexion coupling of the paretic elbow, wrist, and fingers, is caused by and proportional to the amount of shoulder abduction effort and limits reaching function. A wearable exoskeleton capable of predicting movement intent could augment abduction effort and therefore reduce the negative effects of distal joint flexion synergy. However, predicting movement intent from abnormally-coupled torques or EMG signals and subsequent use as a control signal remains elusive. One control strategy that has proven viable, effective, and computationally efficient in myoelectric prostheses for use in individuals with amputation is linear discriminant analysis (LDA)-based pattern recognition. However, following stroke, shoulder effort has been shown to have a negative effect on classification accuracy of hand tasks due to the multi-joint torque coupling of abnormal synergy. This study focuses on the evaluation of an LDA-based classifier to predict individual degrees-of-freedom of the shoulder and elbow joints.

**Methods**

Six degree-of-freedom load cell data along with eight channels of EMG data were recorded during eight tasks (shoulder abduction and adduction, horizontal abduction and adduction, internal rotation and external rotation, and elbow flexion and extension) and used to create feature sets for LDA-based classifiers to distinguish between these eight classes.

**Results**

Cross-validation yielded functional offline classification accuracies (>90%) for two of the eight classes using EMG-only, four of the eight classes using load cell-only, and six of the eight classes using a combined feature set with average accuracies of 83%, 91%, and 92% respectively.

**Conclusions**

The most common misclassifications were between shoulder adduction and internal rotation followed by shoulder abduction and external rotation. It is unknown whether the strategies used were due to abnormal synergy or other factors. LDA-based pattern recognition may be a viable control option for predicting movement intention and providing a control signal for a wearable exoskeleton assistive device. Future work will need to test the approach in a more complex multi-joint task, specifically one that attempts to tease apart shoulder abduction/external rotation and adduction/internal rotation.

Trial Registration: N/A

**Keywords**

hemiparesis, stroke, flexion synergy, shoulder, pattern recognition, linear discriminant analysis

## 2.2 Background

Nearly 800,000 people in the U.S. and 16 million people worldwide suffer a stroke each year [8]. Of these, an estimated 50% result with chronic hemiparesis [9] and up to 80% may have residual upper-extremity impairments [10]. Commonly these survivors present with abnormal movement patterns referred to as abnormal synergies [1,11] described as loss of independent joint control due to coactivation of muscles across multiple joints [12]. Proximal shoulder abduction effort causes involuntary elbow, wrist, and finger flexion, as well as forearm supination proportional to the amount of shoulder effort and is referred to as the flexion synergy [13-15]. In the same manner, shoulder adduction produces involuntary elbow extension, wrist and finger flexion, and forearm pronation and is referred to as the extension synergy. The loss of independent joint control resultant from abnormal synergies is thought be the result of increased utilization of contralesional corticoreticulospinal tract [16,17].

When shoulder effort is reduced, there is a proportional reduction in the expression of loss of independent joint control, enabling access to a greater functional workspace, with full support of the shoulder leading to near maximal reaching range of motion [13,18]. While targeting this impairment with progressive abduction loading therapy has provided small benefit [19,20] the complete restoration of movement remains elusive. Therefore, one possible solution to aid these stroke survivors with persistent loss of independent joint control is to support their arm with a wearable exoskeleton. This exoskeleton could provide smart-support possibly leading to long-term improvements in workspace. At a minimum, a wearable device could assist and enable a survivor of stroke by minimizing the effects of abnormal synergy and therefore maximizing their functional work area, better engaging their environment, and/or supporting interventions for their hand, wrist,

and elbow. Powered exoskeletons, for both upper- [21] and lower- [22] extremity, are becoming more commonplace and are beginning to emerge as viable sources of rehabilitation and assistance. However, design requirements and feasible control techniques that consider the expression of abnormal synergy/loss of independent joint control have not been established.

The application of wearable robotic technology has found success in individuals with amputation[23] paving the way for potential use in individuals with stroke. Historically, these devices were controlled using simple amplitude-based thresholds, but recently the use of linear discriminant analysis (LDA) based pattern recognition has proven to be both accurate and computationally efficient and enables intuitive control of a greater number of degrees of freedom [23-25]. Although LDA-based pattern recognition is often focused on controlling distal joints, pattern recognition of shoulder motions of healthy controls has been explored for the purposes of application to the population with amputation and have achieved classification accuracies above 90% [26,27]. 90% is significant, as it has been implicated as a transitional value between high functionality and extremely variable levels of functionality of a myoelectric prosthesis based on the user, classifier, and their interaction [28].

Pattern recognition has been implemented with individuals with stroke with varying degrees of success. Electromyography (EMG) data from the forearm has been used to predict movement with low [29], mixed [30], and high [31] levels of accuracy. Additionally, EMG has been used to predict goal-directed horizontal reaching in both impaired and healthy controls reporting insufficient and sufficient accuracy respectively [32]. Importantly, a limitation to these applications in individuals with stroke was that the participant's arms were supported, minimizing the expression of the abnormal synergy and potentially inflating classification accuracies compared to

what they would be during active shoulder use common in activities of daily living. In fact, classification accuracy for determining an individual's desire to open their hand is significantly reduced when lifting as little as 25% of their abduction maximum [15,33]. Advanced offline techniques for correcting synergy-induced classification errors only appreciably improved one subject's accuracy [15]. Even if these classification errors could be corrected, the effects of abnormal synergy at the elbow, wrist, and fingers (unintentional activation of muscles) would still exist, possibly limiting range of motion or requiring an exoskeleton to mechanically overpower each affected joint. To reduce synergy presentation and achieve success in classifying distal movement intent, abduction support (less required abduction torque generation) is required. With the advancement of wearable robotics, it is feasible to envision a device that could do this. Actively and smartly controlling abduction support would be desirable in hopes of both facilitating recovery and avoiding "slacking" (tendency to over utilize device support leading to increased weakness). Accurate classification of movement intent at the shoulder and perhaps the elbow would be required to realize this goal but has never been demonstrated. Therefore, as a first step, this study aims to determine if LDA-based pattern recognition of shoulder and elbow joints can achieve functionally useable classification accuracies (>90%) despite the existence of the abnormal synergies in a rigorously controlled and quantitative paradigm.

Sensor fusion from multiple sources has been shown to supplement LDA-based pattern recognition to predict ambulation [34,35]. The utilization of force and moment load cell data, is a unique and potentially powerful control option available for application of pattern recognition in individuals with stroke that is not available to individuals with amputation; the incorporation of which may augment the accuracy of a solely EMG-based classifier for individuals with stroke.

This study investigates how effectively LDA-based pattern recognition techniques applied to load cell, joint torque, EMG, and combined data, classify between maximal isometric torque tasks in eight different directions (shoulder abduction/adduction, shoulder horizontal abduction/adduction, shoulder internal/external rotation, and elbow flexion/extension). It was hypothesized that the combination of load cell and EMG data would result in the largest number of tasks with classification accuracies >90%.

## 2.3 Methods

### *2.3.1 Participants*

Informed consent was obtained from participants to complete the protocol approved by Northwestern's Institutional Review Board. Thirty-five participants with chronic stroke and upper-extremity Fugl-Meyer assessment (UE-FMA) scores between 10 and 45, classifying their motor impairment as moderate or severe, were recruited to participate in the experiment. Six participants were excluded; two for corrupted or absent data which resulted in less than three useable trials in a given direction and four for profound external rotation weakness. These four participants were unable to produce external rotation torque with the exception of that which occurred as a secondary torque (i.e. when testing in a different direction). Characteristics from the remaining 29 participants: 21% female, 38% with affected/hemiparetic right arm, average UE-FMA score of 27.4/66 ± 6.4 (15-43), average age of 57.1 ± 9.2 years (37.1-68.7), average time post-stroke 7.2 ± 4.9 years (.98-24.6). Characteristics are presented as percentage or as average value ± standard deviation (minimum value – maximum value).

### *2.3.2 Setup and instrumentation*

Participants were seated in a rigid chair (Biodex, Shirley, NY; Model 830-110) and secured with two chest straps and a lap belt to minimize shoulder girdle and torso movement with feet supported by a footrest. Their paretic forearm, wrist, and hand were then casted using fiberglass casting material to provide rigid coupling to a load cell and prevent synergy induced wrist and finger flexion. Using a Delrin ring the forearm was attached to a 6-degree of freedom (DOF) load cell (JR3 Inc., Woodland, CA, USA; Model 45E15A) that provided instantaneous forces in three orthogonal directions and the moments about each of the three axes which enabled the calculation of joint torques at the elbow and shoulder. The custom device was then adjusted to place their paretic arm in a position of approximately 90° of abduction, 45° of horizontal adduction, neutral humeral internal-external rotation, and 90° elbow flexion resulting in the entire arm being in the transverse plane located at shoulder height (Figure 1). Skin was prepared using a dry scrub pad and alcohol wipe and electrode gel was applied to eight surface-EMG bipolar differential electrodes with 1cm interelectrode spacing (Delsys, Cambridge, MA, USA; 16 channel Bagnoli) that were attached over the following muscles: anterior deltoid, intermediate deltoid, posterior deltoid, pectoralis major, biceps brachii, triceps long head, triceps lateral head, and brachioradialis. Electrodes were placed

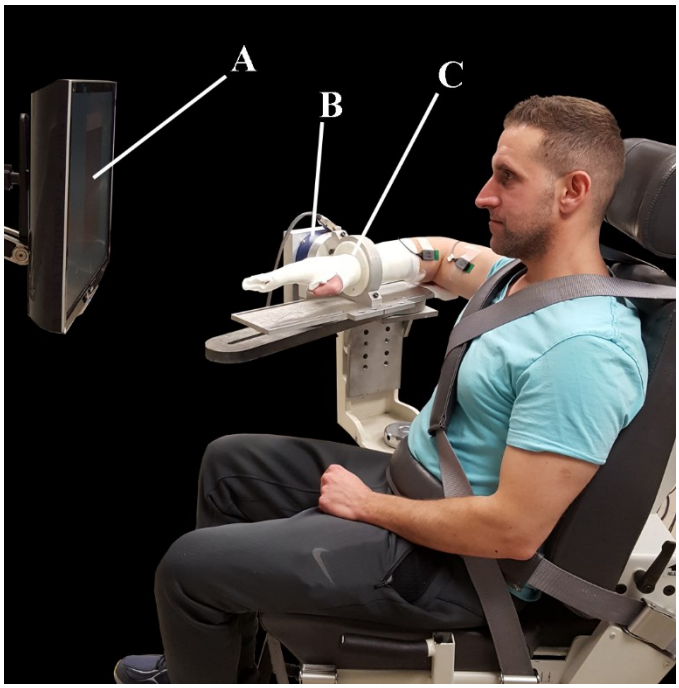


Figure 1. Setup in Biodex chair with participant attached to load cell via rigid cast. Labels identify the following: A) Feedback display, B) Load cell, C) Delrin ring and cast.

by a physical therapist via use of anatomical landmarks and palpation as prescribed by the book *Anatomical Guide for the Electromyographer* [36]. A ground reference electrode was placed over the acromion. These muscle sites were chosen as they could all be reached by the participants with intent to mimic feasible self-applied electrode sites for future applications. This choice became a limitation as EMG data from rotator-cuff muscles and latissimus dorsi may have improved differentiation between classes.

### *2.3.3 Experimental Protocol*

Maximum isometric voluntary torques were tested in eight different directions: shoulder abduction (AB) and adduction (AD), horizontal abduction (HAB) and adduction (HAD), internal rotation (IR) and external rotation (ER), and elbow flexion (EF) and extension (EE). Here we define shoulder abduction as the torque around an axis in the transverse plane running through the glenohumeral joint perpendicular to the humerus. Abduction would cause the humerus to rotate cranially while adduction would cause the humerus to rotate caudally, down toward the torso. Horizontal adduction torque would cause rotation around the vertical axis running through the glenohumeral joint in which the humerus would rotate in the transverse plane toward the front of the body and horizontal abduction would rotate the humerus out to the side and then behind the body. Internal rotation torque is similar to what is used in arm-wrestling or overhand throwing and causes rotation of the humerus along the long-axis of the bone. Internal rotation is what allows individuals to reach the small of their back while external rotation allows them to reach behind their head. Torque generated in the testing direction is considered the primary torque while concurrent torques generated in the other directions are labeled as secondary. The order of testing direction was randomized. Each direction was tested a minimum of three and maximum of six

trials aiming to satisfy the following criteria: three trial maximum primary torques within 10% of each other with the last trial not being the greatest. Three trials were chosen to allow for adequate data to train and validate each classifier and to allow for some natural variation in task completion without causing fatigue. Verbal directions and visual demonstrations were provided prior to execution of each task. Real-time visual feedback of torque production in the testing (primary) direction was provided via large monitor and custom round dial display. The visual feedback offered additional encouragement in addition to auditory encouragement to ensure maximum torque was attained. Trials were 5 seconds long and recorded at 1 kHz via a data acquisition device (National Instruments, NI-DAQ, Austin, TX, USA). A minimum of one minute of rest was given between trials to ensure adequate recovery time and prevent fatigue. Representative data is presented in Figure 2.

*2.3.4 Data processing*

All data collection, processing, classification, and analysis were accomplished with MATLAB (Release 2012a and 2017a, The MathWorks, Inc., Natick, MA, USA) via custom code. Upon inspection of raw EMG data, a small amount of power line noise was noted, so in addition to the Delsys hardware bandpass filter between 20 to 450 Hz, EMG from each trial was digitally notch filtered between 58 and 62 Hz and subsequent harmonics using a $6^{th}$ order Butterworth to remove the power line noise. The proceeding analysis was accomplished for both filtered and unfiltered data and the filtered data performed slightly better, but not significantly (1-2%). An in-depth comparison between these datasets was outside the scope of this study. Isometric joint torques were calculated using a series of matrix translations and rotations of the raw six degree-of-freedom load cell data (three forces and three moments) based on limb anthropometrics and

relative limb and load cell location and orientation. Maximum voluntary torque values were

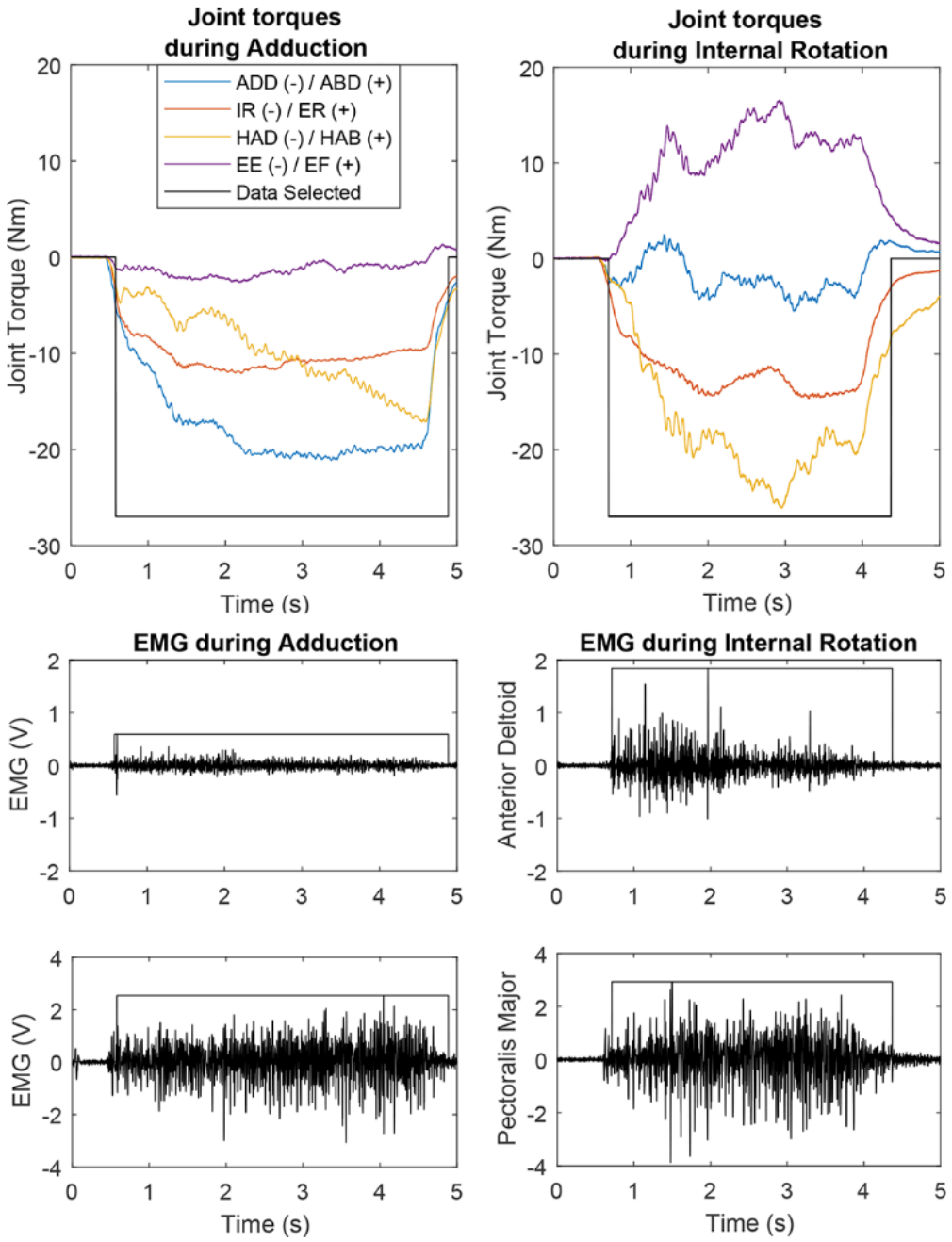


Figure 2. Sample joint torque for one trial of two different shoulder tasks, shoulder adduction and internal rotation with delineation of which data were selected (>20% max in tested direction) for use in the classifier (top). Sample EMG for 2 of the 8 channels: anterior deltoid (used during internal rotation), and pectoralis major (used in adduction and internal rotation). Horizontal abduction (HAB)/adduction (HAD); Abduction (AB)/adduction (AD); External (ER)/internal (IR) rotation; Elbow flexion (EF)/ extension (EE); Newton-meters (Nm); Volts (V); Milliseconds (ms).

calculated using a 200 ms moving average. Data were used from the three trials with maximum torque values. Within each trial, automatic segmentation when the primary torque was >20% of the maximum generated torque for that direction was used for subsequent analysis (classification). Only data when the torque in the primary direction was greater than 20% was used. This somewhat arbitrary cutoff of 20% was used to help ensure that the participant was actually doing what they were tasked to do as well as ensure there was sufficient data to train and validate the classifier for all participants. True maximum strength values are normally achieved for approximately 1 second, so additional data was used to create a richer and lengthier dataset.

*2.3.5 Classification*

To evaluate the possibility of predicting user-intent during these shoulder tasks, pattern recognition analyses were performed which considered the following signal sources: raw measurements from the load cell only, computed joint torques of the shoulder and elbow only, EMG signals only, and a combination of load cell and EMG sensor sources. The pattern recognition system used in this work is similar to a real-time pattern recognition control system that has been developed to control advanced upper-limb prostheses [37]. The control algorithm contains three basic functions: data windowing, feature extraction, and classification. Windows were formed from 200 ms of data and decisions were made every 25 ms (ie 175 ms of overlapping data) which maximizes decision density and minimized delay without significant loss in accuracy [38]. The features used depended on the input signals: for load cell data and computed joint torques, only the mean of each of the channels over each window was used, while for EMG data, the time-domain features proposed by Hudgins [39] were calculated for each of the eight channels. These included mean absolute value, number of zero crossings and slope sign-changes, and waveform

length. This resulted in a six-dimensional feature set using load cell, four dimensional set for joint torque data (shoulder abduction/adduction, shoulder horizonal abduction/adduction, shoulder external rotation/internal rotation, and elbow flexion/extension), 32-dimension set for EMG, and 38 for a combined set (6 dimensions from load cell data and 32 from EMG). The extracted features were supplied to an LDA-based classifier. A trial wise leave-one-out-cross-validation was used in which each set of two trials was used to train a classifier which was then tested against the third and the accuracies averaged.

**2.4 Results**

This study takes a focused look at classifying movement patterns at the shoulder and elbow post-stroke following prior work reporting challenges in classifying movements at the forearm, wrist, and hand. Confusion matrices for the load cell and the EMG time-domain feature sets are shown in Tables 1 and 2 respectively. Accuracies above 90% have been shown to be functionally useable while accuracies between

Table I. Confusion matrix of all 8-classes using load cell dataset

| Load cell dataset | | **Predicted Class** | | | | | | | |
|---|---|---|---|---|---|---|---|---|---|
| | | *EF* | *AB* | *ER* | *HAB* | *EE* | *AD* | *IR* | *HAD* |
| **Actual Class** | | | | | | | | | |
| **Flexion** | *Elbow Flexion (EF)* | **92** | 4 | 3 | 1 | 0 | 0 | 0 | 0 |
| | *Abduction (AB)* | 3 | **87** | 10 | 0 | 0 | 0 | 0 | 0 |
| | *External Rotation (ER)* | 2 | 8 | **89** | 1 | 0 | 0 | 0 | 0 |
| | *Horizontal Abduction (HAB)* | 0 | 0 | 2 | **97** | 0 | 0 | 0 | 0 |
| **Extension** | *Elbow Extension (EE)* | 0 | 0 | 0 | 0 | **98** | 1 | 0 | 0 |
| | *Adduction (AD)* | 0 | 0 | 1 | 0 | 1 | **84** | 13 | 0 |
| | *Internal Rotation (IR)* | 0 | 0 | 0 | 0 | 1 | 14 | **83** | 2 |
| | *Horizontal Adduction (HAD)* | 0 | 0 | 0 | 0 | 1 | 0 | 2 | **96** |

Table I. Confusion matrix for classifier using the load cell data. Movements implicated in flexion synergy are in upper/left portion of table while extension synergy movements are in lower/right portion. Larger bordered box delineates classes that are most often confused for each other. *Flexion synergy*: Elbow flexion (EF), shoulder abduction (AB), external rotation (ER) and horizontal abduction (HAB). *Extension synergy*: elbow extension (EE), shoulder adduction (AD), internal rotation (IR), and horizontal adduction (HAD).

Table II. Confusion matrix of all 8-classes using EMG dataset

| EMG dataset | | Predicted Class | | | | | | | |
|---|---|---|---|---|---|---|---|---|---|
| | | *EF* | *AB* | *ER* | *HAB* | *EE* | *AD* | *IR* | *HAD* |
| **Actual Class** Flexion | *Elbow Flexion (EF)* | **88** | 5 | 3 | 2 | 0 | 0 | 1 | 1 |
| | *Abduction (AB)* | 6 | **76** | 17 | 1 | 0 | 0 | 0 | 0 |
| | *External Rotation (ER)* | 2 | 17 | **76** | 4 | 0 | 0 | 0 | 0 |
| | *Horizontal Abduction (HAB)* | 2 | 1 | 6 | **91** | 0 | 0 | 0 | 0 |
| Extension | *Elbow Extension (EE)* | 0 | 0 | 0 | 0 | **89** | 5 | 3 | 2 |
| | *Adduction (AD)* | 0 | 0 | 0 | 0 | 3 | **78** | 17 | 2 |
| | *Internal Rotation (IR)* | 0 | 0 | 0 | 0 | 3 | 18 | **76** | 4 |
| | *Horizontal Adduction (HAD)* | 0 | 0 | 0 | 0 | 1 | 3 | 6 | **90** |

Table II. Confusion matrix for classifier using EMG data. Refer to Table 1 text for description. Larger classification errors using EMG alone as compared to other classifiers.

65% and 90% may or may not be, depending on the user, the classifier, and their interaction [28]. Both matrices show error primarily occurring "within synergy", i.e. between directions that have been implicated in the typical abnormal movement patterns (identified by the major row and column divisions). Classification errors between abduction and external rotation and adduction and internal rotation are the highest and are most commonly confused for each other as indicated by the bordered boxes in the middle of two quadrants of the confusion matrix.

Table III. Classification Accuracies for each dataset

| | Dataset | | | |
|---|---|---|---|---|
| Class | EMG-TD | Torque | Load cell | EMG+LC |
| EF | 88 | 89 | **92** | **94** |
| AB | 76 | 85 | 87 | **90** |
| ER | 76 | 87 | 89 | **90** |
| HAB | **91** | **97** | **97** | **97** |
| EE | 89 | **97** | **98** | **97** |
| AD | 78 | 80 | 84 | 87 |
| IR | 76 | 76 | 83 | 87 |
| HAD | **90** | **96** | **96** | **98** |
| Average | 83 | 88 | **91** | **92** |

Table III. Summary of classification accuracies for each classifier across all participants. EMG-TD refers to EMG time-domain features, Torque to the mean-absolute value (MAV) of torques generated at the shoulder and elbow only, load cell refers to MAV from the raw load cell data, and EMG+LC are the EMG time-domain features and the MAV from the raw load cell data combined together. Bold indicates ≥ 90% accuracy.

A summary of classification accuracies across all participants for each data set is displayed in Table 3. It is clear that the

classifier using the load cell dataset outperforms the one using the EMG features dataset and that EMG features add a small improvement when used in conjunction with load cell data, especially with adduction and internal rotation. Abduction, external rotation, adduction and internal rotation have the lowest average accuracies across all datasets.

Figure 3a parses out how each class performs using the load cell classifier across all participants. The load cell based classifier generally classifies well (>90%) for 20 of 29 of the participants. Figure 3b shows the same information but only for the four most confused classes. The classification accuracy for these four classes was as low as 50%, 48%, 42%, and 3% for abduction, adduction, external rotation, and internal rotation respectively.

In attempt to understand why the classifier was less accurate with these nine participants in these directions, the normalized abduction/adduction joint torque was plotted against the corresponding external/internal rotation joint torque. Trials of representative participants that had low, moderate, and high classification accuracy in these four classes (participants 2, 15, and 29 in Fig 3a), are plotted in Figure 4. Although this representation does not take into account all data that are used to train and test each classifier, a trend emerges.

The participant with the low classification accuracy has the greatest overlap between the torques generated during these different shoulder tasks. It appears that this participant is doing the same or a very similar action for both abduction and external rotation as well as adduction and internal rotation. The plot labeled moderate classification accuracy shows some overlap in the torque generation pattern used to accomplish these single-DOF tasks. Finally, the participant with the highest classification accuracy has the greatest difference in torque patterns in these directions.

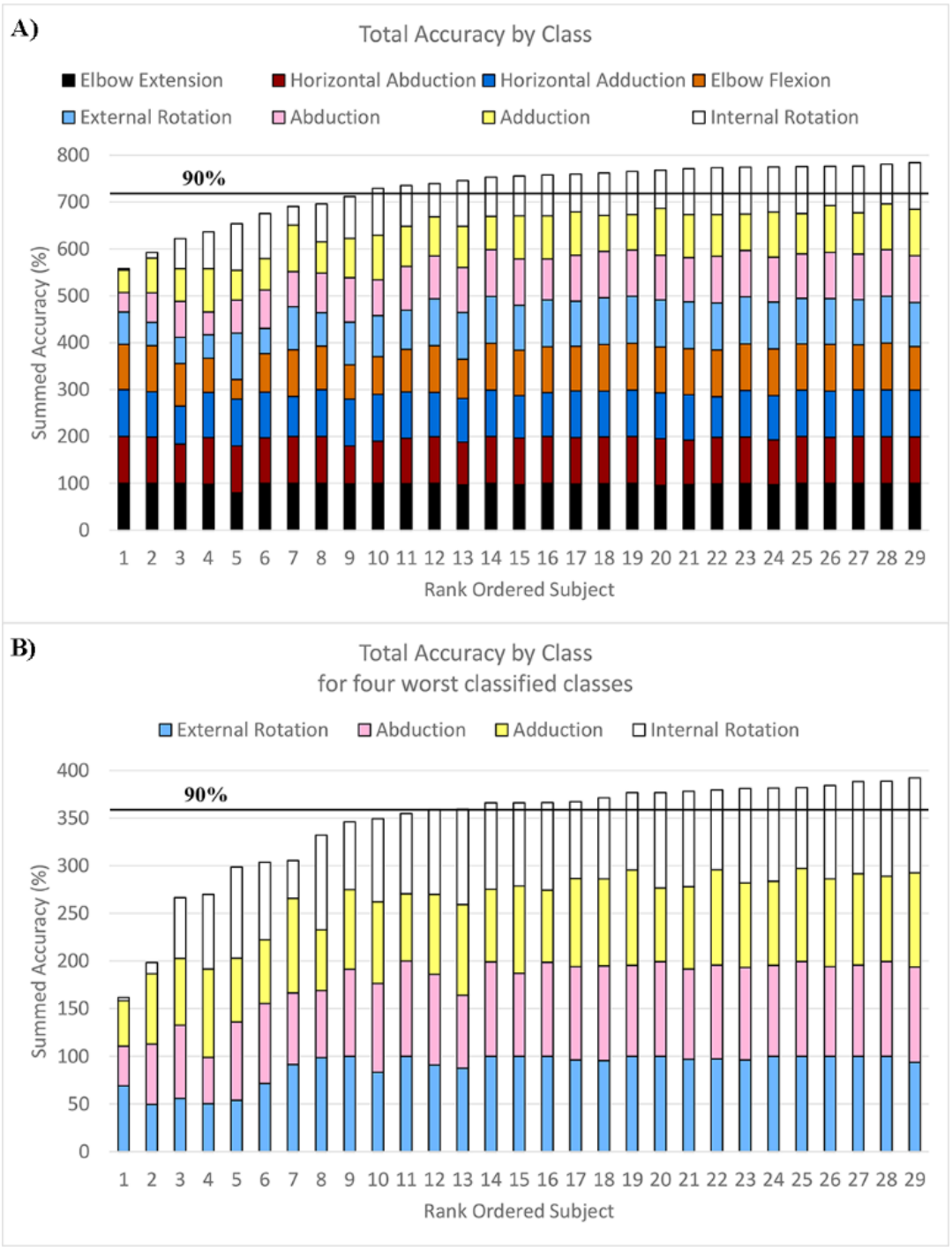


Figure 3. Classification Accuracies by rank ordered subject. A) Stacked bar graph of accuracies from the load cell based classifier for all classes and participants. Classes ordered from most accurate at the bottom to least accurate at the top. B) A simpler representation for the four worst classified classes. Participants rank ordered based on total accuracy of the presented classes. Black horizontal line represents a general cutoff for highly functional levels of classification accuracy (90%). Classification accuracy for these four lowest classes range from 50 to 99%, 42 to 95%, 48 to 99%, and 3 to 99% for External rotation, Abduction, Adduction, and Internal rotation respectively.

A post hoc analysis was completed to explore possible correlation between classification accuracy and synergy presentation, measured clinically with the FMA-UE outcome measure (Fig 5a) and the laboratory-based measure of reaching distance under limb weight (Fig 5b)[20]. Spearman rank correlations were calculated for the FMA-UE scores vs accuracy ($\rho = -0.028$, $p = 0.884$) as the FMA scores are ordinal data and for reach distance vs accuracy ($\rho = 0.12$, $p = 0.554$) due to non-bivariate normality. Neither one showed a significant correlation. An additional Spearman rank correlation was tested using a subset of the Fugl-Meyer assessment data: sections I-IV of the assessment which are focused on the shoulder and elbow ($\rho = 0.15$, $p = 0.430$). Recognizing that our data had

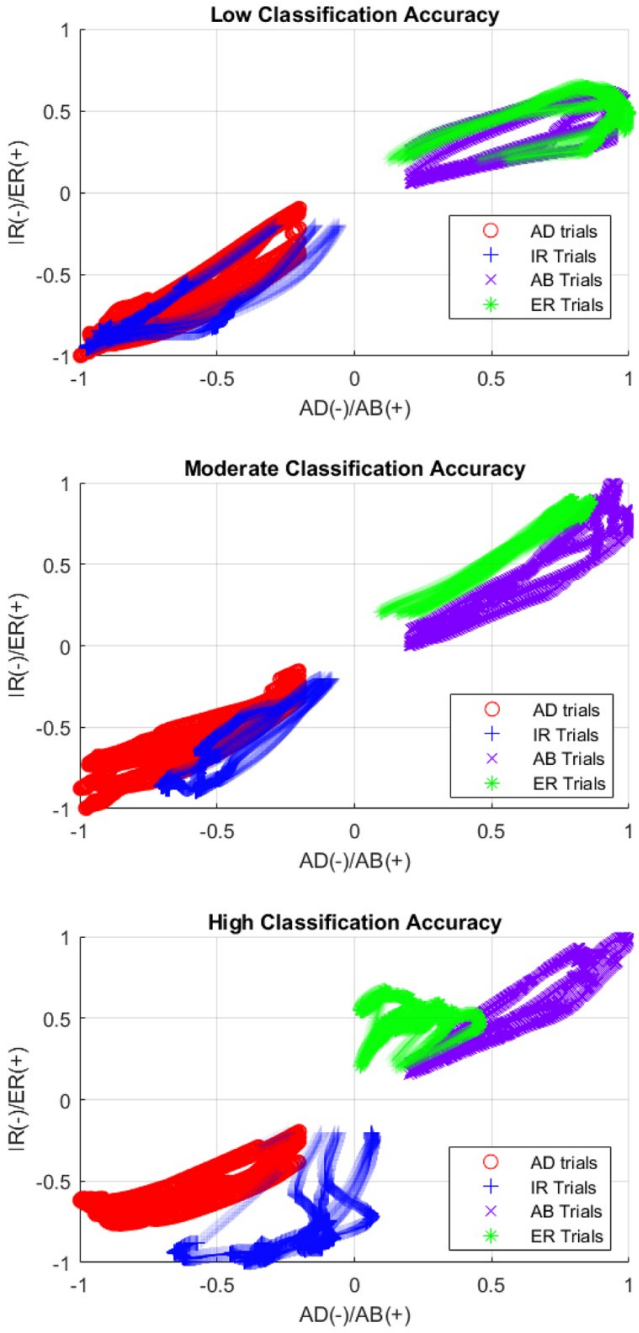


Figure 4. Representative plots of Abduction(AB)/Adduction(AD) vs External rotation (ER)/Internal rotation (IR) normalized torques for 3 participants: low accuracy, moderate accuracy, and high accuracy during all abduction, adduction, internal and external rotation trials. Discrimination between these classes improves as each task is performed in a more unique fashion.

a cluster of scores at a from the twelve participants who had the lowest classification accuracies. No correlations were found in plateau near maximal classification accuracy, these three correlations were repeated using only the data these analyses: FMA-UE vs accuracy ($\rho = 0.29$, $p = 0.358$), reach data vs accuracy ($r = 0.059$, $p = .856$), and FMA-UE sections I-IV ($\rho = 0.20$, $p = 0.520$). Pearson's correlation was used for this correlation of reach data as the removal of the plateau made the data bivariate normal.

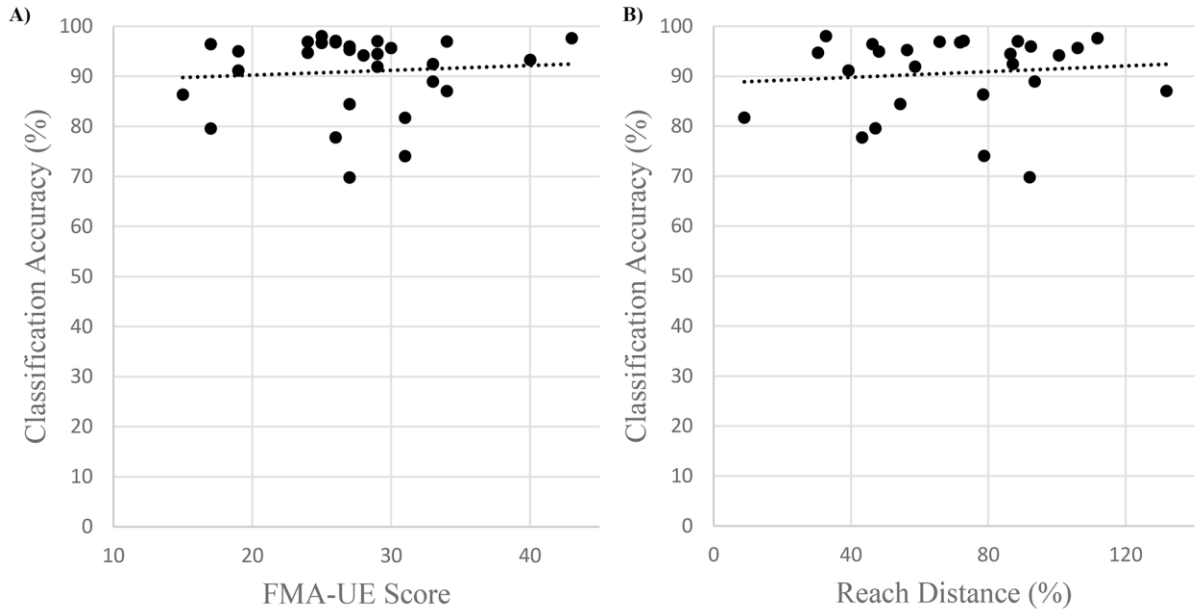


Figure 5. Scatter plots of Classification Accuracy vs UE-FMA (a) and Reach area (b) for all participants. No significant correlations were found using this data or subsets.

## 2.5 Discussion

This is the first time that a pattern recognition analysis has been accomplished on shoulder movements for the population with chronic stroke. The classification accuracies for most participants and classes was greater than 90%, indicating that LDA-based pattern recognition may be a viable control scheme for this population and these tasks. The combination of EMG data with load cell data provided the best classification accuracy averaging 92%, while load cell data alone

averaged 91%, and EMG alone averaged 83%. Classification errors (Table 1 and Table 2) occurred within the defined abnormal synergy movement patterns (*flexion synergy*: shoulder abduction, elbow flexion, external rotation, and horizontal shoulder abduction; *extension synergy*: shoulder adduction, elbow extension, internal rotation, and horizontal shoulder adduction) but primarily between adduction and internal rotation and abduction and external rotation.

Table 3 shows that similar trends in error between adduction and internal rotation and abduction and external rotation apply across all datasets. Classifier accuracy using EMG data is much lower when used on its own compared to the other datasets. This may be influenced by the fact that EMG was only recorded from major muscles of the upper extremity. This likely impacted the accuracy of the classifier and could potentially be improved through EMG acquisition from rotator cuff muscles and other involved muscle groups. For example, high classification accuracies (>92%) have been achieved for shoulder movements within a healthy population using eight channels of EMG over muscles of the back and torso and slightly longer window lengths [26,27]. Despite the aforementioned limitation, the EMG data does a fair job of classifying and, as seen in the combined data set, offers an improvement especially to the most confused classes, increasing the group average for each class closer to the control scheme goal of >90%.

The effect of abnormal synergy within the shoulder joint has been described clinically [1,11] and noted scientifically [12]. However, the results of this work brings question to the validity of using a single-DOF task to quantify this abnormal coupling. In a study using single-DOF tasks, Dewald et al. stated “the control group exhibited a significant coupling between external rotation and abduction and between internal rotation and adduction that was not present in the nonparetic limb of the hemiparetic group”[12]. This is applicable to these findings as 1) coupling was noted in a

control population and 2) was not noted on the non-paretic side of the population with stroke. This suggests that a 1-DOF task may be testing tendency rather than true neurologically mandatory patterns or true ability. The groups exploring the abnormal synergy effect on the elbow, wrist and fingers have moved away from a 1-DOF in favor of a 2-DOF task, which may come closer to testing true ability rather than general tendency. A similar shift in paradigm to a more complex or less constrained task is necessary for testing pattern recognition within the shoulder, as we cannot confidently say if these classification errors were a function of the task, posture, neural constraints of the population after stroke, or lack of ability of the classifier.

To implement a control scheme in a wearable device it would be ideal to have all necessary data come from sites proximal to and including limb segments that are being assisted. In other words, it is best to keep distal and possibly non-supported limb segments free from sensors, thus it is necessary to know if any sensors are required to be placed on the forearm in order to distinguish between these shoulder tasks. Thus, we tested a classifier which used only shoulder and elbow joint torque data as opposed to using all available load cell data. Classification accuracy of a majority of classes was reduced using this dataset, with the most pronounced loss in discriminating adduction and internal rotation (80% and 76% percent accuracy respectively). This indicates that there may be a pronation/supination component, or something else distal to the elbow occurring during adduction, which is different from what is occurring during internal rotation, enabling improved discrimination. Ultimately, this classifier shows promise in being able to control a device without more distal torque information, but further testing is required to determine if higher levels of discrimination between adduction and internal rotation is possible without it.

For many participants, these classifiers adequately discriminated between abduction/external rotation and adduction/internal rotation, but for others they did not. One reason these tasks were not classified as accurately for a cohort of participants is that these individuals were accomplishing different tasks similarly. Those supporting the idea that abnormal synergy is affecting task performance might say that these participants are physically unable to produce torque in those directions without also generating torque in unintended (secondary) directions. Meaning that these participants are locked into typical or predictable patterns due to their neurophysiologic adaptation to their stroke. If so, classification accuracy would be generally associated with the severity of expression of abnormal synergy. In an ad hoc exploration, we looked for, but did not find, a correlation between the UE-FMA outcome measure and classification accuracy (Figure 5a). Because this outcome measure has limited resolution, classification accuracies were also compared to reaching distance data available for most of these participants from a recent study [20] but similarly, were not associated (Figure 5b). The reported reach distance is presented as a percent of excursion attained toward a standardized target near end range of motion under limb weight. This does not indicate that these measures are a poor measure of abnormal joint coupling, but that abnormal coupling within the shoulder may not exist or at least not to the same extent as more distal joints (elbow, wrist, fingers). This may also indicate that an alternative explanation is more likely. It is possible that due to the nature of an isometric task, the posture selected for this study, or of being told to push or pull as hard as they can, these participants used strategies to maximize their torque production that serendipitously or veraciously reflected the previously described constrained abnormal synergy pattern (shoulder adduction and internal rotation or shoulder abduction and external rotation). This suggests that single-DOF

isometric torque generation tasks are either not as accurate at quantifying loss of independent joint control as multi-DOF tasks such as reaching dynamics under differing loads [40], or are possibly inadequate altogether. Another alternative is that these participants were not performing the same task consistently during the three analyzed trials, causing increased classification error. Considering each of these possibilities, application of the classifier on a more complex task is warranted to determine accuracies in a task that truly represents impairment such as the ability to move outside of these patterns. While a correlation between classification accuracies and expression of abnormal synergy may emerge, the present data would lead one to hypothesize that adequate classification accuracies are possible.

Other features and other classification techniques were not used or explored in this initial analysis as many participants had adequate classification accuracy and we do not feel the loss of accuracy for the others was due to lack of classifier abilities. Rather we think that these participants completed the task in a different way than the others. Specifically, in an attempt to maximize their torque generation, they may be coupling these directions producing a similar pattern whether attempting to elicit torque in one direction or another. The degree to which this multi-joint pattern observed during the single-joint task represents abnormal synergy in unclear. Future work will need to explore classification accuracies in multi-DOF movements outside of these patterns as well as attempt to automatically detect the onset of expression of abnormal synergy in order to move toward real-time control of a wearable shoulder assistive device during functional movements.

## 2.6 Conclusion

Here we have demonstrated the possibility to classify user-intent of these eight upper-extremity directions to an adequate level for control for most of the individuals (20 of 29) in this

study. For some individuals, the classifier had difficulty discriminating between shoulder adduction and internal rotation and shoulder abduction and external rotation. It is unknown if this is due to manifestation of the negative effects of abnormal synergy, a limitation inherent in the posture chosen, or a volitional strategy to maximize torque production. This warrants the evaluation of a more complex multi-DOF task representing a pattern outside of the abnormal synergy. Evaluation of the LDA-based classifier under these conditions including the use of sensors on rotator cuff muscles may also improve accuracies for the challenging torque combinations of abduction/external rotation and adduction/internal rotation.

Accurate classification of movement intent is necessary for the successful implementation of a sensor-driven actuated exoskeleton. This work provides initial evidence supporting the ability to differentiate shoulder and elbow movements despite previous challenges in differentiating more distal upper extremity actions. This suggests that continued work is warranted to investigate if an LDA-based classifier can be an effective solution for the control of a more proximal assistive device. Such a device would have both assistive and restorative potential.

# Chapter 3: Pattern Recognition of Partly Dynamic Shoulder Tasks

Kopke JV, Ellis MD, Hargrove LJ. Determining User Intent of Partly Dynamic Shoulder Tasks in Individuals With Chronic Stroke Using Pattern Recognition. Ieee T Neur Sys Reh. 2020;28(1):350-358.

## 3.1 Abstract

Stroke remains the leading cause of long-term disability in the US. Although therapy can achieve limited improvement of paretic arm use and performance, weakness and abnormal muscle synergies—which cause unintentional elbow, wrist, and finger flexion during shoulder abduction—contribute significantly to limb disuse and compound rehabilitation efforts. Emerging wearable exoskeleton technology could provide powered abduction support for the paretic arm, but requires a clinically feasible, robust control scheme capable of differentiating multiple shoulder degrees-of-freedom.

This study examines whether pattern recognition of sensor data can accurately identify user intent for 9 combinations of 1- and 2- degree-of-freedom shoulder tasks. Participants with stroke (n=12) used their paretic and non-paretic arms, and healthy controls (n=12) used their dominant arm to complete tasks on a lab-based robot involving combinations of abduction, adduction, and internal and external rotation of the shoulder. We examined the effect of arm (paretic, non-paretic), load level (25% vs 50% maximal voluntary torque), and dataset (electromyography, load cell, or combined) on classifier performance.

Results suggest that paretic arm, lower load levels, and using load cell or EMG data alone reduced classifier accuracy. However, this method still shows promise. Further work will examine

classifier–user interaction during active control of a robotic device and optimization/minimization of sensors.

*Index Terms*—Linear discriminant analysis, Pattern recognition, Stroke, Robotic therapy.

## 3.2 Introduction

Stroke remains the leading cause of serious long-term disability in the US [41]. An estimated 7 million individuals in the United States, and 82.9 million individuals worldwide, have experienced a stroke [41] and approximately 30-66% live with permanent upper extremity impairment [42,43]. In addition to limb weakness (paresis), involuntary co-activation of upper limb muscles after a stroke impedes coordinated use of the paretic arm [44]. This motor discoordination—sometimes described as primitive, automatic, reflexive, obligatory, stereotypical, or whole-limb movement patterns, and referred to here as *abnormal flexion or extension synergies*—significantly increases difficulty in accomplishing activities of daily living (ADLs) [45]. Abnormal synergies may stem from a neurophysiological reliance on more diffuse cortico-bulbar-spinal pathways to compensate for damage to, or loss of corticospinal projections due to stroke [16].

*Flexion synergy* in the upper extremity is observed when lifting the arm against gravity (shoulder abduction), which causes unintentional co-activation of elbow, wrist, and finger flexors, limiting functional use of the affected limb [46]. The complete flexion pattern includes scapular retraction and elevation, shoulder abduction, and external rotation, elbow flexion, forearm supination, and flexion of wrist and digits [47]. However, with support or reduction of proximal shoulder effort, flexion synergy intensity decreases [46], with a subsequent increase in reach distance [45,48].

Conversely, upper-extremity *extension synergy* occurs when adducting the humerus against resistance, causing involuntary elbow extension. The full extension synergy includes protraction of the scapula, shoulder adduction and internal rotation, elbow extension, and forearm pronation [47]. The effects of extension synergy on wrist and finger activity are not as predictable, but most commonly still result in flexion of both the wrist and fingers. However, extension synergy is typically not as important or detrimental as flexion synergy, as there is rarely a need to adduct the humerus against resistance.

Both flexion and extension synergies present in proportion to effort. For flexion synergy, small yet significant improvements in unsupported reach distance have been obtained using a training paradigm that takes advantage of this relationship [19,20]. By progressively increasing the abduction load as reaching goals are met, individuals with stroke are able to reach further without external physical support. However, the maximal potential benefits of this rehabilitation strategy are unknown, possibly due to unknown effects of dosage and limitations on participation/intervention time.

A wearable device that reduces shoulder effort based on user intent and need may provide a novel solution to address activity limitations caused by weakness and abnormal synergies, allowing the user to better engage with their environment, and facilitating other therapeutic interventions to restore elbow, wrist, and hand function. Such devices have been proposed [49-51], and some have recently become commercially available for healthy individuals [52,53], but appropriate control strategies for individuals with stroke with abnormal synergies are lacking.

Machine learning techniques such as support vector machines, neural networks, and linear discriminant analysis (LDA) have been used with sensor data—e.g., force, acceleration, muscle

activity (i.e., electromyography, EMG)—to predict user intent [54]. In individuals with amputation, EMG pattern recognition has been used to determine user intent to control powered upper [37,55] and lower [56-58] limb prostheses. LDA-based classifiers have enabled control of multiple degree-of-freedom (DOF) myoelectric prostheses; are generally considered to be accurate, robust, and computationally efficient [23-25]; and have been cleared for commercial sale for individuals with amputation [59,60].

Successful application of wearable robotic technology in individuals with spinal cord injury [61] or with amputation [23] has paved the way for use in other populations, including individuals with stroke. However, accurately and reliably controlling a wearable robotic device will be a challenging problem in individuals with stroke due to pathological muscle activation.

Incorporating user intent information into the control strategy overcomes the disadvantages of passive or pre-planned movement patterns (i.e., "slacking" and restricted freedom of movement, respectively) by requiring user effort and active participation [62]. Pattern recognition of EMG during shoulder movement was explored as a control system for persons with amputation, and classification error rates below 10% were achieved in a healthy control population [26,27]. However, for individuals with stroke, classification of user intent for simply opening and closing the paretic hand was negatively affected by lifting at the shoulder at only 25% of maximum effort [15,33]. EMG from the paretic forearm predicts intended movement with a broad range of outcomes including high [31], mixed [30], and low [29] error rates. EMG has also been used to predict goal-directed reaching with sufficient accuracy in a healthy control population but insufficient accuracy for individuals with stroke[32]. Our previous work [63] demonstrated low classification error (<10%) for 8 isometric shoulder and elbow tasks in a majority of participants with stroke. However, some participants had

high error rates, possibly because in our experimental design only a single-DOF was being tested or controlled at any one time. It is possible that participants were consciously or unconsciously completing different tasks using a similar multi-DOF strategy to maximize strength readings. For example, they could have simultaneously maximized external rotation and abduction effort and used that strategy for both external rotation and abduction testing, making the torque and muscle activation patterns similar and difficult to distinguish.

Our present work aims to understand how abnormal synergies due to stroke affect the ability of an LDA-based classifier to discriminate between different 1- and 2-DOF shoulder tasks. We extended our preliminary analysis [64] to evaluate performance of classifiers using data from non-paretic arms of individuals with stroke as well as age- and gender-matched healthy controls. Additionally, we evaluated the effect of lifting-load (25% or 50% maximal voluntary torque) and dataset type (EMG, load cell, or a combined data set) on classification error rate.

We hypothesized that, due to muscle co-activation patterns caused by abnormal synergy after a stroke, classification accuracy of control participants would be higher than that for the paretic arm of the participants with stroke. Classifier performance on the non-paretic (or less-affected [65]) arms was hypothesized to be higher than paretic but lower than control classifier performance. We also hypothesized that classification error for the paretic arm would be higher at higher levels of proximal shoulder effort due to increased synergy presentation. Finally, we hypothesized that the accuracy of classifiers using EMG would be lower than those using raw load cell data, and that classifiers using a single data set would be lower than those using a combined data set.

## 3.3 Methods

### *3.3.1 Participants*

All participants provided informed consent to participate in the protocol, which was approved by the Northwestern University Institutional Review Board (IRB #: STU00205835). We recruited 12 age- and gender- matched control participants and 14 participants with chronic (> 1 year) hemiparetic stroke with moderate to severe motor impairments, as determined by a score on the upper-extremity portion of the Fugl-Meyer assessment (FMA-UE) of > 10 and < 45. These individuals exhibit flexion synergy at levels of effort less than limb weight (approximately 50% shoulder abduction strength) and could benefit from using a powered assistive device for the shoulder. Two participants with stroke were excluded from the study: one was unable to accomplish the dual-task protocol and the other had no external rotation strength. Consequently, 12 participants with stroke (50% female, who were, on average, 60.8±10.3 years old, with an FMA-UE score of 26.9 ± 8.4, and 16.8 ± 8.3 years post-stroke, along with 12 control participants (50% female, mean age 59.1 years old ± 9.9) completed the study. For participants with stroke, both arms were tested (non-paretic then paretic); for control participants, only the dominant arm was tested.

### *3.3.2 Setup and instrumentation*

To measure maximal isometric strength, participants were seated in a rigid chair (Biodex, Shirley, NY; Model 830-110). Torso movement was minimized by securing them with a lap belt and two chest straps and placing their feet on a foot rest. A fiberglass cast was applied to their anatomically neutral forearm, wrist, and hand to rigidly and securely attach their arm to a 6-DOF

load cell (JR3 Inc., Woodland, CA, USA; Model 45E15A). This custom setup was adjusted to place the participant's arm in 90° of abduction, 45° of horizontal adduction, and 90° of elbow flexion. A licensed physical therapist applied bipolar EMG electrodes (Delsys, Cambridge, MA, USA; 16 channel Bagnoli), with 1cm interelectrode spacing, over 11 muscles—deltoid (anterior, intermediate, and posterior), upper-trapezius, supraspinatus, infraspinatus, latissimus dorsi, teres complex, pectoralis major sternal fibers, biceps brachii, and triceps lateral head)—located using guidelines set forth in *Anatomical Guide for the Electromyographer* [36] using palpation and anatomical landmarks. A ground electrode was placed over the acromion. Maximal torque measurements (Section II.C) were collected in this setup to minimize wear on the ACT$^{3D}$ robot (Section II.D)

### *3.3.3 Isometric maximal voluntary torque measurements*

Maximal isometric voluntary torques were determined for six movements: shoulder abduction, adduction, external and internal rotation, and elbow flexion and extension and used to inform the second part of the experiment. Verbal encouragement was provided to ensure maximal effort. Forces, moments, and EMG were collected at 1 kHz.

### *3.3.4 Dual task setup on ACT$^{3D}$*

Participants were then moved to a customized ACT$^{3D}$ haptic master robot [40,66] with a 6-DOF load cell (JR3 Inc., Woodland, CA, USA; Model 51E20A) attached under the end effector. The load cell allows precise control of abduction and adduction (vertical) loading while simultaneously measuring forces and moments in three orthogonal directions. Participants were secured in the rigid chair as described in Section II.B and connected to the ACT$^{3D}$ with a custom setup that

centered the medial epicondyle (center of rotation of elbow) over the load cell. The custom device clamped the medial and lateral epicondyles between foam pads, and secured the cast to the device at the forearm (Fig. 1A, top). The arm position was similar to that described for isometric torque measurements. Movement in the transverse plane was constrained and a "ceiling" and "floor" were created to prevent elbow movement beyond 5 cm above and below 90° of abduction, respectively. This enabled movement in the vertical direction equating to approximately ± 10° of abduction/adduction while minimizing change of alignment of the medial epicondyle over the load cell (0.4 cm).

### *3.3.5 Dual task protocol*

Participants were required to abduct (lift, +) and adduct (depress, -) at 0, ± 25, and ± 50% of their maximum joint torque determined by isometric testing. For 0%, the entire limb weight was supported by the ACT$^{3D}$, which is equivalent to no effort. Each trial lasted 10 seconds. For the first 5 seconds the participant was asked to move and maintain their arm between the ceiling and floor, with proprioceptive and visual feedback from their limb. At 5 seconds the participant was provided a verbal and visual cue via a graphical user interface (Fig. 1A middle) to begin either maximal isometric external or internal rotation while continuing to keep their arm off the horizontal surfaces. The order of testing conditions was randomized. A minimum of 3 and a maximum of 10 trials of each condition were completed with the goal of having 3 trials with isometric humeral rotation maximums within 10% of each other and at least 3 seconds of active rotation. This resulted in data for 3 trials of 10 conditions (0, ± 25, ± 50% abduction/adduction for both external and

internal rotation).

### *3.3.6 Data Processing*

The Delsys EMG collection system bandpass filtered signals between 20-450 Hz, and force and moment data were transformed to joint torques. External and internal rotation was calculated for

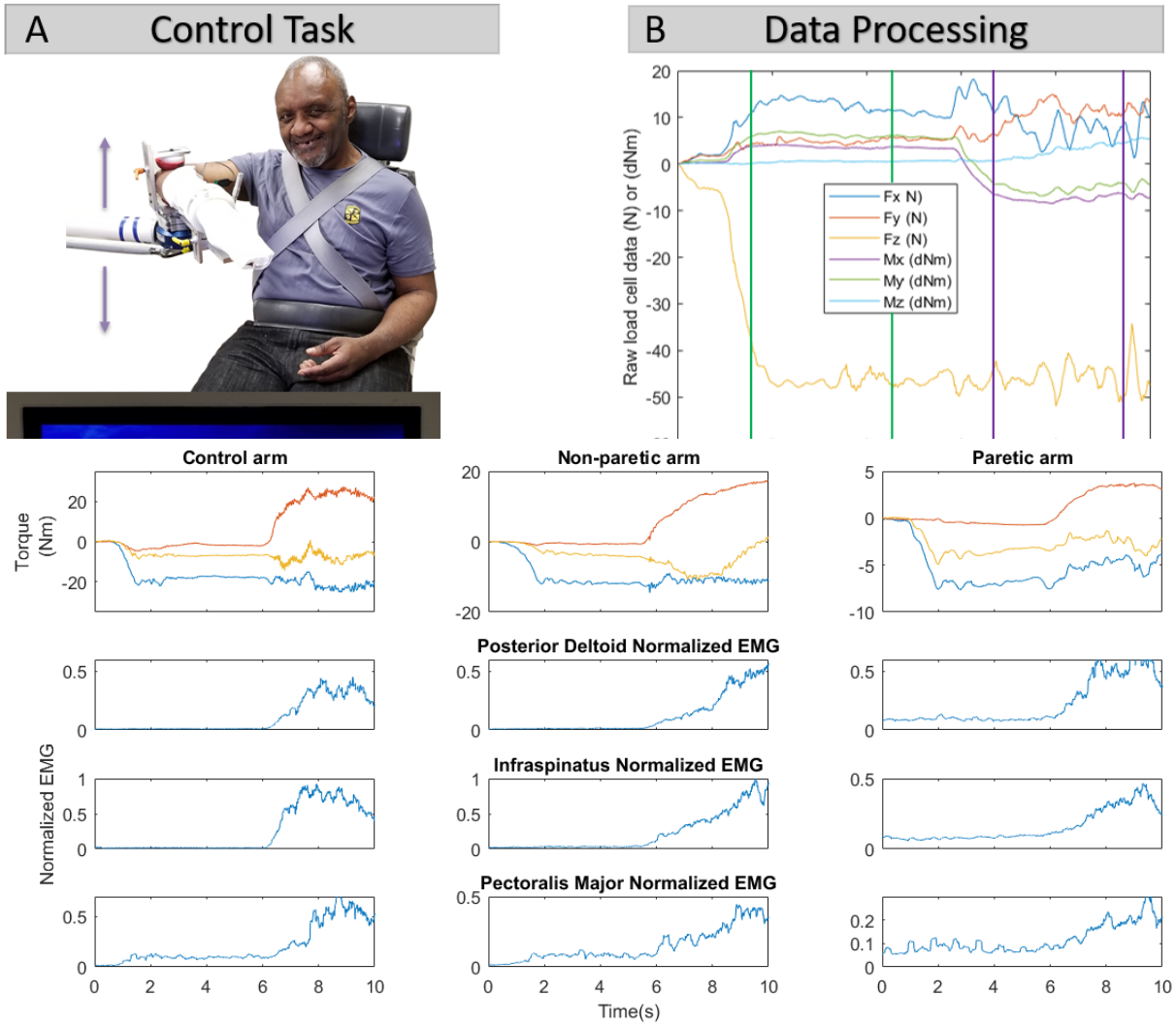


Figure 7. Visual comparison of representative trials of participants from each arm type for 25% adduction (first 5 seconds) followed by external rotation (last 5 seconds). Top row is calculated shoulder joint torques (blue = adduction(-)/abduction(+), red = internal rotation(-)/external rotation(+), yellow = horizontal adduction (-)/abduction(+). Bottom 3 rows are normalized root mean squared EMG over 200 ms windows for the posterior deltoid, infraspinatus, and pectoralis major muscles.

each trial. For the subsequent analysis, we used the three trials from each condition in which the greatest humeral rotational torques were achieved and the arm was maintained off of the horizontal surfaces during the periods of interest (1.5s-4.5s and 6.5-9.5s). Representative joint torques and normalized EMG data for each group are presented in Fig. 2. The purpose of two time segments was to extract pure abduction-, adduction-, or no- loading time (occurs during first 5 seconds) as opposed to dual-task time (occurs during last 5 seconds). Different load-levels (0, 25, and 50% of abduction and adduction) were used in attempt to elicit different degrees of the abnormal synergy so we could run an analysis of the effect of lifting effort on classification accuracy.

### *3.3.7 Classification*

Two sets of LDA-based classifiers were created from each dataset type: EMG data, raw load cell data, and a combined dataset (EMG and raw load cell data, appended post feature extraction). One set of classifiers was created using the 0% and ±25% lifting condition data and the second set of classifiers was created using the 0% and ±50% lifting condition data. The data from the 0% lift condition was used as a baseline in both sets of classifiers to create no movement, external rotation only, and internal rotation only classes.

Data collected between 1.5s to 4.5s and between 6.5 and 9.5s in each trial were extracted and labeled according to the task being accomplished during each time period. Data were windowed into 200ms windows using 20ms steps (180ms overlap). This allowed the load cell data recorded at 50 Hz and the EMG data recorded at 1000 Hz to be combined after windowing without down-sampling. Four time-domain features (mean absolute value, zero-crossing, slope sign change, and waveform length) [67] were extracted from EMG data and mean absolute values were extracted for

load cell data. These features have proven accurate and robust in other myoelectric control applications [68].

Classifiers were trained and tested using a trial-wise leave-one-out cross validation, i.e., two of the three trials were used to create a classifier and tested against the third. Each combination was tested and classification accuracies for each dataset were averaged within and across participants for comparison.

### *3.3.8 Statistics*

Two linear mixed-effects models (equation 1) were used to test the effect of the fixed factors: arm type (non-paretic vs paretic and non-paretic vs control), load level (25%, 50%), and dataset type (EMG, load cell, combined) on classification error rate. Two models were used since only the dominant arm of the control group was tested making the design unbalanced. One benefit of using a linear model is that it allows an analysis of the effect of each factor (magnitude and direction) as opposed to a pure comparison of group means. A mixed-effect model was chosen to allow individuals to be treated as random effects so each could have their own response. The model also included arm*load and arm*dataset interaction terms to detect any interaction between these terms. This would be expected if, as we hypothesized, load level or dataset behaved differently for each arm-group; specifically we expected that load level and paretic arm would have an interaction with heavier lift, yielding greater error rates due to increased presentation of abnormal synergy. These models and post-hoc statistical analysis were completed using MiniTab® Statistical Software (Minitab, Inc., State College, PA, USA). Main effects (arm, load, dataset) are implicit in this model.

$$error\ rate \sim 1 + arm * load + arm * dataset + (1 \mid participant) \quad (1)$$

## 3.4 Results

### *3.4.1 Linear mixed-effects model (LMEM)*

A summary of results from the two models is presented in Tables I (paretic vs non-paretic) and II (control vs non-paretic). No interaction terms were significant for either model. Significant differences exist between non-paretic and paretic arms (p = <0.00001) and lift at 25% vs 50% (p=0.00083) with estimated pattern recognition classification error differences of -8.6% and 3.63%, respectively. Thus classification error for paretic arms increased by 8.6% compared to non-paretic arms and lifting at 50% maximum joint torque improved classification by 3.63% over lifting at 25%. The model also predicted the model coefficient for the combined dataset classifier as better than the load cell data classifier by 4.09%, and the load cell classifier was better than the EMG classifier by 3.14%. Similar results were found in the comparison between the control group and the non-paretic arm group (Table II). The classifiers built using the control arm, 50% load level, and the combined dataset performed better than all other classifiers.

Table IV. Non-paretic vs Paretic LMEM Results

| NP vs P | F | p-value | Compare | Δ coef |
|---|---|---|---|---|
| Arm | 66.22 | <0.0001 | NP vs P | -8.62 |
| Load Level | 11.73 | 0.0008 | 25% vs 50% | 3.63 |
| Dataset | 16.31 | <0.0001 | Comb vs LC | -4.09 |
| | | | EMG vs LC | 3.14 |

Table V. Control vs Non-paretic LMEM Results

| C vs NP | F | p-value | Compare | Δ coef |
|---|---|---|---|---|
| Arm | 9.8 | 0.0049 | C vs NP | -4.52 |
| Load Level | 8.22 | 0.0049 | 25% vs 50% | 2.00 |
| Dataset | 12.69 | <0.0001 | Comb vs LC | -2.45 |
| | | | EMG vs LC | 0.87 |

### *3.4.2 Classifier Performance*

Table III shows the confusion matrix for the combined dataset of the participants with stroke for the 50% load level condition. Each row represents what the user intended (actual) while the predicted classes are represented by the columns. Grey shading indicates single-DOF conditions.

Table VI. Confusion Matrix for Paretic Arm, 50% Lift, Combined Dataset

| 50% Comb. | No Mvt | AD | AB | ER | ER+AD | ER+AB | IR | IR+AD | IR+AB |
|---|---|---|---|---|---|---|---|---|---|
| No Mvt | 94 | - | 1 | 2 | - | - | 3 | 1 | - |
| AD | 2 | 92 | - | - | 4 | - | 1 | 1 | - |
| AB | 1 | - | 95 | 1 | - | 2 | - | - | - |
| ER | 10 | - | - | 86 | - | 2 | 1 | - | - |
| ER+AD | 1 | 9 | - | 2 | 87 | 1 | - | - | - |
| ER+AB | - | - | 9 | 2 | - | 86 | - | - | 3 |
| IR | 10 | 2 | 1 | 1 | - | - | 85 | - | 1 |
| IR+AD | 4 | 4 | - | - | 2 | - | - | 90 | - |
| IR+AB | - | - | 4 | - | - | 3 | 1 | - | 92 |

AD = adduction, AB = abduction, ER = external rotation, IR = internal rotation, Mvt = movement.

Group averages of classification error rate for the 25% lift condition are presented in Table IV and the 50% lift condition in Table V, with standard deviations presented within parentheses (n=12 for each group and condition).

Table VII. Average Classification Error for 25% Lift Condition

| 25% | EMG | LC | Comb | Avg. |
|---|---|---|---|---|
| P | 24.2 (13.7) | 20.0 (11.6) | 14.0 (11.3) | 19.4 (12.6) |
| NP | 11.3 (6.7) | 11.0 (10.4) | 4.9 (4.1) | 9.1 (7.9) |
| C | 5.1 (3.1) | 6.4 (7.9) | 2.3 (2.1) | 4.6 (5.2) |
| Avg. | 13.5 (11.9) | 12.4 (11.3) | 7.0 (8.5) | |

Table VIII. Average Classification Error for 50% Lift Condition

| 50% | EMG | LC | Comb | Avg. |
|---|---|---|---|---|
| P | 18.3 (10.3) | 14.1 (9.3) | 9.7 (7.0) | 14.1 (9.4) |
| NP | 8.4 (4.2) | 8.3 (5.3) | 4.7 (3.5) | 7.1 (4.7) |
| C | 1.9 (1.0) | 4.0 (3.9) | 1.7 (2.6) | 2.5 (2.9) |
| Avg. | 9.5 (9.3) | 8.8 (7.6) | 5.4 (5.8) | |

P = paretic, NP = non-paretic, C = Control arms; LC = load cell data, Comb = combined data; Avg. = average.

Averaged results from each group and dataset are presented in Fig 3. Although the 50% lift condition was significantly better than the 25% condition, the two levels are averaged for figure clarity since their differences were relatively small.

Post-hoc comparisons of dataset performance revealed that the combined dataset performed significantly better than both the load cell and EMG dataset ($p=0.0005$, $p<0.0001$ respectively for paretic vs non-paretic and $p<0.0001$, $p=0.0005$ respectively for control vs non-paretic).

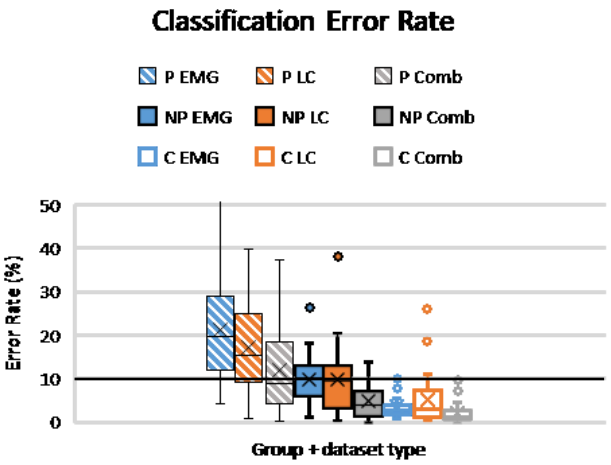


Figure 8. Summary of classifier error rates for all groups and dataset types. Rectangular boxes indicate 1st-3rd interquartile range, with 'X' indicating means, horizontal bars are medians, and error bars indicate standard deviation. The bold horizontal line denotes a 10% error rate controllability cutoff for myoelectric devices [44]. P = paretic, NP = non-paretic, C = Control arms; LC = load cell data, Comb = combined data.

Performance of load cell and EMG datasets alone were not significantly different from each other ($p=0.212$ for paretic vs non-paretic and $p=0.679$ for control vs non- paretic).

### 3.5 Discussion

The aim of our study was to investigate the feasibility of determining user intent for movement of the shoulder of the paretic limb in individuals with stroke. This approach could allow future development of an exoskeleton to provide abduction support for the paretic arm. In particular, we were interested in the relationship between controlling internal/external rotation and shoulder abduction/adduction simultaneously. Overall, we found that using a pattern recognition system based on the combination of EMG and load cell information in individuals with stroke resulted in an average error rate as low as 9.7%. These results are promising as related work in controlling myoelectric prostheses has shown that systems with error rates in the range of 0 – 10% allow good control of a device [28]. Control system error rates as high as 35% can be used, but result in greater variability in performance between individuals. Thus, our next phase of research is to implement the combined control system on an embedded system to allow real-time control of a lab-based robot.

We hypothesized that classification of control limb data would be better than non-paretic arm data, which would be better than paretic arm data. Our results support this hypothesis. Differences in classifier error rate between paretic and non-paretic arms are likely due to stroke sequelae (weakness, spasticity, etc) caused by the damage to the cortical neurons. Additional weakness could be attributed to limb disuse.

Classification accuracies using data from non-paretic limbs were significantly lower than from control arm data, although still within a useable range. We speculate that the difference may be related to damage due to stroke, possibly in structures that are bilaterally activated. We did not use imaging to locate stroke-related damage nor did we control for stroke location. While the FMA-UE confirmed hemiparesis within a specified range, this test has a known ceiling effect for detecting deficits in a non-paretic limb [69]. A more detailed evaluation of the non-paretic limb was beyond the scope of this study; however, we acknowledge that the "less affected" limb is known to have subtle impairments after stroke [65] that may have reduced classifier accuracy compared to controls.

Abnormal flexion synergy that presents proportional to proximal shoulder effort [48] and represents the primary impairment contributing to reaching dysfunction [70], did not seem to explain any error since greater shoulder effort caused an improvement in classification accuracy similar to the other groups. In fact, the 50% lift condition was significantly better than the 25% condition. Thus, we reject our hypothesis that the greater loading condition (50%) has a negative effect on classification accuracy. It may be that even at low loading levels, abnormal synergy is fully expressed in the shoulder DOFs, thus higher loads do not cause a further decrease in classification accuracy. Evaluation of torque coupling within the shoulder was beyond the scope of this discussion but may shed light on the possibility. These results are intuitive in retrospect, if we ignore the possible effects of abnormal synergy, due to the inner workings of an LDA. An LDA linearly separates groups by maximizing distance between means and minimizing overlap of variance. A higher load level would create greater distance between data clusters, which would result in better classification accuracy. The paretic arms were weaker, as expected post-stroke, thus

reducing separation between the classes. Additionally, the no-movement class was based on 0% effort which may have some amount of torque generated in other directions and/or co-contraction with concurrent EMG generation. Greater abduction and adduction effort required in the 50% condition generate greater distance between data clusters from the 0% condition compared to the 25% condition, thus increasing classification accuracy.

Classifier performance using load cell data was not statistically different than using EMG data; however, the combination of both types of data performed significantly better. Therefore, we can accept the hypothesis that the combined data set provided the best classification accuracy yet reject the hypothesis that load cell data would perform better than EMG. This indicates that the load cell and the EMG sensors provide some complementary information as Huang et al also found [35]. We expected that the load cell data would outperform EMG because EMG signals are noisy and difficult to measure from small or deep muscles involved in movement while load cells are sensitive and accurate to all changes in forces and moments. Since we used 11 EMG sensors on the back, shoulder, and arm, it is possible that we were able to overcome these disadvantages. Unlike the muscles in the forearm or arm which are commonly used to control many degrees of freedom of the hand, wrist, and elbow after amputation, the muscles that accomplish the actions tested in this study are larger and have a greater amount of separation possibly enabling higher levels of classification accuracy. Surface EMG sensors are inexpensive, non-invasive, and easy to apply but come with their own disadvantages including sensitivity to sweat, movement, and fatigue and must be applied generally in the correct area and orientation [71]. Implantable EMG sensors could be a solution to these disadvantages and is a promising avenue of exploration. Further analysis is needed to determine if common muscle sites provided the most useful information

across participants or groups and how much the number of sensors could be reduced. We suspect there is an optimal subset of surface EMG channels, maybe 4 to 6, for each individual that may not be shared across groups or participants similar to the results found in Hargrove 2007 [72]. A detailed analysis extends beyond the scope of the present study.

While mounting a load-cell to the ACT$^{3D}$ robot was straightforward, incorporating a load cell to measure forces and moments from a paretic limb in a portable wearable device has challenges. Although not considered in this study, data from other sensors could be incorporated into a pattern recognition approach. For example, force sensitive resistors used to measure interface pressures or inertial sensors to measure joint orientation could provide valuable information. Classification error rates were higher using single sources of information compared to using combined EMG and load cell data, but still showed promise. EMG data may be sufficient on its own but classification accuracy could be improved using other sensors that would be easier to implement than a load cell [35,71].

As depicted by the confusion matrix of paretic arm data in Table III there were increased errors between the single task motions, internal and external rotation, and the no movement class. Additional significant error existed between the external rotation dual-tasks and their corresponding 1-DOF lift condition counterpart (e.g. adduction + external rotation being confused as pure adduction). Determining the underlying cause of these errors is outside the scope of this study but we offer two hypotheses to explain them.

These sources of error could be explained by arm weakness; participants may not generate enough torque or EMG during these tasks to allow these classes to be distinguished from others. In addition to rotating the humerus, rotator cuff muscles are also used to maintain dynamic stability

within the glenohumeral joint [73]. Additionally, muscles that adduct (latissimus dorsi, pectoralis major, and teres major) also internally rotate the humerus [74]. Together, these factors may limit the amount of external rotation torque that can be generated during adduction. These anatomical/neuromuscular phenomenon are present in all arms/populations but may only affect the classification accuracies of the paretic arm due to its underlying weakness.

Additionally, a loss of independent DOF control within the shoulder joint, similar to that observed between joints (shoulder, elbow, and hand) [46,75,76], could account for diminished classification accuracies in the paretic arm. In the present example, a reduced ability to produce external rotation torque during adduction would be considered a "task-dependent weakness" in the context of loss of independent joint/DOF control [77], further reducing the distance between means and increasing classification error in an LDA. In fact, abnormal co-contraction of each part of the deltoid has also been found in paretic arms of individuals with stroke [78].

We performed an offline analysis to compute the classification error rate of the collected data. The relationship between offline analysis and real-time performance is an open topic with some studies showing weak or no correlation [79], with others showing positive correlation within certain ranges of the classification error rate metric [28]. One drawback of offline analyses of pattern recognition for amputees is that they do not have proprioceptive or visual feedback of their attempted movements. In our study, participants had force and proprioceptive feedback from their limbs (although these feedback mechanisms may have been altered as a result of the stroke) and real-time visual feedback from their arm and the graphical user interface. Thus while our analysis was performed offline, the participants were attempting to perform real-time movements and did

have access to feedback. Future work controlling an actual device will investigate how users' response to generated errors affects their performance.

This study is limited by the small sample size for the number of conditions tested, the minimal amount of movement permitted only in one degree of freedom, and the use of a large amount of sensors, possibly limiting the generalizability of these findings to an entire population or to a future control scheme. Despite these limitations, this work is a logical and necessary step towards understanding user-in-the-loop control of a device that can minimize expression of abnormal synergy within the paretic population.

This work extends our prior work [63] by comparing the non-paretic arm and healthy control arms with the paretic arm. Additionally, instead of a pure isometric 1-DOF task we used a mixed, partly-dynamic partly-isometric task enabling intuitive control of an additional DOF. In our previous study, participants were asked to generate their maximum strength in one of eight directions without regard to what torques were being generated in the other directions. This made it impossible to determine if classification errors were due to limitations caused by the stroke or by selection of a strategy or preference in completing the task. By imposing a dual task paradigm, we ensured that each participant was controlling what was happening in the directions that were most commonly confused in the previous study (abduction/adduction and internal/external rotation). By incorporating a mixed dynamic and isometric task, we moved towards a less constrained task and enabled intuitive control of torque generation in one degree of freedom while measuring maximum torque generation in the other. As a result, we believe that the higher error rates in our prior work were caused by the strategy selected by certain participants to achieve the

task rather than their impairments due to stroke or the capability of a pattern recognition system to classify the data.

### 3.6 Conclusion

Using a testing paradigm that enabled control of the level of effort in one DOF via dynamic movement along with inherent proprioceptive and visual feedback enabled us to begin to better discern the ability of an LDA-based classifier to determine user intent in single- and dual- shoulder tasks after a stroke. Using linear mixed-effects models, estimates of contribution to classifier accuracy, in addition to group differences were obtained. This provided insight not only into which groups were different but in which direction and by how much. Although the classifier trained with paretic arm data performed the worst, sufficient classification accuracies suggest that future work is warranted to examine active control of a robotic device using LDA-based classification for this population.

# Chapter 4: Shoulder Joint Torques during Dual-Task

Mechanical Coupling of Shoulder Joint Torques of Individuals with Chronic Stroke Mirrors Controls, with Additional Non-Load-Dependent Negative Effects in Dual-Task

Authors: Joseph V. Kopke, Levi J. Hargrove, Michael D. Ellis

## 4.1 Abstract

Background: After stroke, motor control is often negatively affected leaving survivors with less strength, less coordination, and increased tone throughout their affected upper-extremity. Humeral internal and external rotation has been included in the definitions of abnormal synergy but have yet to be studied in-depth.

Objective: Determine ability of the paretic, non-paretic, and control shoulders to generate internal and external rotation torque under different abduction and adduction loads.

Methods: 24 participants, 12 with impairments after stroke and 12 controls completed this study. A robotic device controlled abduction and adduction loading to 0, 25, and 50% of maximum strength in each direction. Once established against the vertical load, each participant generated maximum internal and external rotation torque.

Results: Linear mixed-effects models tested the effect of group (control, non-paretic, and paretic), load (0, 25, 50% adduction or abduction), and their interaction. Group was significant in all task combinations. Paretic arms were less able to generate dual-task normalized torque across loads. There was a significant effect of load in three of four load/task combinations. Load-level and group interactions were not significant. This indicates that abduction and adduction loading affected each

group in a similar manner. Open-Sim modeling was used to confirm a biomechanical basis for the commonly observed behavior.

Conclusion: Biomechanical constraints explain limitations in external and internal rotation strength during adduction and abduction dual-tasks respectively. Additional non-load-dependent effects cause a negative offset in dual-task strength in individuals with stroke. These results do not support the existence of load-dependent "abnormal synergy" during these tasks (abduction or adduction with simultaneous maximal internal or external rotation) after stroke, but rather support the presence of a more global effect such as hypertonia.

## 4.2 Background

Approximately 610,000 new strokes occur each year in the US and 16.9 million worldwide [41]. Currently 6.6 million Americans are living post stroke and approximately 30-60% of whom are expected to have chronic upper extremity motor impairments [42,43], Impairments after stroke include weakness, loss of coordination, hypertonicity, and spasticity. Weakness and loss of coordination may affect a majority of activities of daily living involving the upper-extremity requiring control of proper arm position, stiffness, damping, and inertia [80] to enable the hand to accomplish a task including eating, dressing, preparing food, carrying objects, opening doors, etc.

One factor that contributes to the loss of coordination after stroke is an unintentional co-contraction of muscles throughout a limb and is described as abnormal synergy or the loss of independent joint control [1,11,75]. Shoulder abduction is reported as being accompanied by shoulder external rotation, elbow flexion, supination, and wrist and finger flexion while adduction is often accompanied by shoulder internal rotation, elbow extension, and wrist and finger flexion [47].

Using an isometric task in single directions, Dewald et al. compared control, non-paretic, and paretic internal and external rotation torques generated during abduction and found inconsistencies compared with the expectations of the abnormal synergy hypothesis [12]. Specifically, the paretic and control groups had similar secondary torque generation patterns in internal and external rotation which was different from the non-paretic arm group. The group has henceforth largely ignored this degree of freedom in preference of investigation of the more robust effects of abductor drive on distal joints including elbow, wrist, and fingers [16].

We have also moved away from analyzing secondary torques (torques generated in directions that participants are not instructed to control or have feedback on) during single direction isometric tasks because of the difficulty in determining if those torques are pathologic (mandatory), normal physiologic, or just how these individuals chose (consciously or unconsciously) to perform the task [75,81]. We have subsequently moved towards multi-degree of freedom (DOF) tasks which tests ability in two or more directions simultaneously [13,40]. Although adding a possible confounding cognitive load, the tasks are simple enough that we believe allow us to better test true limitations, whether neural or mechanical, after stroke. This dual-task paradigm has not been completed for within shoulder movements such as internal and external rotation during abduction. This is an important step for understanding the underlying impairment and how to target it in rehabilitation.

Although normative strength data exists for an unimpaired population, there is minimal work published which attempts to quantify torque generation capacity at the shoulder (glenohumeral joint) during multi-DOF tasks. Baillargeon et al. recently published a study examining feasible torque space of the shoulder in young healthy adults [82]. They noted that external

rotation during adduction and internal rotation during abduction were the weakest directions of the shoulder. Although these data are from unimpaired individuals, these torque combinations are considered to be the "out of synergy" in individuals with stroke. Beer et. al confirmed that hemiparetic external rotation weakness was profound (33%) however this weakness was unrelated to reaching performance while supported and against gravity [83]. Humeral rotation impairments after stroke have been assumed to be resultant of abnormal neural drive limiting "out of synergy" strength but it remains to be demonstrated.

This study examines dual-task internal and external rotation torque generation ability (strength) during abduction and adduction using a two-DOF task utilizing the capabilities of a robot to precisely control the required torques in one direction (abduction/adduction) while testing maximal isometric strength in another (internal/external rotation). This paradigm is similar to that first described by Beer et. al. investigating "task dependent weakness" albeit measuring elbow flexion/extension during abduction/adduction [77]. In line with the described clinical presentation and laboratory-based findings of multi-joint synergistic movement and posturing following a stroke, we hypothesized that the paretic arm would reflect abnormal synergy within the DOFs of the glenohumeral joint such that external rotation would be weaker during adduction and stronger during abduction and conversely internal rotation would be stronger during adduction and weaker during abduction in comparison to individuals without stroke.

### 4.3 Methods

Fourteen participants with chronic hemiparetic stroke with moderate to severe upper-extremity motor impairments were recruited and provided consent to participate. A licensed physical therapist determined moderate to severe motor impairment using the upper-extremity

portion of the Fugl-Myer Assessment with a score between 10 and 45 out of 66. Two of these participants were excluded from analysis, one was not able to generate any external rotation torque and another was unable to execute the required dual-task. Twelve age- and gender- matched participants without stroke were also recruited to serve as controls. Thus, 12 participants with hemiparetic stroke with chronic motor impairments (50% female, who were, on average, 60.8 ± 10.3 years old, with a Fugl-Myer Upper-Extremity Assessment score of 26.9 ± 8.4, and were 16.8 ± 8.3 years post-stroke), along with 12 control participants (50% female, mean age 59.1 ± 9.9 years old) completed the study. The non-paretic (NP) then the paretic (P) arms were tested in those with stroke, while only the dominant (right) arm was tested in control participants. All participants provided written consent to participate in the study in accordance with Northwestern University Institute Review Board (IRB #: STU00205835).

### *4.3.1 Setup and Instrumentation*

Once seated in a rigid chair (Biodex, Shirley, NY; Model 830-110) with waist and shoulder straps fastened and secured, each participant's arm was placed in 90° of abduction, 45° of horizontal adduction, and 90° of elbow flexion using a custom setup which put the arm in the transverse plane at shoulder height. The forearm was rigidly attached to the custom setup via a fiberglass cast which covered the hand, wrist, and forearm enabling a 6-DOF load cell (JR3 Inc., Woodland, CA, USA; Model 45E15A) to measure 3-axis force and moment data.

### *4.3.2 Single-DOF Isometric Strength*

Isometric strength was collected via a single-DOF isometric task in six different directions in the following order: shoulder abduction, shoulder adduction, external rotation, internal rotation, and elbow flexion and extension. Five second trials with verbal encouragement and visual

feedback of real-time torque were repeated until three trials were collected in which the maximum torques in the testing direction was within 10% of each other and the last one was not the greatest. Load cell data and the corresponding anthropometrics for each participant were used to calculate maximal joint torques, a precision measurement of strength. The maximal adduction and abduction joint torque was used as input to the subsequent dual-task strength protocol.

### *4.3.3 Dual-Task Strength Setup*

Participants moved from the isometric setup to a customized robotic setup which was comprised of a modified ACT$^{3D}$ HapticMaster with an added 6-DOF load cell (JR3 Inc., Woodland, CA, USA; Model 51E20A) at the end effector. Each participant sat in a similar chair as described above. Participants were rigidly connected to the load cell using a custom device that secured the medial and lateral epicondyles between foam centered over the load cell and attached the casted forearm to a rigid bar extending from the load cell as depicted in Fig. 1. The elbow was centered over the load cell to minimize sensitivity to measurement error. The robot and the participants were adjusted so their arm position was the same as in the isometric single-DOF strength testing (90° abduction, 45° horizontal adduction, and 90° elbow flexion).

Figure 9. Dual-task setup. Custom ACT$^{3D}$ with load cell (in blue under elbow) with casted arm attached via custom device. Movement of the robot was limited to the vertical direction. This participant's arm is resting on lower horizontal surface.

### *4.3.4 Dual-Task Strength Testing*

Using the maximal abduction and adduction joint torque data from the isometric single-DOF strength testing, vertical loads (accounting for limb weight) were calculated and programmed into the device. These loads would require each participant to use 0, 25, or 50% of their maximal abduction or adduction strength to move the robot vertically depending on the condition being tested (5 loading conditions). An upper- and lower- vertical limit was created as a ceiling, 5 cm above and floor, 5 cm below 90° of abduction (joint position) to control how far the shoulder could abduct or adduct. Forces applied by the robot during adduction trials forced the at-rest limb to the ceiling while abduction loads would force it to the floor. During each trial the participant was required to adduct or abduct the specified load off of the limit and maintain it there (quasi-static/dynamic). Each trial consisted of 5 seconds of single task abduction or adduction off of the limit (5 levels: 0, ± 25, ± 50%) followed by 5 seconds of maximal isometric internal or external rotation. Internal and external rotation torques that were generated while the limb made incidental contact with the floor or ceiling were not included in the analysis. A digital screen provided feedback of real-time calculated internal and external rotation joint torque. A visual and audible cue was given for both the start to the lift condition (first 5 seconds) and the lift plus rotation condition (last 5 seconds). Our lab has found that quasi-static/dynamic control of shoulder abduction and adduction position while under load alleviates the cognitive burden of the dual-task as it is more functionally intuitive than a fully isometric dual-task. Conditions were randomized between the abduction/adduction loads and between internal and external rotation efforts resulting in 10 conditions (5 levels for external rotation and the 5 levels for internal rotation). Trials were repeated within each condition until 3 trials were acquired in which the maximal internal or external rotation torque was within 10% of each other and the last one was not the greatest. Fig 2.

shows representative trials for each combination of tasks (abduction or adduction paired with external or internal rotation) of a participant in each group.

### *4.3.5 Data Processing*

Load cell data was transformed into joint torques using anthropometric measurements and a series of coordinate transformations for both the single- and the dual-task. All data were smoothed/averaged over 200ms windows. The highest internal and external rotation torque was identified within each trial. As mentioned, torques acquired while contact was made with the ceiling or the floor limit were ignored. The largest torque for each condition and each participant was used for the analysis below. This resulted in one external rotation torque and one internal rotation torque for each of the 5 load-levels (-50, -25, 0, 25, 50%) representing the humeral rotation strength as a function abduction/adduction load.

### *4.3.6 Data Analysis*

Four linear mixed-effects models were generated from normalized dual-task strength data to test the effects of group, load-level, and their interaction on internal and external rotation strength (equation 1). Abduction and adduction data were separated as were external and internal rotation data. The 0% data was used in both the adduction and the abduction analyses resulting in the use of 3 torques for each person in each group. Gender was initially included as a main effect but removed due to lack of significance and was not our primary comparison of interest. The models were formulated as follows with group and load as main factors and participant as a random factor:

$$Eq\ 1: Rotation\ torque \sim group\ +\ load + group * load\ +\ (1|participant)$$

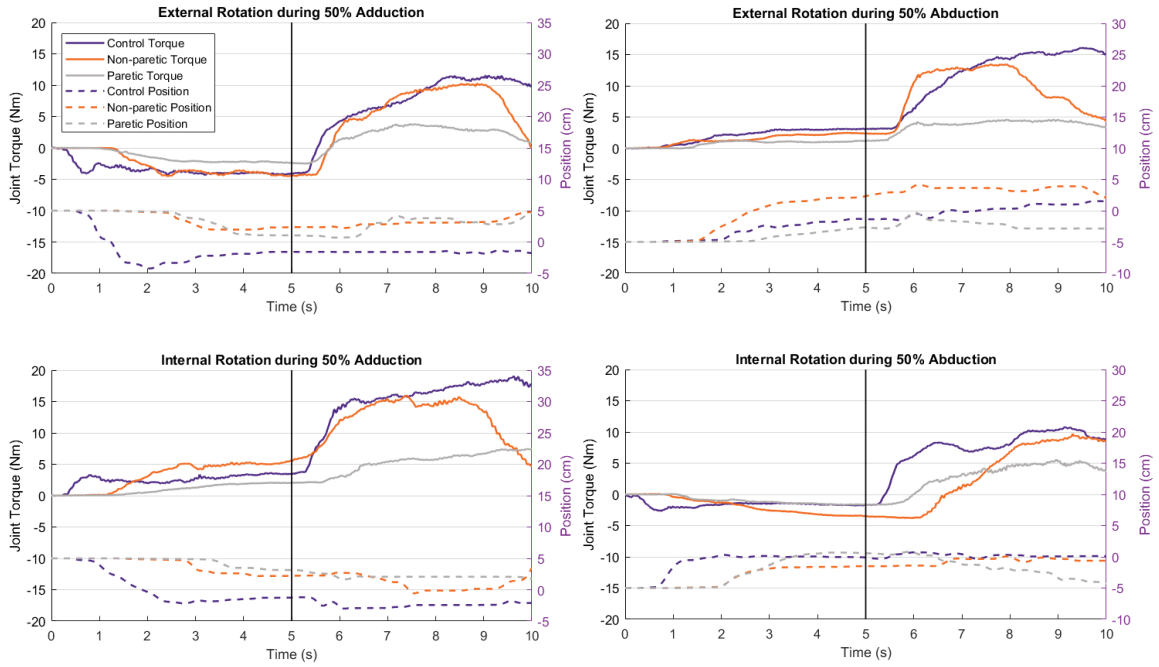


Figure 10. Representative trials for each lifting/humeral rotation direction combination for each group. Solid lines are the isometric humeral rotation joint torques (Nm; External Rotation(+) in the top panels, Internal Rotation(+) in the bottom panels) indicated by the left y-axis. Dashed lines are the vertical position of the robot (cm; 0 indicating midpoint between ceiling (+) and floor (-) limits) during the task indicated by the right y-axis. The starting position of the vertical position on the left two plots was 5cm illustrating the participant beginning in contact with the ceiling limit. Similarly, the starting position of the vertical position on the right two plots was -5cm illustrating the participant beginning in contact with the floor limit. The vertical black line indicates the transition cues (visual and verbal) from the single-task to the dual-task.

## 4.4 Results

Isometric strength values are summarized in Table I for all groups and directions presented as group mean (standard error) with N = 6 for each group and gender. Raw strength values were averaged by gender since we did not collect or control for muscle mass or cross-sectional area and a known relationship exists between gender and muscle mass and muscle mass and strength resulting in gender differences in strength of 40 or 50% [84,85]. Combined results for women and men is also provided for comparison with other published data that may not have been split by gender. Paired (P-NP) t-tests were run for internal and external rotation strength for both men and women and all four tests were significant at $\alpha$=0.05 indicating that the paretic arms are significantly

weaker than the non-paretic arms in these two directions (Women IR: p=0.028, Women ER: p=0.001, Men IR: p=0.007, Men ER: p= 0.005). A family-wise correction factor for multiple t-tests was not used as it was deemed overly conservative and weakness is an established impairment following stroke. Relative strength ratios between each group are provided to give a general indication of how the strengths compared between groups. Strength ratios presented in Table I are ratios of the group averages since participants were not matched at the individual level. The strength of the paretic arms generally ranges between 25 and 50% compared to the non-paretic arms and controls.

Table IX Single-DOF Isometric Strength (torque, Nm)

| Women | AB | AD | ER | IR | EF | EE |
|---|---|---|---|---|---|---|
| C | 39.6 (1.3) | 38.9 (1.5) | 19.4 (1.7) | 16.6 (1.1) | 38.8 (2.1) | 24.4 (1.3) |
| NP | 25.8 (3.6) | 28.7 (3.5) | 16.7 (1.7) | 14.7 (2.3) | 32.2 (1.2) | 22.2 (1.9) |
| P | 16.3 (2.0) | 19.5 (2.6) | 4.6 (1.0) | 7.8 (1.1) | 15.8 (1.1) | 10.6 (2.5) |
| NP/C | 0.65 | 0.74 | 0.86 | 0.88 | 0.83 | 0.91 |
| P/NP | 0.63 | 0.68 | 0.28 | 0.53 | 0.49 | 0.48 |
| P/C | 0.41 | 0.50 | 0.24 | 0.47 | 0.41 | 0.44 |

| Men | AB | AD | ER | IR | EF | EE |
|---|---|---|---|---|---|---|
| C | 66.4 (8.6) | 66.8 (6.9) | 38.2 (4.9) | 33.6 (3.2) | 70.4 (9.4) | 41.3 (4.5) |
| NP | 57.7 (4.9) | 59.1 (6.9) | 35.8 (3.3) | 32.0 (3.4) | 67.2 (8.4) | 47.1 (6.7) |
| P | 28.1 (2.9) | 30.6 (5.0) | 10.3 (2.4) | 12.3 (2.2) | 32.2 (5.5) | 19.7 (3.9) |
| NP/C | 0.87 | 0.89 | 0.94 | 0.95 | 0.96 | 1.14 |
| P/NP | 0.49 | 0.52 | 0.29 | 0.38 | 0.48 | 0.42 |
| P/C | 0.42 | 0.46 | 0.27 | 0.37 | 0.46 | 0.48 |

| Combined | AB | AD | ER | IR | EF | EE |
|---|---|---|---|---|---|---|
| C | 53.0 (5.8) | 52.8 (5.4) | 28.8 (3.8) | 25.1 (3.0) | 54.6 (6.6) | 32.9 (3.4) |
| NP | 41.8 (5.6) | 43.9 (5.9) | 26.3 (3.4) | 23.4 (3.3) | 49.7 (6.6) | 34.7 (5.0) |
| P | 22.2 (2.1) | 25.0 (3.0) | 7.5 (1.5) | 10.1 (1.0) | 24.0 (2.2) | 15.1 (1.7) |
| NP/C | 0.79 | 0.83 | 0.91 | 0.93 | 0.91 | 1.05 |
| P/NP | 0.53 | 0.57 | 0.28 | 0.43 | 0.48 | 0.44 |
| P/C | 0.42 | 0.47 | 0.26 | 0.40 | 0.44 | 0.46 |

AB=Abduction, AD=Adduction, ER=External Rotation, IR=Internal Rotation, EF=Elbow flexion, EE=Elbow Extension, C=Control, NP=Non-paretic, P=Paretic

Dual-task results are presented in Fig 3. as bar plots of the internal and external rotation strength at each load-level for each group (Fig 3.a-d presents actual joint torque, Fig 3.e,f presents joint torques normalized to each individual's maximal voluntary torque in the corresponding direction).

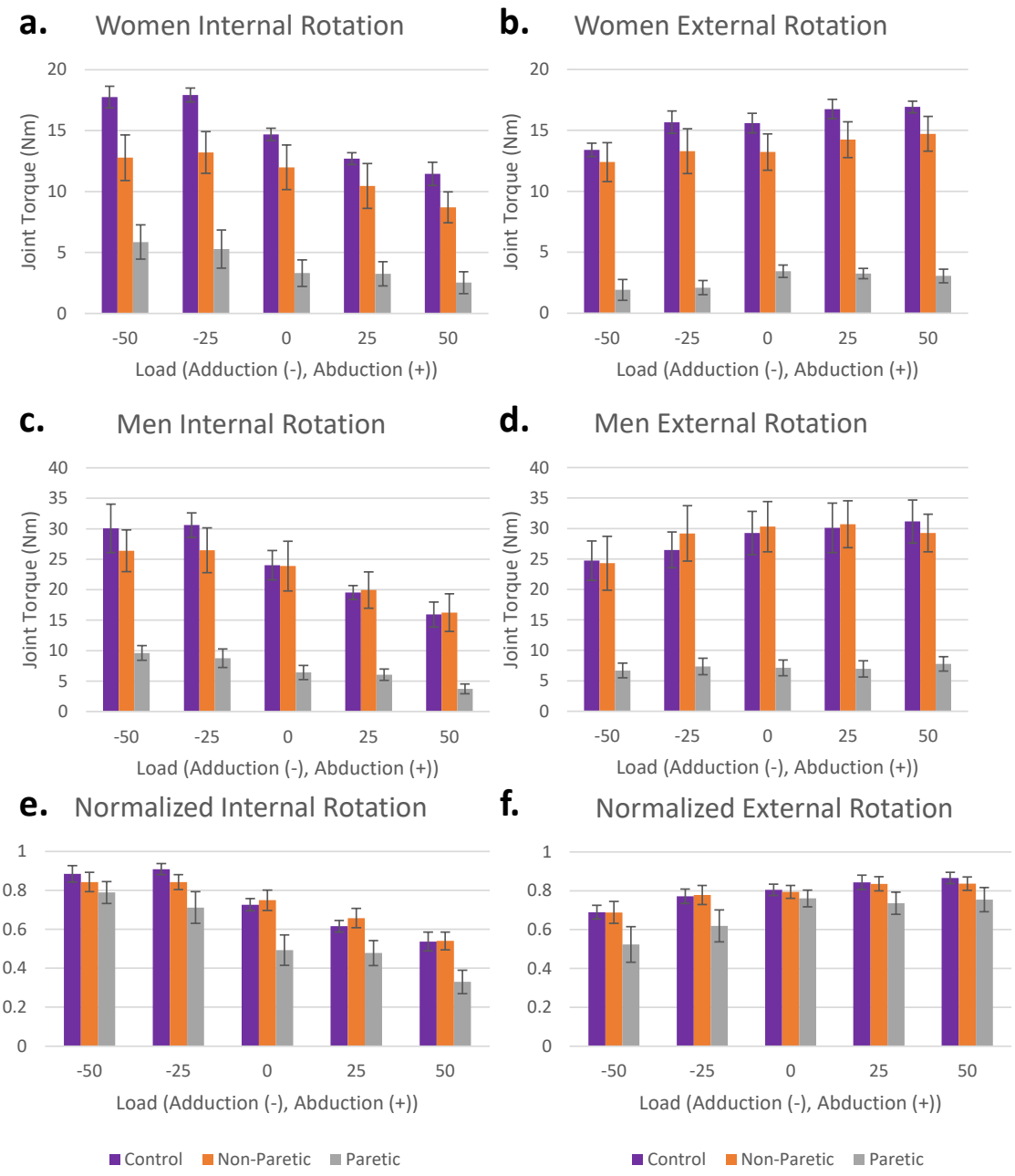


Figure 11. Dual-task performance. Bar plots with standard error of the isometric internal (a, c) and external (b, d) rotation torque generated under the different loading conditions for women (n=6/group) and men (n=6/group). Negative x-axis is % max adduction while positive x-axis is % max abduction and 0 indicating the unloaded or arm-weight fully supported condition. The bottom plots (e, f) depict the average internal and external strengths of the 12 participants in each group normalized to their maximal strengths.

Table II shows the results of the four linear mixed-effects models (LMM) on the normalized strength data. External rotation (ER) and internal rotation (IR) during adduction are listed first while external rotation and internal rotation during abduction are listed last. Each linear model was run within one task combination (e.g. external rotation during adduction). The 0% load condition was used in both the adduction as well as the abduction models resulting in four models with three load-levels and three groups

Table X Linear Mixed Models

External Rotation during Adduction

| | DF Num | DF Den | F-Value | P-Value |
|---|---|---|---|---|
| Group | 2 | 46.91 | 5.96 | 0.0049 |
| Load-Level | 2 | 78.87 | 8.98 | 0.0003 |
| Group*Load | 4 | 78.87 | 0.85 | 0.4988 |

Internal Rotation during Adduction

| | DF Num | DF Den | F-Value | P-Value |
|---|---|---|---|---|
| Group | 2 | 51.5 | 8.96 | 0.00046 |
| Load-Level | 2 | 80.67 | 12.45 | 0.00002 |
| Group*Load | 4 | 80.67 | 1.2 | 0.32 |

External Rotation during Abduction

| | DF Num | DF Den | F-Value | P-Value |
|---|---|---|---|---|
| Group | 2 | 45.65 | 4.17 | 0.022 |
| Load-Level | 2 | 78.07 | 0.69 | 0.50 |
| Group*Load | 4 | 78.07 | 0.41 | 0.80 |

Internal Rotation during Abduction

| | DF Num | DF Den | F-Value | P-Value |
|---|---|---|---|---|
| Group | 2 | 49.01 | 18.32 | 0.00000 |
| Load-Level | 2 | 79.85 | 13.12 | 0.00001 |
| Group*Load | 4 | 79.85 | 0.35 | 0.84 |

As seen in Table II, group was a significant main effect for each combination of adduction or abduction with external rotation or internal rotation. In each of the task combinations, paretic arms generated less torque (relative to their maximum) compared to the control and non-paretic arms averaged across all load-levels (ER during Adduction: $p=0.0049$, IR during Adduction: $p=0.00046$, ER during Abduction: $p=0.022$, IR during Abduction: $p<0.00000$).

Load-level was significant for all task combinations except for external rotation during abduction (ER during Adduction: $p=0.0003$, IR during Adduction: $p=0.00002$, ER during Abduction: $p=0.503$, IR during Abduction: $p=0.00001$). This indicates that abduction and adduction loading has an effect on internal and external rotation torque generation in each group for all combinations except the abduction external rotation task.

**4.5 Discussion**

This study examined single-DOF, and for the first time, dual-task internal and external rotation strength after stroke. Importantly, it attempted to better understand the contributing factors to the conventional inclusion of internal/external rotation in stroke-related stereotypical or synergy patterns of movement.

We hypothesized that the paretic arm would be less able to generate external rotation torque during adduction and less able to generate internal rotation torque during abduction secondary to the elicitation of the abnormal synergy. As shown in Fig. 3a-d and even more so in Fig. 3e-f, a common trend emerges across groups: all groups appear to behave as the paretic arm was expected to, being less able to generate “out of synergy” joint torques. The group and load-level interaction was not significant in any task combination indicating that the differences in external and internal rotation strength across load-levels was not different between groups (their slopes are the same).

These results agree with recent results from Baillargeon et al, 2019 in which the weakest torque directions in a young healthy population were combinations of abduction and internal rotation as well as adduction and external rotation suggesting an alternative explanation for multi-DOF coupling in the glenohumeral joint [82].

The unexpected finding that the ability to generate "out of synergy" torques was not different between individuals with stroke and control supports the alternative explanation that there is a primary mechanical constraint limiting behavior. We posit that biomechanical constraints due to muscle attachments and their corresponding actions naturally limit control of DOFs within the glenohumeral joint. Specifically, the primary adductors (latissimus dorsi, pectoralis major, and teres major) have moment arms with a strong component acting in internal rotation as well as in adduction [74,86,87]. Conversely, aside from the subscapularis (a more pure internal rotator), those same muscles are the primary internal rotators with a significant component of the muscle pull acting in adduction. Thus, when a task requires adduction, the pectoralis major and latissimus dorsi are activated and intrinsically generate internal rotation torque thus limiting the amount of net external rotation that can be generated. Conversely, when a task requires internal rotation, adduction torque will automatically be generated opposing any desired abduction torque generation. Thus, in a dual-task where the abduction load must be controlled, the amount of internal rotation that can be generated will be limited by the amount of abduction that can offset or negate the biomechanically coupled adduction torque that occurs during internal rotation.

We found that paretic arms are weaker (decreased single-DOF strength). This is consistent with the conventional stroke sequela of hemiparesis or weakness. Our results appear generalizable since the magnitude of weakness observed in the present study is similar to prior work.

Specifically, our data reflect previously reported baseline strength values for abduction (25Nm), adduction (33Nm), external rotation (8Nm), and internal rotation (12Nm) in a similar but larger cohort (N=32) as part of a recent chronic stroke rehabilitation trial [20]. We accounted for the profound strength impairment by normalizing dual-task strength by the single-DOF strength prior to evaluating the effect of load-level and group.

With this lack of strength accounted for, we found a negative offset in performance of the paretic arm resulting in an effect of group in all four task conditions. Because there was no difference in slope (no interaction effect of group by load-level) we believe the load-dependent abnormal synergy could not be responsible, but instead perhaps another stroke-related sequela such as hypertonia (generalized increase in background muscle activity) that presents during tasks or movement [88-91].

The scaled down performance of the affected arm could also reflect changes in cognitive motor planning and subsequent execution of the dual-task. This is less likely since performance was not different between the non-paretic and control arms implying that participants with stroke were cognitively capable of completing the task in similar fashion to controls.

We conducted musculoskeletal modeling via OpenSim using a previously validated model of the shoulder [92,93] to expound how external rotation during adduction and internal rotation during abduction can be limited in both individuals with and without stroke. We matched the model posture to our experimental setup which equated to 40° “elevation angle”, 90° “shoulder elevation”, 50° “shoulder rotation”, and 90° of “elbow flexion”. Muscle parameters for muscles crossing the shoulder were extracted and provided to customized optimization software written in MATLAB (Release 2017a, The MathWorks, Inc., Natick, MA, USA).

Prior work identified that this model under-predicts the moment arm of the teres minor compared to values found via cadaveric testing so we extracted values for the teres minor as well as for the other rotator cuff muscles from anatomical moment arm studies to better approximate the rotator cuff musculature [74,87]. Additionally, the model is based on the 50% male size and young male muscle volume. Muscle volume (peak force) was adjusted by multiplying each muscle by its ratio between an older adult male or female and the young male adult data that was used to generate the model [94,95].

Hypothetical joint torque maximums were acquired by using the customized software to optimize muscle activations to maximize the joint torques in each of the directions (abduction, adduction, external rotation, and internal rotation). Next, abduction and adduction loading was simulated by creating inequality constraints

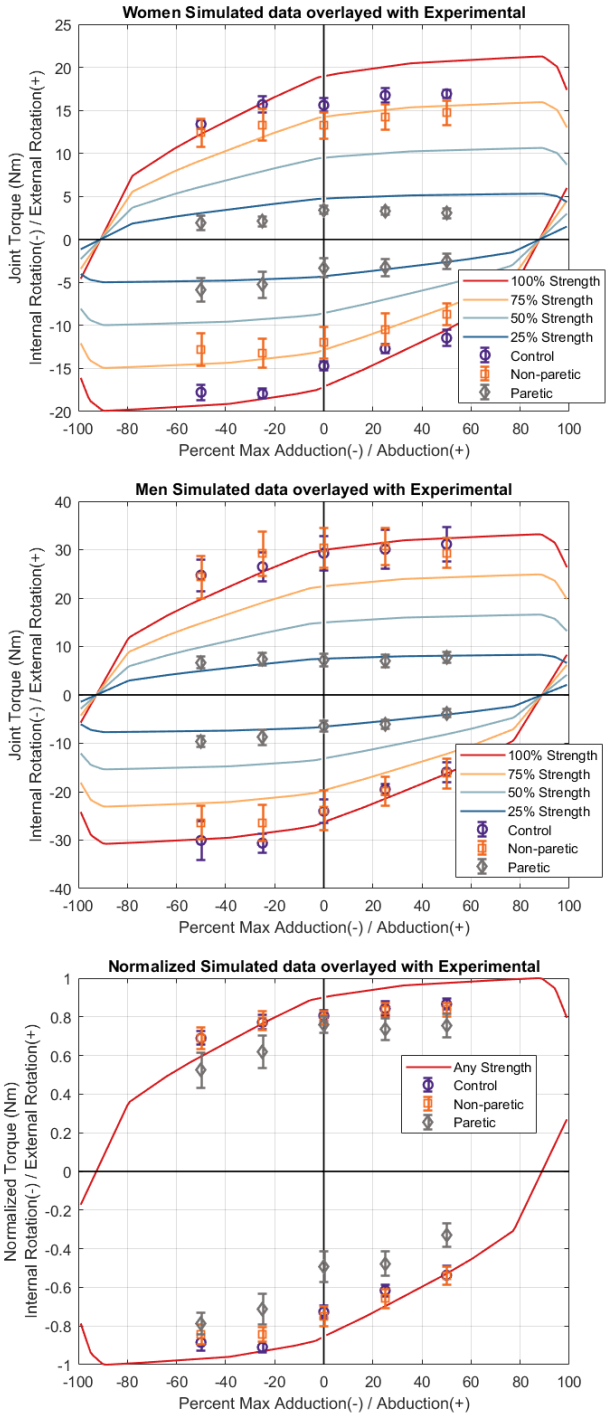


Figure 12. Modeled dual-task strength. Solid lines are simulated maximal joint torques using OpenSim setup with similar posture to the prescribed protocol. Experimental data overlayed with mean (± standard error). Top) Women, Middle) Men, Bottom) All normalized to maximum humeral rotation torque (external or internal). For comparison with Figure 3, note that internal rotation here is represented differently as a negative number.

of abduction and adduction loads ranging between 0% and 100% ±1% of the maximum torque. The optimization was then run to maximize torque in internal and external rotation while simultaneously meeting the abduction or adduction loading constraints. This resulted in simulations of the described dual-task protocol but across all possible load-levels. The red lines in Fig. 4 depict the simulated joint torques across all load-levels -100% (maximal adduction) to 100% (maximal abduction).

To better simulate the weakness experienced after stroke and to cause the model to generate torques closer to those expressed by our participants with stroke, all muscle forces were simulated as having strength that was 25%, 50%, or 75% of the maximal strength (Fig 4). Each of these limits was applied across all 18 muscles included in the model. The optimization was run again to maximize internal and external rotation torque under the prescribed strength and load constraints. As seen in the blue and gold lines of Fig. 4, study data from all of our participants are reflected in the results of the biomechanical model. This observation supports our conclusion that there is a biomechanical constraint due to muscle attachments and lines of action that limits internal rotation and external rotation during abduction and adduction. Of note, there was no detected difference between non-paretic and control arm performance in these tasks indicating that all participants had the cognitive resources to understand and perform the task.

What is left to explain then is why the paretic arms had a global limitation in normalized dual-task strength (they were less able to generate dual-task internal or external rotation torque compared to their maximum under all loading conditions). This is apparent in the effect of group resulting in negative offset in performance of the paretic arms as compared to the others. Further work is needed, but we hypothesize that the reliance on of upregulation of different neural tracts

secondary to the damage due to stroke, specifically the extrapyramidal corticobulbospinal tracts such as the reticulospinal tract, contributes to this phenomenon. This tract has been shown to be upregulated in stroke on the impaired side[16,96]. This tract is also implicated in control of postural adjustments and muscular tone[97]. We postulate that the increased activity of the reticulospinal tract results in increased global background activity or hypertonia during effortful tasks. The implications of this for the dual-task in this study is that there will be increased activity of the **antagonists** resulting in added constraints limiting the amount of internal or external rotation torque that can be generated. The increased background activity of the **agonists** is overshadowed by or incorporated with their intentional activation to complete the task.

The fact that we do not see a load-dependence specific to stroke as seen in work with more distal joints is that the proximal effort required to maximize internal or external rotation exists under all load conditions and possibly activates or recruits the reticulospinal tract to its maximal extent even without any abduction or adduction loading.

Limitations in this model include that it assumes intact/unimpaired motor control, cognition, vision/perception, and other common stroke sequelae. While these are mostly accounted for through study inclusion/exclusion criteria, they may partly explain differences between model output and study participant performance. The model was also built using bone and muscle size/length equivalent to the 50$^{th}$ percentile male and while adjustments to muscle volume were made, adjustments to bone size and length were not. This may explain why the fit to the female data is not as close as it is for the male data.

Finally, the overall study design had some relevant limitations. Despite significant main effects, the small sample size and increased variance within individuals with stroke may have

underpowered the statistical evaluation of an interaction effect of group x load. However, the striking similarity with the musculoskeletal model minimizes this possibility. Regarding methodology, we did not test at higher load-levels (>50% abduction/adduction strength) during the dual task paradigm that is known to maximize upper extremity synergy expression. While testing at higher loads becomes difficult secondary to motor control, fatigue, and discomfort, it may expose a minimal contribution of abnormal synergy to performance of the affected arm that was not observed in the present study.

### 4.6 Conclusion

This study examined humeral rotation strength under different abduction and adduction loads in an attempt to evaluate the underlying factors impacting the control of the glenohumeral joint. With generalized stroke-related weakness accounted for (task performance normalized to maximal strength values), we conclude that a mechanical constraint (muscle action) is the primary contributor to the ability to control multiple DOFs within the glenohumeral joint. This effect was common across all groups, paretic, non-paretic, and controls. A load-dependent change (abnormal synergy) was not detected for the participants with stroke that was different from the other groups. However, a negative effect of stroke limiting dual-task performance was detected across all loads and may be attributed to hypertonicity, another sequela of stroke, caused by the upregulation of or greater reliance on brainstem motor pathways.

# Chapter 5: Human-In-The-Loop Myoelectric Pattern Recognition Control of an Arm-Support Robot

Human-In-The-Loop Myoelectric Pattern Recognition Control of an Arm-Support Robot to Improve Reaching in Stroke Survivors

Authors: Joseph V. Kopke, Michael D. Ellis, Levi J. Hargrove

## 5.1 Abstract

Vertical arm support improves reaching ability in persons with stroke. Whereas static control mechanisms for arm support are well established, dynamic control based upon an individual's real-time muscle activations has the potential to offer patient-specific applications and advance existing strategies. Muscle activation impairments after stroke include paresis, hypertonia, loss of inter-joint coordination, hyperactive stretch reflexes, and altered timing resulting in heterogeneous signals challenging implementation of dynamic control. However, in individuals with stroke, supporting the arm compensates for gravity and diminishes neural drive to proximal muscles, partially ameliorating these impairments and improving reaching ability. A machine learning (linear discriminant analysis)-based myoelectric pattern recognition system was used to control incremental changes (in 25ms windows) in either vertical position or vertical support-force during a reach and retrieve task, with the goal of improving reaching function based upon movement intent as determined by real-time muscle activation. Both vertical support paradigms were successfully implemented and resulted in greater forward reaching performance as demonstrated by increased elbow extension and horizontal shoulder adduction compared to reaching under

normal gravitational loading. Muscle activation levels with real-time support were lower than for the no-support condition and similar to those observed during static support paradigms. The computational power of machine learning prevailed despite the abnormal muscle activations associated with stroke and should be considered in the development of future rehabilitation approaches.

## 5.2 Introduction

Worldwide, an estimated 80 million people have survived a stroke (7 million in the US), 17 million strokes occur each year (800,000 in US), and 36-44% of survivors are left with chronic disability.[41,98,99] Most commonly, this entails upper extremity impairments including weakness, hypertonia, loss of joint coordination, spasticity, and abnormal muscle activation timing,[44,100-102] each of which affect, and often limit, daily function. These impairments contribute to differing electromyographic (EMG) signal patterns compared to those of non-injured persons such as alterations in signal amplitude,[103,104] increased background activation,[105] and stereotypical abnormal activation patterns.[12,106]

Some of these impairments present in proportion to the amount of neural drive, or simply, muscular effort.[13,70,107] Movement of the arm at the shoulder requires greater effort than movement of the distal upper-extremity joints, as the shoulder must move greater mass at a greater distance against the force of gravity (i.e., the shoulder does more mechanical work). Anti-gravity (shoulder abduction) assistance at the shoulder alleviates the severity of stroke-related impairments by reducing hypertonia, abnormal synergy, and abnormal excitation, thus enabling more joint excursion, better coordination, and greater reaching.[13,76] Additionally, pattern recognition of hand grasp intent seems to improve when the shoulder is supported.[33] Research groups have used a

broad range of devices, from simple surfaces or limb-weight support systems to complex robotic systems to support the arm in different ways, both to achieve and explore this phenomenon.[40,108]

Exoskeletal devices to address the above impairments have been designed for all joints of the upper extremity, either to assist in therapeutic intervention or in accomplishing activities of daily living.[109-112] However, support at the shoulder is crucial in this population due to the negative functional effects of exerting effort at the shoulder (e.g., reduced reach distance; increased unintentional flexion throughout the elbow, wrist, and hand; reduced accuracy of classifying hand movement intention), which these devices must then overcome. Few devices have used a human-in-the-loop approach to control the amount of support applied at the shoulder. Makowski et al. used a neural network to predict and apply *horizontal* planar forces during reaching on a modified HapticMaster with some success (i.e., slightly improved reach but impaired control and movement characteristics).[113] They also reported an equal improvement in reach distance but no detriment to movement characteristics when a static *vertical* force-offset, equal to half of the participants' limb weight, was applied. These results, in addition to our finding that providing a horizontal surface or off-loading the weight of the limb reduces impairments and maximizes reach distance, led us to explore real-time control of *vertical* support.

Here we demonstrate real-time myoelectric pattern recognition control of a robotic arm (modified HapticMaster) to provide two types of vertical support in a small sample (n=5) of individuals with chronic moderate stroke. The goal of this study was to test the feasibility of this approach and enable preliminary analysis of its effectiveness in improving reaching ability. We hypothesized that real-time control of vertical support, either through position or force, would enable greater elbow and horizontal shoulder adduction excursion compared to the no-support condition

reflecting the conventional mode of static vertical limb-weight support. The dynamic vertical support mechanism developed here has the potential to advance existing rehabilitation strategies such as progressive abduction loading therapy[20] by utilizing a physiological signal to determine optimal vertical support/loading.

### 5.3 Results

Participants completed 10 reaching trials under five different vertical support conditions: no support (requiring the participant to lift the full weight of their limb), tabletop support, full limb-weight support, and two conditions in which real-time pattern recognition was used to control (i) vertical velocity or (ii) the time rate of change in vertical force, across each time window (25ms). The tabletop condition was simulated by generating a vertical lower limit within the robot's workspace located in the transverse plane at 90° of humeral elevation, and the limb-weight support was provided by directing the robot to apply a vertical force equivalent to the weight of the limb. These two support conditions did not change throughout the trial (static support) while the two controller-based conditions incrementally changed either the vertical position or the supporting force every 25ms (dynamic support).

Each trial consisted of four arm movement components: lift, reach, return, and lower. Lift required the arm to be moved into a target window between 80° and 100° of shoulder abduction. Reach consisted of the participant reaching as far out in front as possible. Reach distance was decomposed into both horizontal shoulder adduction angle and elbow extension angle to aid in understanding where improvements or limitations in reach distance originated. Results for each participant, as well as average maximal joint angles during the five support conditions are displayed in figure 1. Data were only used if the participant's arm was within the vertical target window.

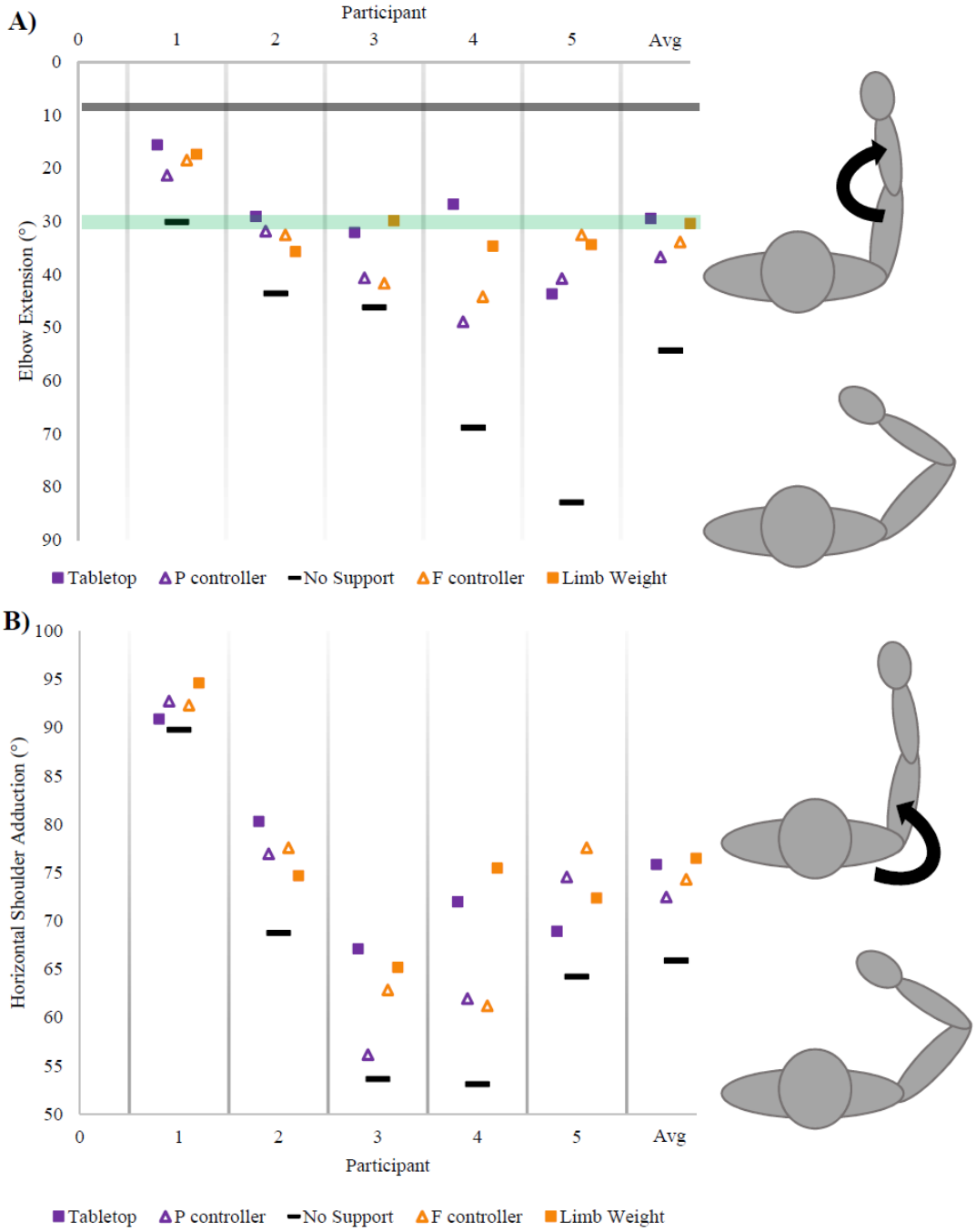


**Figure 13. Maximum Reach Characteristics.** A) Maximum elbow extension and B) maximum horizontal shoulder adduction attained during forward reach under five conditions: Tabletop support (arm resting on rigid frictionless horizontal surface provided by robot), ΔP controller (position based real-time control), No support (participant lifting the full weight of limb), ΔF controller (force based real-time control), Full Limb-Weight Support (by the robot). Averages of each condition are provided on right side of each plot. Squares represent static (unchanging) support conditions, while triangles represent dynamic (changing) support conditions based on the output of the controller. Purple represents position based support and orange represents force based support. The green horizontal bar indicates functional elbow extension, and black bar indicates near-full elbow extension.

EMG signal amplitude was recorded to assess relative effort and to identify abnormal control

patterns across different tasks. EMG data were rectified and a moving average applied using 200ms windows, followed by normalization of each channel to the maximal value recorded throughout each study session. Normalized EMG from all trials of each condition and participant were averaged. Figure 2 displays a time series heatmap depicting relative EMG activity for four channels involved in lifting the arm against gravity (anterior, intermediate, and posterior deltoid and upper-trapezius) across *all* trials of each condition. These data indicate the amount of proximal muscle activation required during reaching for each condition.

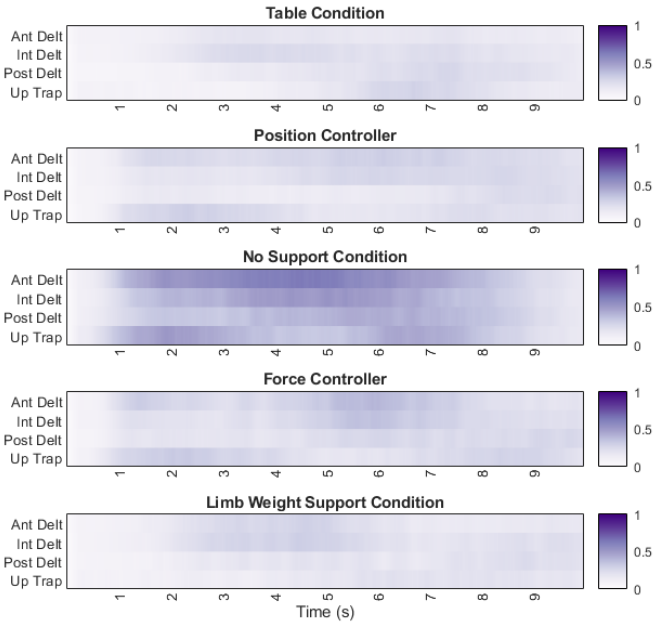


**Figure 14 Average normalized EMG during each condition.** Averaged smoothed (200ms) normalized EMG is shown for all participants across all trials. Ant – Anterior, Int – Intermediate, Post – Posterior, Up – Upper, Trap – Trapezius. Note that the no support condition is positioned in the middle to allow easier comparison between the support

As well as providing intended support, the controller should avoid directing unintended changes in support during other unrelated movements such as movement at the elbow, hand, or bringing the arm across the chest (horizontal adduction). As the increased tone and common muscle activity patterns that emerge after stroke might prevent successful discrimination between shoulder abduction or adduction (vertical movements) and other movements, we also explored the feasibility of using pattern recognition to control a wearable exoskeleton while the upper extremity is moving in other directions and in other ways.

Additional data acquired from a subset of study participants (n=3) were examined to determine the ability of the classifier to identify untrained and unrelated (i.e., not vertical abduction or adduction) activities as "no-movement". Four combinations of tasks were selected: horizontal shoulder adduction and abduction, internal and external (isometric) rotation, elbow flexion and extension, and hand open and close. Each combination of tasks was accomplished in an alternating fashion under two different conditions, limb-weight support and tabletop support, simulating the ideal support that could be provided via the real-time controllers. As above, limb-weight support entailed the robot providing a supportive force equivalent to 100% of the limb weight while the tabletop support was a rigid and frictionless horizontal plane, similar to a smooth table.

Forty-five seconds of each combination of tasks was recorded during three, 15 second trials. EMG data were subsequently classified offline using the classifier established for the real-time control described above. Classification of these motions should result in one of three possible classes (abduction, adduction, or neither/no-movement). Since this control scheme is concerned with only controlling vertical support, ideally all data from these other movements would classify as no-movement. Successful discrimination would indicate that characteristics of these tasks are more similar to the no-movement class than to the abduction and adduction movement classes and would eliminate the need to include training data from these motions into a future classifier. Tables I (device providing limb-weight support) and II (device providing tabletop support) show the average percentage of data windows for each unrelated movement that were classified as one of these three options.

To evaluate the *potential* (best case scenario) of offline classification using this experimental setup and data, we averaged the *best* performance of each participant and task combination, resulting in

classification accuracies of 91, 90, 100, and 94%, respectively, for the four tasks during the limb-weight support condition and 84, 89, 96, and 85%, respectively, for the four tasks during the tabletop support condition.

Table XI Limb-Weight Support

| Unrelated Movement Classification | No Movement | Abduction | Adduction |
|---|---|---|---|
| Horizontal Add/Abd | 78 | 6 | 16 |
| Internal/External Rot | 70 | 15 | 15 |
| Elbow Flex/Extend | 96 | 3 | 1 |
| Hand Open/Close | 84 | 16 | 1 |
| Average – all tasks | 82 | 10 | 8 |

Table XII Rigid Tabletop Support

| Unrelated Movement Classification | No Movement | Abduction | Adduction |
|---|---|---|---|
| Horizontal Add/Abd | 63 | 13 | 23 |
| Internal/External Rot | 74 | 20 | 6 |
| Elbow Flex/Extend | 88 | 7 | 6 |
| Hand Open/Close | 75 | 24 | 0 |
| Average – all tasks | 75 | 16 | 9 |

Add - Adduction, Abd - Abduction, Rot - Rotation.

**5.4 Discussion**

In this study, we assessed the feasibility of using human-in-the-loop myoelectric pattern recognition controllers to control a robot that provided vertical shoulder support after stroke, to enable the user to accomplish a voluntary forward reaching task. The controllers were used to provide vertical support via position or force, both known to improve reaching performance when provided statically.[40] Additionally, we examined relative EMG activity under each condition and, in a subset of participants, the ability of the classifier to discriminate other non-related tasks.

Reaching performance, in terms of both elbow and shoulder horizontal adduction excursion, improved in all participants for both controllers. This indicates that each participant was able to interact with the pattern recognition controllers well enough to accomplish the task and that both types of support improved reaching performance compared to the no-support condition. Assuming

reach performance would be at least as good as the no-support condition, a one-tailed paired t-test showed that both types of control were statistically significantly better than no support, even given the small study cohort (elbow: p=0.028 for position, p = 0.033 for force, shoulder: p=0.0098 for position, p = 0.0059 for force); the larger variability in elbow excursion improvement reduced the test statistic (t-score) of this difference.

Participants 3 and 4 showed a marked reduction in reaching performance (Fig. 1a and 1b) when using the dynamic support offered by the controllers (triangles) compared to static support (squares). We postulate that this difference could be reduced through additional time using and getting accustomed to the control system.[114]

Makowski et al used functional electrical stimulation (FES) to assist humeral elevation after stroke in attempt to reduce post-stroke impairments and improve reach with mixed results.[115] FES has limitations including muscle fatigue due to recruitment of larger more fatigable muscle fibers first as well as reduced ability to determine user-intent once stimulation is on. Makowski et al also attempted to use EMG to control anterior-posterior horizontal reaching forces with robotic assistance.[113] They found reaching was better assisted with non-changing vertical support (equal to half the weight of the limb) alone or vertical support in combination with EMG triggered horizontal support. Our technique enables real-time control of vertical support force up to the entire weight of the limb or even slightly over which should enable even greater reaching ability. Other groups have examined classification of shoulder movements but without application to real-time control of a device.[26,116-118]

When participants used the online controller, EMG activity was reduced to levels similar to those of the static support conditions, indicating that the participants were using less effort than during

the no-support condition, which manifested as improved reaching performance. Furthermore, this indicates that the participants were working with, rather than against the robot during the specified tasks. These results are similar to those of Lenzi et al who used proportional surface EMG control of robotic assistance at the elbow.[119]

Qualitative feedback from participants on how they felt about using real-time control included the following comments: “this is great, I feel like I am hardly working at all,” “the first one [referring to the position-based controller] was a bit jerky, kind of like driving a big truck,” and “I really like this one [the force-based controller] since it is smoother and helps me reach further without having to work so hard.” Modifications to the control scheme, including the possible use of velocity filters or rate-limiters, may reduce the feeling of jerkiness but this would require further development and testing.

Using the classifier to discriminate between abduction and adduction and other unrelated motions in offline tests resulted in high error rates. The precise relationship between online and offline performance for pattern recognition myoelectric controllers is not well understood. In online control tasks, subjects have the opportunity to correct small mistakes, which may not impact completion of the task. We also note that the offline error rates were within the range expected for a usable online controller.[28] Furthermore, the trials with the highest accuracy for each participant and task combination show what may be possible even without real-time adjustments. The addition of training data incorporating these or other unrelated movements to the classifier may improve the ability to discriminate between abduction/adduction and other unrelated movements not requiring a change in vertical support. Of course the hope would be to minimize required training data.

Tabletop support resulted in greater prediction errors for abduction and adduction than during full limb-weight support. This may be because participants could engage other muscles or generate forces up or down without a change in vertical position as happens in the limb-weight support condition. It is possible that, during the tabletop support condition, participants were engaging the abnormal muscle co-activation pattern of shoulder adductor/elbow extensor that are common after stroke as they attempted to move their limb. The limb-weight support condition would reduce the participant's ability to utilize such abnormal patterns because use of abductors or adductors would cause the limb to move outside of the required vertical target window. The offline nature of this analysis limits our ability to assess what would happen in real-time use specifically with the position control as mentioned above. This finding has implications for how control of a future device should be implemented: position control may enable greater range of motion and even better task performance but possibly at the expense of allowing abnormal muscle activation patterns. Preventing reinforcement of the neural pathways underlying such patterns may require either use of force-based support or ensuring that any abnormal patterns result in an unwanted vertical movement that the user must attempt to avoid.

Elbow flexion and extension movements, which were included in the classifier as part of the supported reach and return components in the training data, had the lowest classification errors. However, horizontal shoulder adduction and abduction movements had significant misclassification rates as vertical adduction. These errors may have resulted from only using EMG from the pectoralis major, the primary horizontal adductor, in this study and not including EMG from the latissimus dorsi or teres major, which would be active during vertical adduction tasks but less active in horizontal adduction tasks. Thus addition of EMG data from the latissimus dorsi and

possibly the teres complex may reduce these errors. Accuracy of classification of the internal and external rotation task was confounded by the fact that it was isometric and thus participants could not perceive how their arm would move in response to their effort, and no joint torque feedback was provided. Our prior work has shown that these degrees of freedom can be discriminated to a level that should enable real-time control of a device.[120,121] A different device or at minimum a different method of connecting the participant to the device would be necessary to free and enable testing of this degree-of-freedom. The hand open and close data most prominently showcases the abnormal muscle patterns attributed to stroke, which explains why attempts to open and close the hand were misclassified as shoulder abduction. Since no quantitative limits or criteria were used to determine the amount of effort participants expended during these movements, it is possible that participants were trying really hard to open or close their hand, tasks which are often severely impaired after stroke and not always possible. Although the classifier was able to classify other unrelated and untrained motions as no (vertical) movement most of the time, further work using an online controller with additional EMG sensors and more degrees of freedom would help in clarifying what is possible.

Study limitations include the small number of participants, which limits the generalizability and statistical power of the study, and the absence of a shoulder tracking task, although we believe there are many ways in which the body can be positioned and moved to accommodate and compensate for minor errors in position. Comparison of the efficacies of the two types of control (force and position) is not possible without a larger cohort. Additionally, without running an online analysis in which the user can learn and attempt to adjust to misclassifications, an offline analysis offers limited insight aside from the fact that initial results were promising.

Ultimately we have shown that control of vertical support via myoelectric pattern recognition is feasible and efficacious after stroke despite heterogeneous muscle activation patterns. Both the position and force-based controllers improved elbow and shoulder joint excursion during forward reach compared to the no-support condition, enabling greater reaching distance. Providing support reduces the effort needed to counter gravity throughout the task, reducing muscular activity and the subsequent movement impairments experienced post stroke.

Immediate next steps include a multi-session study to determine the extent to which the use of the controller can be learned to maximize reaching and an online assessment of the interaction between the participant, the classifier, and unrelated movements. Including additional EMG channels and even force sensitive resistors followed by optimization may also be beneficial. Future steps include the design and application of these techniques to a wearable device that supports the shoulder in similar ways.

Future work could incorporate these techniques into a rehabilitation program helping users to identify and avoid the abnormal muscle activation and movement patterns as they recover. Optimization of limb support could be systematically implemented thereby mimicking "progressive abduction loading therapy" proposed by Ellis et al.[19] but utilizing a direct physiological signal as opposed to task performance to progress the intervention. Ultimately, incorporating smart support into daily life and activities of daily living with a wearable device could help expand and explore a new avenue of stroke rehabilitation.

## 5.5 Materials and Methods

Ten participants consented to enroll in this study, which was approved by the Northwestern University IRB (IRB# STU00210805). Inclusion criteria included having had a unilateral stroke more than six months prior to the study, with motor deficits limited to one side, and having moderate motor impairment as determined by the upper-extremity portion of the Fugl-Myer Assessment (10<score<40). Participants also had to be able to follow a set of 4-step sequential instructions. Exclusion criteria included lack of shoulder or elbow volitional control or proprioception, any range of motion limitations that prevented safe participation and interaction with the parameters set for the robot (100° of shoulder abduction/scaption with neutral humeral rotation), any shoulder or spine pain, and any major medical conditions that may preclude safe participation. Four individuals did not qualify due to motor impairments that were too minor (2) or too major (2), and one participant's body type together with a contracture of their pectoralis major caused the load cell to consistently touch their body, so they were removed from the study due to safety concerns. Thus, five participants completed this single session, four-hour, feasibility study and were included in the data analysis.

### *5.5.1 Experimental Setup*

The participant was positioned in the Biodex chair (Biodex Medical Systems, Inc., Shirley, NY), with their affected arm/shoulder abducted 90º and horizontally adducted 45º from the frontal plane. The participant was then strapped into the

**Figure 15 Setup.** Participant setup in the ACT$^{3D}$.

Biodex chair with nylon belts to constrain movement of the upper body and torso. A lightweight fiberglass cast was applied to the participant's paretic forearm (not crossing the elbow or wrist joints) and then attached to the ACT$^{3D}$ haptic device end effector via custom hardware (Fig. 3). The ACT$^{3D}$ consists of the admittance-controlled HapticMaster robot (Moog Inc., The Netherlands) with a six-degree-of-freedom load cell end effector (JR3, Woodland, CA).

The robot was programmed to allow free unconstrained movement in the transverse (horizontal) plane (including horizontal shoulder abduction/adduction and elbow flexion/ extension). Internal and external rotation were constrained due to the design of the gimbal and the way the participant was secured to the robot. Virtual rigid surfaces were programmed to limit the amount of vertical movement to between 70° and 100° shoulder abduction to protect the shoulder.

Twelve pairs of Ag/Ag-Cl gel EMG electrodes were placed over the following muscle sites, according to the guidelines in the Anatomical Guide for the Electromyographer: anterior, middle, and posterior deltoid, upper-trapezius, pectoralis major, supraspinatus, infraspinatus, and biceps brachii, with two pairs over the wrist and finger extensors and two over the flexors. A custom amplifier system based on the Texas Instruments ADS1299 was used to sample EMG at a frequency of 1 kHz, with a gain of 1k, and with band pass filtering of 70-350Hz.

*5.5.2 Position- and Force- Controller Description*

Although it is possible to use other inputs to a controller, myoelectric pattern recognition, which is successfully used by persons with an amputation, was chosen both because it allowed us to take advantage of the lead time that occurs prior to the intended movement in order to minimize response delay.[34,122,123]

A linear discriminant analysis–based pattern recognition controller consisting of three classes was used to control the robot in the vertical direction in two different ways: position-control and force-control. The position-based controller consisted of applying classifier output (class and speed) at and across each decision window (25ms) to the vertical position of the robot. More explicitly, a velocity was applied across each 25ms window that was proportional as described in Equations 1, 2, and 3 from Scheme et al.[124] Similarly, for the force-based controller, incremental changes were made to the vertical force using the direction and magnitude output from the proportional control classifier. In this way the robot responded to the intent of the user each 25ms.

$$PC_i = \left( \frac{1}{C_i} \sum_{j=1}^{N_{CH}} S_{i,j} MAV_j \right)^2 \qquad (1)$$

where $PC_i$ is the proportional control output for each class for a given window, $N_{CH}$ is the number of channels used, $MAV_j$ is the mean absolute value of channel $j$ within the given window, $S_{i,j}$ is the stored set of values representing the *centers* of each class and channel that were calculated and stored during classifier training by (2)

$$S_{i,j} = \frac{1}{K_{i,j}} \sum_{k=1}^{K_{i,j}} MAV_{i,j,k}^{Tr} \qquad (2)$$

where $MAV_{i,j,k}^{Tr}$ is the mean absolute value of the training data from class $i$, channel $j$, and computation window $k$, and $K_{i,j}$ is the total number of computation windows ($k$) for class $i$ and channel $j$. $C_i$ is the stored set of per-class *normalization factors* calculated and stored during classifier training by using (3). These are the channel-sum of squared *centers* found using (2) in the following:

$$C_i = \sum_{j=1}^{N_{CH}} S_{i,j}^2 \qquad (3)$$

Additional gains to the proportional control for each class and controller-type were adjusted to each participant based on the following guidelines: gains were lowered if the participant consistently lifted their arm directly into the ceiling limit upon first effort to lift their arm; conversely, gains were increased if their elbow was lifting off the load cell or it appeared that the participant was waiting on the robot to respond. Different gains were used for the position and force paradigms as well as between the positive and negative vertical directions. A graphical depiction of the control scheme is presented in figure 4.

*5.5.3 Control System Training*

Training data consisted of three sets of two, 10-second trials of each movement type (abduction, adduction, no movement) with each set occurring at a different horizontal adduction position (0°, 45°, and 90°). Additionally, five supported reach trials on a rigid table-like surface at 90° abduction and five limb-weight supported reach trials were included into the no-movement class training data. Supported reaching trials were included to aid the classifier in discriminating between pure abduction and adduction and reaching, since common muscle activation patterns across movements, as well as generalized increased muscle tone during tasks occur after stroke. In total, 28, 10-second trials were used as training data.

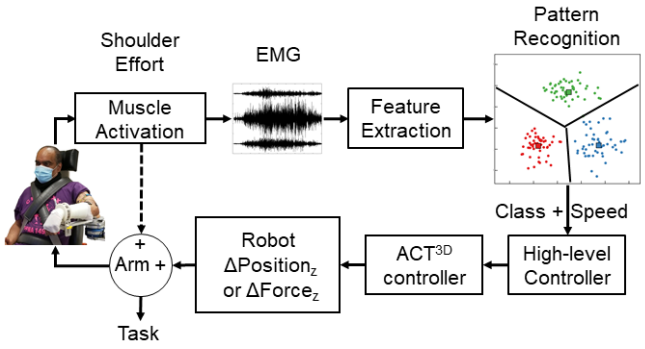


**Figure 16 Block diagram of control schemes.** Dashed line indicates that only during the force-based control can muscle activity *directly* affect the movement or stiffness of the arm.

*5.5.4 Data Segmentation and Feature Extraction*

Similar procedures were used for segmentation and feature extraction for both online and offline classifiers and analyses. All 12 channels of EMG were processed using 200ms windows and 25ms steps (175ms overlap). Within each window, the Hudgin's feature set (mean absolute value, number of slope sign changes, number of zero-crossings, and waveform length) was extracted in addition to 6$^{th}$ order autoregressive features. In total, 12 channels, each with 10 feature vectors, for a total of 120 features, were used to train and test both the online and offline classifiers.[67]

*5.5.5 Lift and Reach Task Description*

The two controllers were then used to control the robot in a reaching task, which was also completed under a no-support condition, a tabletop condition, and a limb-weight supported condition. The tabletop and limb-weight support conditions were added as hypothetical best cases for comparison with the real-time control data. Ten lift-reach-return-lower trials were performed under each condition. The participant was required to lift their arm to achieve a vertical target window between 80 and 100 degrees of abduction, then reach out straight in front of them as far as they could, return to the starting position, and lower their arm below 80° abduction. Although ultimately arbitrary, these limits were implemented to protect the glenohumeral joint and because many compensations can accommodate inaccuracies in shoulder control. During the supported conditions, the limb was already in the vertical target window, so only the forward reach and return portions of the task were required. Verbal instructions to participants generally included phrases such as "lift, reach out in front of you as far as you can, return, and lower your arm." No mention was made of speed, as ballistic motions are not used functionally. Figure 5 depicts joint kinematic data as well as forces provided and sensed during a position control trial as well as a force control trial.

For each participant, the order of support conditions was randomized. Data recorded for each trial included calculated joint angles, position and velocity of the end effector, the forces and moments

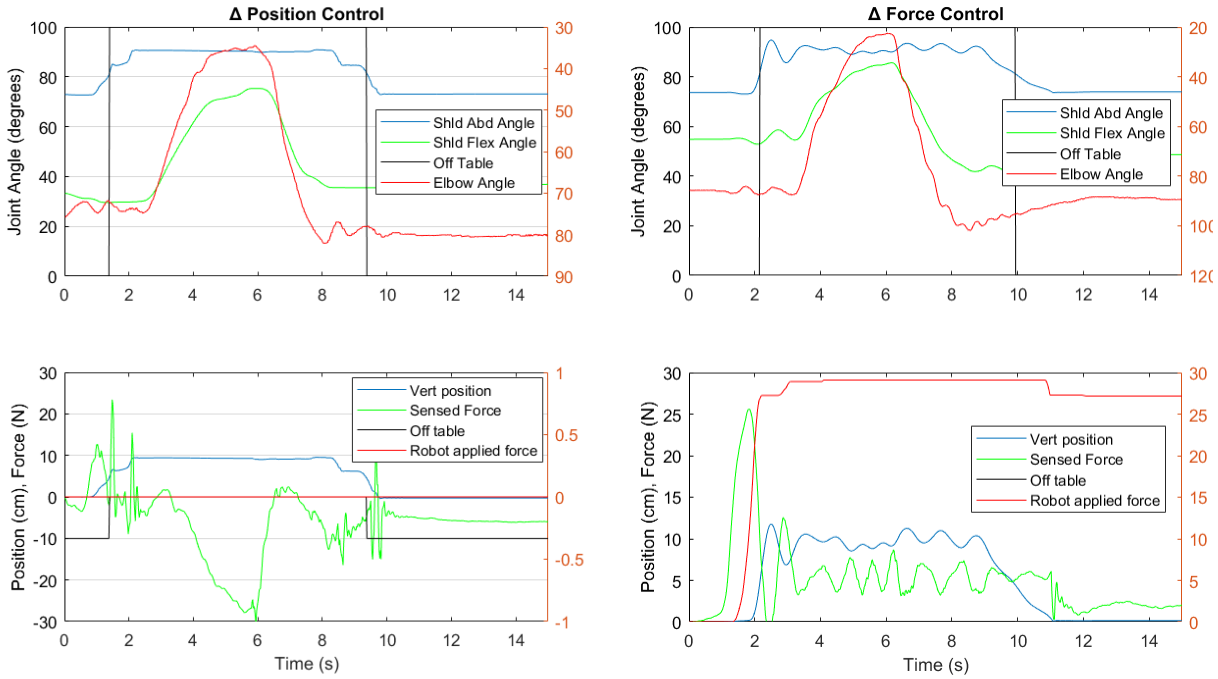


**Figure 17 Representative trials.** Representative lift and reach trials of each control type: position control (left) and force control (right) with joint kinematics (top) and robot forces (bottom). The large negative force (-30N) displayed in the bottom left is a participant engaging an abnormal synergy pattern in order to maximize reach; the controller successfully identified the reach and prevented the robot from lowering its vertical position outside of the target window to enable a greater reach. In the bottom right at the end of the reach around 11 seconds can be seen a minimal drop in support force as the classifier has difficulty recognizing adduction when the arm only need be relaxed in order to lower to the starting position.

at the load cell under the end effector, and 12 channels of surface EMG.

### *5.5.6 Unrelated Movement Task*

In order to test how well the classifier could inherently discriminate other (non-trained and non-controlled) degrees of freedom, an offline task and analysis was performed. Four sets of two paired tasks including horizontal shoulder adduction and abduction, isometric internal and external rotation, elbow flexion and extension, and hand open and close were performed in random order under two types of vertical support: tabletop support and limb-weight support. Each participant

attempted the four sets of movements, through their full range of motion, for a total 45 seconds for each pair. Internal and external rotation were isometric so participants were asked to “use about the same strength that is required to move your arm like this” (and an external rotation motion moving from neutral to 90° while the humerus was abducted to 90° was demonstrated). The transverse plane was unconstrained. Data for this task was collected in three of the five participants.

# Chapter 6: Concluding Remarks

## 6.1 Summary

This collection of work has attempted to understand control of the shoulder after stroke, the feasibility of using muscle signals as a control signal for a powered device, and applied machine learning techniques to control robotic arm support to test its effect on reaching distance. Specifically, weakness, increased tone (increased activation of all muscles throughout the limb), and loss of independent joint control (abnormal synergy causing patterned activation of all flexors or extensors throughout the limb) were all implicated as possibly having a negative effect on correctly determining user-intent after stroke.

A major takeaway from this collection of work is that using myoelectric pattern recognition to control either the vertical force or vertical position of a robotic support device is possible and efficacious for individuals after stroke. Key contributions from each chapter are outlined here:

Chapter 2: Even under isometric and maximum voluntary contraction conditions, in which we would expect the greatest presentation of abnormal synergy, a Load cell and EMG-based classifier was able to distinguish to a satisfactory (>90%) level of accuracy, 4 of the 8 classes of movement, two at the shoulder and two at the elbow. External rotation and abduction were often confused for each other as were internal rotation and adduction. Although the results were promising, we questioned whether the misclassifications were due to the nature of the task and the setup or whether they were true limitations in pattern recognition of the shoulder after stroke.

Chapter 3: attempted to examine the questions uncovered in Chapter 2, mainly, could the four motions identified as most challenging, be correctly discriminated. A specially designed apparatus connecting the participants arm to the $ACT^{3D}$ attempted to isolate humeral long-axis rotation (internal and external rotation) from abduction and adduction. The robot required certain levels of abduction and adduction effort prior to requiring maximal internal and external rotation. This study demonstrated that indeed these four motions could be detected and discriminated but only for a partly dynamic task. This indicates that the isometric setup and single-DOF task negatively affected the classifiers ability to discriminate between motions as the participant could perform the same combined motion to maximize torques for two different degrees of freedom.

Chapter 4: explored some neuromechanistic implications in regards to the biomechanics of the shoulder and the joint torques generated under the four different dual-tasks presented in Chapter 3. Paretic, non-paretic, and control shoulders followed similar patterns across the different load levels. This at least partly dispels conventional thought that these patterns are part of the abnormal synergy due to stroke. All groups were better able to generate external rotation during abduction and less able to generate it during adduction. The opposite was true for internal rotation, with participants generating increased torque during adduction and decreased internal rotation during abduction. The paretic arms were less able to generate normalized internal and external rotation torques across all load levels, possibly indicating the presence of a more global effect such as hypertonicity, causing co-activation of both agonists and antagonists simultaneously, limiting torque generation under all of the conditions.

Chapter 5: attempted to realize the techniques examined in the previous chapters and test their effect on reaching distance. Participants were able to control both the vertical force and the vertical position using online real-time myoelectric pattern recognition control of the ACT$^{3D}$ robot. This is the first documented success of real-time control of vertical shoulder support in stroke. Participants raised their arm into a vertical target window and reached out as far as they could. Participant's elbow and shoulder excursion improved significantly with the real-time support as compared to the no support condition. Their muscle activity was reduced to levels near those of the fully supported condition

## 6.2 Implications

Although this work did not include the design of a wearable device, it moves us one step closer to a realization of one. The techniques explored here could be used to control a device in two distinct manners, assistive or rehabilitative. Assistive referring to a mode that would maximize performance and would be provided for as long as it is needed. Alternatively, rehabilitative referring to a mode that would attempt, as the name implies, to rehabilitate function of the users arm; little by little improving the ability to activate the shoulder and distal upper extremity outside the typical patterns and with reduced tone. Once a wearable device is realized, therapy could be incorporated into all activities of daily living, maximizing meaning, dose, and repetition. Support could be modified over time ensuring that participants are having to work while simultaneously being assisted to be more successful. In either case, it may be possible to use machine learning to help individuals understand and avoid when they are trying too hard and engaging negative patterns.

## 6.3 Limitations

Generally the studies within this body of work were small, especially Chapter 6 which was adversely affected by the presence of COVID-19, thus limiting the strength of conclusions and broader generalization. This thesis used surface EMG which is non-invasive but has its own unique set of limitations, especially considering future application requiring daily or long-term use. This work also used two different types of LDA based classifiers with limited number of features. There are many more classifier algorithms as well as features out there that could be explored and that may ultimately provide some benefit. All studies used nylon straps to minimize movement of the torso and scapula but movement, especially of the latter, still occurred. For more specific limitations of each study, please refer to the discussion section of each chapter and appendix.

## 6.4 Future Directions

I believe that good science brings some answers, but more importantly brings more good questions, progressively stepping closer and closer to truth. This body of work is only one step of many that hopes to bring permanent positive change to those negatively affected by stroke. This thesis specifically explored the feasibility and efficacy of using myoelectric pattern recognition to control a future powered shoulder device after stroke. Logical next steps then might include expanded testing on the $ACT^{3D}$ or other comparable device with increased online testing with a couple more EMG channels as mentioned in Chapter 6. Some thought would need to be given as to what would constitute successful control of shoulder support beyond what was attempted here. Another somewhat straightforward step may include the use of implantable electrodes to minimize the limitations of using surface electrodes.

Although this thesis explored control for use on a powered device, a single-DOF passive shoulder device, similar to that presented in Cole Simpson's dissertation[125] could also provide the support needed to minimize abnormal co-activation of the affected limb. With minor modifications, a motor and non-backdrivable gearbox could be mounted on the exoskeletal system proposed by Simpson. Once a powered version of a single-DOF shoulder support device is developed, comparisons could be made between the manual- and the powered- versions. Insight could also be gained as to timing and dose (volume and intensity) of intervention as Ellis has shown a positive effect of arm support intervention training on the $ACT^{3D}$ without note of a ceiling effect.

It would be interesting to investigate the use of a powered wearable exoskeleton as an intervention. The machine learning techniques tested here could be used to help users avoid the tendency to engage the abnormal synergy and the maximal amount of support could be modified over time as strength and ability to operate outside the synergy improves.

Ultimately, combinations of simpler more robust exoskeletal systems may enable modular application to individuals, thus tailoring assistance and intervention possibilities to target the specific and unique impairments of each person. I can imagine a single-DOF shoulder support device working alongside a hand opening/closing device that is mechanical, electrically stimulated, or both to aid or rehabilitate reach and grasp function after stroke.

# References


1. Twitchell TE. The restoration of motor function following hemiplegia in man. *Brain.* 1951;74(4):443-480.
2. Langhorne P, Coupar F, Pollock A. Motor recovery after stroke: a systematic review. *Lancet Neurol.* 2009;8(8):741-754.
3. Hatem SM, Saussez G, Della Faille M, et al. Rehabilitation of Motor Function after Stroke: A Multiple Systematic Review Focused on Techniques to Stimulate Upper Extremity Recovery. *Front Hum Neurosci.* 2016;10:442.
4. Dobkin BH. Clinical practice. Rehabilitation after stroke. *N Engl J Med.* 2005;352(16):1677-1684.
5. Krebs HI, Hogan N, Volpe BT, Aisen ML, Edelstein L, Diels C. Overview of clinical trials with MIT-MANUS: a robot-aided neuro-rehabilitation facility. *Technol Health Care.* 1999;7(6):419-423.
6. Rodgers H, Bosomworth H, Krebs HI, et al. Robot assisted training for the upper limb after stroke (RATULS): a multicentre randomised controlled trial. *Lancet.* 2019;394(10192):51-62.
7. Veerbeek JM, Langbroek-Amersfoort AC, van Wegen EE, Meskers CG, Kwakkel G. Effects of Robot-Assisted Therapy for the Upper Limb After Stroke. *Neurorehabil Neural Repair.* 2017;31(2):107-121.
8. Benjamin EJ, Virani SS, Callaway CW, et al. Heart Disease and Stroke Statistics-2018 Update: A Report From the American Heart Association. *Circulation.* 2018.

9. Kelly-Hayes M, Beiser A, Kase CS, Scaramucci A, D'Agostino RB, Wolf PA. The influence of gender and age on disability following ischemic stroke: the Framingham study. *J Stroke Cerebrovasc Dis.* 2003;12(3):119-126.

10. Mayo NE, Wood-Dauphinee S, Ahmed S, et al. Disablement following stroke. *Disabil Rehabil.* 1999;21(5-6):258-268.

11. Brunnstrom S. Motor testing procedures in hemiplegia: based on sequential recovery stages. *Phys Ther.* 1966;46(4):357-375.

12. Dewald JP, Beer RF. Abnormal joint torque patterns in the paretic upper limb of subjects with hemiparesis. *Muscle Nerve.* 2001;24(2):273-283.

13. Sukal TM, Ellis MD, Dewald JPA. Shoulder abduction-induced reductions in reaching work area following hemiparetic stroke: neuroscientific implications. *Exp Brain Res.* 2007;183(2):215-223.

14. Miller LC, Dewald JPA. Involuntary paretic wrist/finger flexion forces and EMG increase with shoulder abduction load in individuals with chronic stroke. *Clin Neurophysiol.* 2012;123(6):1216-1225.

15. Lan YY, Yao J, Dewald JPA. The Impact of Shoulder Abduction Loading on Volitional Hand Opening and Grasping in Chronic Hemiparetic Stroke. *Neurorehab Neural Re.* 2017;31(6):521-529.

16. McPherson JG, Chen A, Ellis MD, Yao J, Heckman CJ, Dewald JPA. Progressive recruitment of contralesional cortico-reticulospinal pathways drives motor impairment post stroke. *J Physiol.* 2018.

17. McMorland AJ, Runnalls KD, Byblow WD. A neuroanatomical framework for upper limb synergies after stroke. *Front Hum Neurosci.* 2015;9:82.

18. Ellis MD, Sukal T, DeMott T, Dewald JPA. Augmenting clinical evaluation of hemiparetic arm movement with a laboratory-based quantitative measurement of kinematics as a function of limb loading. *Neurorehab Neural Re.* 2008;22(4):321-329.

19. Ellis MD, Sukal-Moulton T, Dewald JPA. Progressive Shoulder Abduction Loading is a Crucial Element of Arm Rehabilitation in Chronic Stroke. *Neurorehab Neural Re.* 2009;23(8):862-869.

20. Ellis MD, Carmona C, Drogos J, Dewald JPA. Progressive Abduction Loading Therapy with Horizontal-Plane Viscous Resistance Targeting Weakness and Flexion Synergy to Treat Upper Limb Function in Chronic Hemiparetic Stroke: A Randomized Clinical Trial. *Front Neurol.* 2018;9:71.

21. Gopura RARC, Bandara DSV, Kiguchi K, Mann GKI. Developments in hardware systems of active upper-limb exoskeleton robots: A review. *Robot Auton Syst.* 2016;75:203-220.

22. Young AJ, Ferris DP. State of the Art and Future Directions for Lower Limb Robotic Exoskeletons. *Ieee T Neur Sys Reh.* 2017;25(2):171-182.

23. Geethanjali P. Myoelectric control of prosthetic hands: state-of-the-art review. *Med Devices (Auckl).* 2016;9:247-255.

24. Scheme E, Englehart K. Electromyogram pattern recognition for control of powered upper-limb prostheses: state of the art and challenges for clinical use. *J Rehabil Res Dev.* 2011;48(6):643-659.

25. Hakonen M, Piitulainen H, Visala A. Current state of digital signal processing in myoelectric interfaces and related applications. *Biomed Signal Proces.* 2015;18:334-359.

26. Rivela D, Scannella A, Pavan EE, Frigo CA, Belluco P, Gini G. Analysis and Comparison of Features and Algorithms to Classify Shoulder Movements From sEMG Signals. *IEEE Sensors Journal.* 2018;18(9):3714-3721.

27. Buerkle VR, Englehart K, Hudgins B. Pattern recognition of single and combined motions from the shoulder complex. *Conf Proc IEEE Eng Med Biol Soc.* 2006;1:3419-3422.

28. Young AJ, Hargrove LJ, Kuiken TA. The effects of electrode size and orientation on the sensitivity of myoelectric pattern recognition systems to electrode shift. *IEEE Trans Biomed Eng.* 2011;58(9):2537-2544.

29. Zhang SQ, Zhang X, Cao S, Gao XP, Chen X, Zhou P. Myoelectric Pattern Recognition Based on Muscle Synergies for Simultaneous Control of Dexterous Finger Movements. *Ieee T Hum-Mach Syst.* 2017;47(4):576-582.

30. Lu Z, Tong RKy, Zhang X, Li S, Zhou P. Myoelectric Pattern Recognition for Controlling a Robotic Hand: A Feasibility Study in Stroke. *Ieee T Bio-Med Eng.* 2018:1-1.

31. Zhang X, Zhou P. High-Density Myoelectric Pattern Recognition Toward Improved Stroke Rehabilitation. *Ieee T Bio-Med Eng.* 2012;59(6):1649-1657.

32. Cesqui B, Tropea P, Micera S, Krebs HI. EMG-based pattern recognition approach in post stroke robot-aided rehabilitation: a feasibility study. *J Neuroeng Rehabil.* 2013;10.

33. Lan YY, Yao J, Dewald JPA. The Impact of Shoulder Abduction Loading on EMG-based Intention Detection of Hand Opening and Closing After Stroke. *2011 Annual International Conference of the Ieee Engineering in Medicine and Biology Society (Embc).* 2011:4136-4139.

34. Hargrove LJ, Young AJ, Simon AM, et al. Intuitive Control of a Powered Prosthetic Leg During Ambulation A Randomized Clinical Trial. *Jama-J Am Med Assoc.* 2015;313(22):2244-2252.

35. Huang H, Zhang F, Hargrove LJ, Dou Z, Rogers DR, Englehart KB. Continuous Locomotion-Mode Identification for Prosthetic Legs Based on Neuromuscular-Mechanical Fusion. *Ieee T Bio-Med Eng.* 2011;58(10):2867-2875.

36. Perotto A, Delagi EF. *Anatomical guide for the electromyographer : the limbs and trunk.* 3rd ed. Springfield, Ill., USA: Charles C. Thomas; 1994.

37. Kuiken TA, Miller LA, Turner K, Hargrove LJ. A Comparison of Pattern Recognition Control and Direct Control of a Multiple Degree-of-Freedom Transradial Prosthesis. *IEEE J Transl Eng Health Med.* 2016;4:2100508.

38. Smith LH, Hargrove LJ, Lock BA, Kuiken TA. Determining the Optimal Window Length for Pattern Recognition-Based Myoelectric Control: Balancing the Competing Effects of Classification Error and Controller Delay. *Ieee T Neur Sys Reh.* 2011;19(2):186-192.

39. Hudgins B, Parker P, Scott RN. A new strategy for multifunction myoelectric control. *IEEE Trans Biomed Eng.* 1993;40(1):82-94.

40. Ellis MD, Lan YY, Yao J, Dewald JPA. Robotic quantification of upper extremity loss of independent joint control or flexion synergy in individuals with hemiparetic stroke: a review of paradigms addressing the effects of shoulder abduction loading. *J Neuroeng Rehabil.* 2016;13.

41. Benjamin EJ, Muntner P, Alonso A, et al. Heart Disease and Stroke Statistics-2019 Update: A Report From the American Heart Association. *Circulation.* 2019:CIR0000000000000659.

42. Kwakkel G, Kollen BJ, Krebs HI. Effects of robot-assisted therapy on upper limb recovery after stroke: a systematic review. *Neurorehabil Neural Repair.* 2008;22(2):111-121.

43. Anderson CS, Linto J, Stewartwynne EG. A Population-Based Assessment of the Impact and Burden of Caregiving for Long-Term Stroke Survivors. *Stroke.* 1995;26(5):843-849.

44. Dewald JP, Pope PS, Given JD, Buchanan TS, Rymer WZ. Abnormal muscle coactivation patterns during isometric torque generation at the elbow and shoulder in hemiparetic subjects. *Brain.* 1995;118 ( Pt 2):495-510.

45. Ellis MD, Sukal T, DeMott T, Dewald JP. Augmenting clinical evaluation of hemiparetic arm movement with a laboratory-based quantitative measurement of kinematics as a function of limb loading. *Neurorehabil Neural Repair.* 2008;22(4):321-329.

46. Miller LC, Dewald JP. Involuntary paretic wrist/finger flexion forces and EMG increase with shoulder abduction load in individuals with chronic stroke. *Clin Neurophysiol.* 2012;123(6):1216-1225.

47. O'Sullivan SB, Schmitz TJ. *Physical rehabilitation.* Philadelphia: F.A. Davis; 2007.

48. Sukal TM, Ellis MD, Dewald JP. Shoulder abduction-induced reductions in reaching work area following hemiparetic stroke: neuroscientific implications. *Exp Brain Res.* 2007;183(2):215-223.

49. Simpson CS, Okamura AM, Hawkes EW. Exomuscle: An inflatable device for shoulder abduction support. Paper presented at: 2017 IEEE International Conference on Robotics and Automation (ICRA); 29 May-3 June 2017, 2017.

50. Neill CTO, Phipps NS, Cappello L, Paganoni S, Walsh CJ. A soft wearable robot for the shoulder: Design, characterization, and preliminary testing. Paper presented at: 2017 International Conference on Rehabilitation Robotics (ICORR); 17-20 July 2017, 2017.

51. Lenzi T, Rossi SD, Vitiello N, et al. The neuro-robotics paradigm: NEURARM, NEUROExos, HANDEXOS. Paper presented at: 2009 Annual International Conference of the IEEE Engineering in Medicine and Biology Society; 3-6 Sept. 2009, 2009.

52. Exoskeleton Report: Arm Support. [Online]. 2019; https://exoskeletonreport.com/product-category/exoskeleton-catalog/industrial/shoulder-support-exoskeleton-for-work-and-industry/. Accessed 06 May, 2019.

53. MATE Exoskeleton by Comau Boosts Workers' Strength and Performance without Using Electric Power. [Online]. 2018; https://www.wearable-technologies.com/2018/10/mate-exoskeleton-by-comau-boosts-workers-strength-and-performance-without-using-electric-power/. Accessed 06 May, 2019.

54. Novak D, Riener R. A survey of sensor fusion methods in wearable robotics. *Robot Auton Syst.* 2015;73:155-170.

55. Hargrove LJ, Lock BA, Simon AM. Pattern recognition control outperforms conventional myoelectric control in upper limb patients with targeted muscle reinnervation. 2013;2013:1599-1602.

56. Hargrove LJ, Simon AM, Lipschutz RD, Finucane SB, Kuiken TA. Real-time myoelectric control of knee and ankle motions for transfemoral amputees. 2011;305(15):1542-1544.

57. Hargrove LJ, Young AJ, Simon AM, et al. Intuitive control of a powered prosthetic leg during ambulation: a randomized clinical trial. 2015;313(22):2244-2252.

58. Hargrove LJ, Simon AM, Young AJ, et al. Robotic leg control with EMG decoding in an amputee with nerve transfers. 2013;369(13):1237-1242.

59. Coapt Engineering Technology. [Online]. https://www.coaptengineering.com/technology.html. Accessed 06 May, 2019.

60. IBT Products. https://www.i-biomed.com/products.html. Accessed 06 May, 2019.

61. Nam KY, Kim HJ, Kwon BS, Park JW, Lee HJ, Yoo A. Robot-assisted gait training (Lokomat) improves walking function and activity in people with spinal cord injury: a systematic review. *J Neuroeng Rehabil.* 2017;14(1):24.

62. Blank AA, French JA, Pehlivan AU, O'Malley MK. Current Trends in Robot-Assisted Upper-Limb Stroke Rehabilitation: Promoting Patient Engagement in Therapy. *Curr Phys Med Rehabil Rep.* 2014;2(3):184-195.

63. Kopke JV, Hargrove LJ, Ellis MD. Applying LDA-based pattern recognition to predict isometric shoulder and elbow torque generation in individuals with chronic stroke with moderate to severe motor impairment. *J Neuroeng Rehabil.* 2019;16.

64. Kopke JV, Hargrove LJ, Ellis MD. Application of an LDA Classifier for Determining User-Intent in Multi-DOF Quasi-Static Shoulder Tasks in Individuals with Chronic Stroke: Preliminary Analysis. *Conf Proc IEEE Eng Med Biol Soc.* 2018;2018:2312-2315.

65. Pohl PS, Winstein CJ. Practice effects on the less-affected upper extremity after stroke. *Arch Phys Med Rehabil.* 1999;80(6):668-675.

66. Sukal TM, Ellis MD, Dewald JPA. Evaluation and intervention in the paretic upper extremity following hemiparetic stroke using the ACT (3D) system. *P Ieee Ras-Embs Int.* 2006:809-+.

67. Hudgins B, Parker P, Scott RN. A New Strategy for Multifunction Myoelectric Control. *Ieee T Bio-Med Eng.* 1993;40(1):82-94.

68. Englehart K, Hudgins B. A robust, real-time control scheme for multifunction myoelectric control. *Ieee T Bio-Med Eng.* 2003;50(7):848-854.

69. Wolf SL, Catlin PA, Ellis M, Archer AL, Morgan B, Piacentino A. Assessing Wolf Motor function Test as outcome measure for research in patients after stroke. *Stroke.* 2001;32(7):1635-1639.

70. Ellis MD, Schut I, Dewald JPA. Flexion synergy overshadows flexor spasticity during reaching in chronic moderate to severe hemiparetic stroke. *Clin Neurophysiol.* 2017;128(7):1308-1314.

71. Young AJ, Kuiken TA, Hargrove LJ. Analysis of using EMG and mechanical sensors to enhance intent recognition in powered lower limb prostheses. *J Neural Eng.* 2014;11(5):056021.

72. Hargrove LJ, Englehart K, Hudgins B. A comparison of surface and intramuscular myoelectric signal classification. *Ieee T Bio-Med Eng.* 2007;54(5):847-853.

73. Wilk KE, Arrigo CA, Andrews JR. Current concepts: The stabilizing structures of the glenohumeral joint. *J Orthop Sport Phys.* 1997;25(6):364-379.

74. Ackland DC, Pandy MG. Moment Arms of the Shoulder Muscles during Axial Rotation. *J Orthop Res.* 2011;29(5):658-667.

75. Dewald JP, Sheshadri V, Dawson ML, Beer RF. Upper-limb discoordination in hemiparetic stroke: implications for neurorehabilitation. *Top Stroke Rehabil.* 2001;8(1):1-12.

76. Ellis MD, Sukal T, DeMott T, Dewald JPA. ACT(3D) exercise targets gravity-induced discoordination and improves reaching work area in individuals with stroke. *Int C Rehab Robot.* 2007:890-895.

77. Beer RF, Given JD, Dewald JPA. Task-dependent weakness at the elbow in patients with hemiparesis. *Arch Phys Med Rehab.* 1999;80(7):766-772.

78. Roh J, Rymer WZ, Perreault EJ, Yoo SB, Beer RF. Alterations in upper limb muscle synergy structure in chronic stroke survivors. *J Neurophysiol.* 2013;109(3):768-781.

79. Jiang N, Vujaklija I, Rehbaum H, Graimann B, Farina D. Is Accurate Mapping of EMG Signals on Kinematics Needed for Precise Online Myoelectric Control? *Ieee T Neur Sys Reh.* 2014;22(3):549-558.

80. Mussa-Ivaldi FA, Hogan N, Bizzi E. Neural, mechanical, and geometric factors subserving arm posture in humans. *J Neurosci.* 1985;5(10):2732-2743.

81. Ellis MD, Acosta AM, Yao J, Dewald JPA. Position-dependent torque coupling and associated muscle activation in the hemiparetic upper extremity. *Exp Brain Res.* 2007;176(4):594-602.

82. Baillargeon EM, Ludvig D, Sohn MH, Nicolozakes CP, Seitz AL, Perreault EJ. Experimentally quantifying the feasible torque space of the human shoulder. *J Electromyogr Kinesiol.* 2019.

83. Beer RF, Ellis MD, Holubar BG, Dewald JPA. Impact of gravity loading on post-stroke reaching and its relationship to weakness. *Muscle Nerve.* 2007;36(2):242-250.

84. Janssen I, Heymsfield SB, Wang ZM, Ross R. Skeletal muscle mass and distribution in 468 men and women aged 18-88 yr. *J Appl Physiol (1985).* 2000;89(1):81-88.

85. Heyward VH, Johannesellis SM, Romer JF. Gender Differences in Strength. *Res Q Exercise Sport.* 1986;57(2):154-159.

86. Ackland DC, Pak P, Richardson M, Pandy MG. Moment arms of the muscles crossing the anatomical shoulder. *J Anat.* 2008;213(4):383-390.

87. Kuechle DK, Newman SR, Itoi E, Niebur GL, Morrey BF, An KN. The relevance of the moment arm of shoulder muscles with respect to axial rotation of the glenohumeral joint in four positions. *Clin Biomech.* 2000;15(5):322-329.

88. Knutsson E, Richards C. Different types of disturbed motor control in gait of hemiparetic patients. *Brain.* 1979;102(2):405-430.

89. Chae J, Yang G, Park BK, Labatia I. Muscle weakness and cocontraction in upper limb hemiparesis: relationship to motor impairment and physical disability. *Neurorehabil Neural Repair.* 2002;16(3):241-248.

90. Levin MF, Selles RW, Verheul MH, Meijer OG. Deficits in the coordination of agonist and antagonist muscles in stroke patients: implications for normal motor control. *Brain Res.* 2000;853(2):352-369.

91. Stoeckmann TM, Sullivan KJ, Scheidt RA. Elastic, viscous, and mass load effects on poststroke muscle recruitment and co-contraction during reaching: a pilot study. *Phys Ther.* 2009;89(7):665-678.

92. Delp SL, Anderson FC, Arnold AS, et al. OpenSim: open-source software to create and analyze dynamic simulations of movement. *IEEE Trans Biomed Eng.* 2007;54(11):1940-1950.

93. Saul KR, Hu X, Goehler CM, et al. Benchmarking of dynamic simulation predictions in two software platforms using an upper limb musculoskeletal model. *Comput Method Biomec.* 2015;18(13):1445-1458.

94. Holzbaur KRS, Murray WM, Gold GE, Delp SL. Upper limb muscle volumes in adult subjects. *J Biomech.* 2007;40(4):742-749.

95. Vidt ME, Daly M, Miller ME, Davis CC, Marsh AP, Saul KR. Characterizing upper limb muscle volume and strength in older adults: A comparison with young adults. *J Biomech.* 2012;45(2):334-341.

96. Li S, Chen YT, Francisco GE, Zhou P, Rymer WZ. A Unifying Pathophysiological Account for Post-stroke Spasticity and Disordered Motor Control. *Front Neurol.* 2019;10:468.

97. Lee J MM. Neuroanatomy, Extrapyramidal System. *In: StatPearls [Internet] Treasure Island (FL): StatPearls Publishing;* [Online]. 2020; https://www.ncbi.nlm.nih.gov/books/NBK554542/. Accessed 03 May, 2021.

98. Hankey GJ, Jamrozik K, Broadhurst RJ, Forbes S, Anderson CS. Long-term disability after first-ever stroke and related prognostic factors in the Perth Community Stroke Study, 1989-1990. *Stroke.* 2002;33(4):1034-1040.

99. Hardie K, Hankey GJ, Jamrozik K, Broadhurst RJ, Anderson C. Ten-year risk of first recurrent stroke and disability after first-ever stroke in the Perth Community Stroke Study. *Stroke.* 2004;35(3):731-735.

100. Kamper DG, Fischer HC, Cruz EG, Rymer WZ. Weakness is the primary contributor to finger impairment in chronic stroke. *Arch Phys Med Rehabil.* 2006;87(9):1262-1269.

101. Persson CU, Holmegaard L, Redfors P, Jern C, Blomstrand C, Jood K. Increased muscle tone and contracture late after ischemic stroke. *Brain Behav.* 2020;10(2):e01509.

102. McPherson JG, Ellis MD, Heckman CJ, Dewald JPA. Evidence for Increased Activation of Persistent Inward Currents in Individuals With Chronic Hemiparetic Stroke. *J Neurophysiol.* 2008;100(6):3236-3243.

103. Li X, Suresh A, Zhou P, Rymer WZ. Alterations in the peak amplitude distribution of the surface electromyogram poststroke. *IEEE Trans Biomed Eng.* 2013;60(3):845-852.

104. Tang W, Zhang X, Tang X, Cao S, Gao X, Chen X. Surface Electromyographic Examination of Poststroke Neuromuscular Changes in Proximal and Distal Muscles Using Clustering Index Analysis. *Front Neurol.* 2017;8:731.

105. Chen YT, Li S, Magat E, Zhou P, Li S. Motor Overflow and Spasticity in Chronic Stroke Share a Common Pathophysiological Process: Analysis of Within-Limb and Between-Limb EMG-EMG Coherence. *Front Neurol.* 2018;9:795.

106. Srivastava S, Patten C, Kautz SA. Altered muscle activation patterns (AMAP): an analytical tool to compare muscle activity patterns of hemiparetic gait with a normative profile. *J Neuroeng Rehabil.* 2019;16(1):21.

107. McPherson LM, Dewald JPA. Differences between flexion and extension synergy-driven coupling at the elbow, wrist, and fingers of individuals with chronic hemiparetic stroke. *Clin Neurophysiol.* 2019;130(4):454-468.

108. Masia L, Krebs HI, Cappa P, Hogan N. Design and characterization of hand module for whole-arm rehabilitation following stroke. *Ieee-Asme T Mech.* 2007;12(4):399-407.

109. McConnell AC, Moioli RC, Brasil FL, et al. Robotic devices and brain-machine interfaces for hand rehabilitation post-stroke. *J Rehabil Med.* 2017;49(6):449-460.

110. Lo HS, Xie SQ. Exoskeleton robots for upper-limb rehabilitation: state of the art and future prospects. *Med Eng Phys.* 2012;34(3):261-268.

111. Proietti T, Crocher V, Roby-Brami A, Jarrasse N. Upper-Limb Robotic Exoskeletons for Neurorehabilitation: A Review on Control Strategies. *IEEE Rev Biomed Eng.* 2016;9:4-14.

112. Ona ED, Cano-de la Cuerda R, Sanchez-Herrera P, Balaguer C, Jardon A. A Review of Robotics in Neurorehabilitation: Towards an Automated Process for Upper Limb. *J Healthc Eng.* 2018;2018:9758939.

113. Makowski NS, Knutson JS, Chae J, Crago PE. Control of Robotic Assistance Using Poststroke Residual Voluntary Effort. *Ieee T Neur Sys Reh.* 2015;23(2):221-231.

114. Tabor A, Bateman S, Scheme E. Evaluation of Myoelectric Control Learning Using Multi-Session Game-Based Training. *IEEE Trans Neural Syst Rehabil Eng.* 2018;26(9):1680-1689.

115. Makowski NS, Knutson JS, Chae J, Crago PE. Functional electrical stimulation to augment poststroke reach and hand opening in the presence of voluntary effort: a pilot study. *Neurorehabil Neural Repair.* 2014;28(3):241-249.

116. Rivela D, Scannella A, Pavan EE, Frigo CA, Belluco P, Gini G. Processing of surface EMG through pattern recognition techniques aimed at classifying shoulder joint movements. *Annu Int Conf IEEE Eng Med Biol Soc.* 2015;2015:2107-2110.

117. Zhang X, Dai J, Li X, et al. sEMG-based shoulder-elbow composite motion pattern recognition and control methods for upper limb rehabilitation robot. *Assembly Automation.* 2019;39(3):394-400.

118. Jiang Y, Chen C, Zhang X, et al. Shoulder muscle activation pattern recognition based on sEMG and machine learning algorithms. *Comput Methods Programs Biomed.* 2020;197:105721.

119. Lenzi T, De Rossi SM, Vitiello N, Carrozza MC. Intention-based EMG control for powered exoskeletons. *IEEE Trans Biomed Eng.* 2012;59(8):2180-2190.

120. Kopke JV, Ellis MD, Hargrove LJ. Determining User Intent of Partly Dynamic Shoulder Tasks in Individuals With Chronic Stroke Using Pattern Recognition. *Ieee T Neur Sys Reh.* 2020;28(1):350-358.

121. Kopke JV, Hargrove LJ, Ellis MD. Applying LDA-based pattern recognition to predict isometric shoulder and elbow torque generation in individuals with chronic stroke with moderate to severe motor impairment. *J Neuroeng Rehabil.* 2019;16(1):35.

122. Kuiken TA, Li G, Lock BA, et al. Targeted muscle reinnervation for real-time myoelectric control of multifunction artificial arms. *JAMA.* 2009;301(6):619-628.

123. Hargrove LJ, Simon AM, Lipschutz RD, Finucane SB, Kuiken TA. Real-time myoelectric control of knee and ankle motions for transfemoral amputees. *JAMA.* 2011;305(15):1542-1544.

124. Scheme E, Lock B, Hargrove L, Hill W, Kuruganti U, Englehart K. Motion Normalized Proportional Control for Improved Pattern Recognition-Based Myoelectric Control. *IEEE Trans Neural Syst Rehabil Eng.* 2014;22(1):149-157.

125. Simpson C. Wearable Devices for Physical Assistance: Enhancing Capabilities After Stroke and in Running. In: ProQuest Dissertations Publishing; 2020.

126. Benjamin EJ, Blaha MJ, Chiuve SE, et al. Heart Disease and Stroke Statistics-2017 Update: A Report From the American Heart Association. *Circulation.* 2017;135(10):e146-e603.

127. Ellis MD, Lan Y, Yao J, Dewald JP. Robotic quantification of upper extremity loss of independent joint control or flexion synergy in individuals with hemiparetic stroke: a review of paradigms addressing the effects of shoulder abduction loading. *J Neuroeng Rehabil.* 2016;13(1):95.

128. Marchal-Crespo L, Reinkensmeyer DJ. Review of control strategies for robotic movement training after neurologic injury. *J Neuroeng Rehabil.* 2009;6:20.

129. Mehrholz J, Hadrich A, Platz T, Kugler J, Pohl M. Electromechanical and robot-assisted arm training for improving generic activities of daily living, arm function, and arm muscle strength after stroke. *Cochrane Database Syst Rev.* 2012(6):CD006876.

130. Englehart K, Hudgins B. A robust, real-time control scheme for multifunction myoelectric control. *IEEE Trans Biomed Eng.* 2003;50(7):848-854.

131. Smith LH, Kuiken TA, Hargrove LJ. Real-time simultaneous and proportional myoelectric control using intramuscular EMG. *J Neural Eng.* 2014;11(6):066013.

132. Lum PS, Burgar CG, Shor PC, Majmundar M, Van der Loos M. Robot-assisted movement training compared with conventional therapy techniques for the rehabilitation of upper-limb motor function after stroke. *Arch Phys Med Rehab.* 2002;83(7):952-959.

133. Krebs HI, Volpe BT, Williams D, et al. Robot-aided neurorehabilitation: A robot for wrist rehabilitation. *Ieee T Neur Sys Reh.* 2007;15(3):327-335.

134. Kahn LE, Lum PS, Rymer WZ, Reinkensmeyer DJ. Robot-assisted movement training for the stroke-impaired arm: Does it matter what the robot does? *J Rehabil Res Dev.* 2006;43(5):619-629.

135. Brokaw EB, Nichols D, Holley RJ, Lum PS. Robotic Therapy Provides a Stimulus for Upper Limb Motor Recovery After Stroke That Is Complementary to and Distinct From Conventional Therapy. *Neurorehab Neural Re.* 2014;28(4):367-376.

136. Perotto A, Delagi EF. *Anatomical guide for the electromyographer : the limbs and trunk.* 5th ed. Springfield, Ill.: Charles C. Thomas; 2011.

137. Hargrove LJ, Englehart K, Hudgins B. A comparison of surface and intramuscular myoelectric signal classification. *IEEE Trans Biomed Eng.* 2007;54(5):847-853.

# Appendix A: Preliminary Analysis of Pattern Recognition of Quasi-Static Shoulder Tasks

Kopke JV, Hargrove LJ, Ellis MD. Application of an LDA Classifier for Determining User-Intent in Multi-DOF Quasi-Static Shoulder Tasks in Individuals with Chronic Stroke: Preliminary Analysis. Conf Proc IEEE Eng Med Biol Soc. 2018;2018:2312-2315.

## A.1 Abstract

Abnormal synergies commonly present after stroke, limiting function and accomplishment of ADL's. They cause co-activation of sets of muscles spanning multiple joints across the affected upper-extremity. These synergies present proportionally to the amount of shoulder effort, thus the effects of the synergy reduce with reduced effort of shoulder muscles. A promising solution may be the application of a wearable exoskeletal robotic device to support the paretic shoulder in hopes to maximize function. To date, control strategies for such a device remain unknown. This work examines the feasibility of using two different linear discriminant analysis classifiers to control shoulder abduction and adduction as well as external and internal rotation simultaneously, two primary degrees of freedom that have gone largely unstudied in hemiparetic stroke. Forces, moments, and muscle activity were recorded during single and dual-tasks involving these degrees of freedom. A classifier that classified all tasks was able to determine user-intent in 14 of the 15 tasks above 90% accuracy. A classifier using force and moment data provided an average 94.3% accuracy, EMG 79%, and data sets combined, 94.9% accuracy. Parallel classifiers identifying user-intent in either abduction and adduction or internal and external rotation were 95.4%, 92.6%, and 97.3% accurate for the respective data sets. These preliminary results indicate that it seems possible

to classify user-intent of the paretic shoulder in these degrees of freedom to an adequate accuracy using load cell data or load cell and EMG data combined that would enable control of a powered exoskeletal device.

## A.2 Introduction

Stroke is the leading cause of serious long-term disability in the U.S. [126] and the second leading cause worldwide, with fifteen million strokes occurring annually, 33% of which result in permanent disability [42]. Motor discoordination due to stereotypical movement patterns called abnormal synergies is a major factor in limiting ADLs [45]. These synergies cause involuntary co-activation of muscles throughout the upper-limb impeding coordinated use of upper extremity joints [44]. The upper extremity flexion synergy is expressed during shoulder abduction causing unintentional elbow, wrist, and finger flexion [46]. The flexion synergy limits functional use of the arm, wrist, and hand [45]. However, with assistance or reduction of abduction effort, the amplitude of flexion synergy decreases resulting in an increase in reach distance [45,48] and a decrease in abnormal coupling of wrist and finger flexion [46] commonly seen during functional tasks.

A device that reduces shoulder effort employing real-time sensing may provide a novel solution to activity limitations caused by flexion synergy impairment. Such a device is feasible, but comprehensive design and control requirements remain undefined. Humeral rotation (Fig. 1), for example, is an important degree of freedom (DOF) of movement required for many bimanual tasks such as carrying a load. Although shoulder internal/external rotation is thought to be part of abnormal synergy patterns, it has been largely ignored in static and dynamic

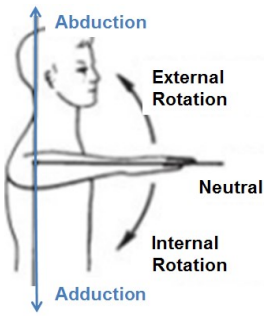


Figure 18. Depiction of humeral internal/external rotation (black) and abduction/adduction (blue)

investigations [45,48,127]. Therefore, it is currently unknown how much humeral rotation is induced due to abnormal synergy and if it can be controlled independently of shoulder abduction/adduction. Knowledge of paretic internal/external rotation capabilities and effects of associated abnormal synergy will help determine if this DOF needs to be actuated, passively supported, or left unaided in order to assist function with a wearable device.

One control paradigm that has proven to work well with wearable human assistive robotics for neuropathological populations is EMG-based control [119]. EMG-based controllers enable a short device response time [119], prevent increasing user-reliance on the device [128], and encourage neuroplastic improvements by requiring active participation [129]. Pattern recognition assumes that distinct recognizable patterns exist within data and that these data can be sorted by those patterns to be used as a control signal [130]. User-intent has been effectively predicted based on muscle activity patterns in individuals with amputation to control powered upper- [37,55] and lower- [56-58] limb prostheses. Linear discriminant analysis (LDA) pattern recognition systems have been found to be more robust, comparably accurate, and less computationally intensive compared to other pattern recognition algorithms [25] thus this method was chosen for this analysis. This paradigm is a good place to start as it is intuitive, requires the user to produce effortful contractions, and has been effective in other populations. Additionally, the level of activation can be monitored and reduced through active support by the device, thus controlling synergy expression.

This work aims to understand functional limitations and synergy presentation post-stroke in a degree of freedom (humeral rotation) that has yet to be explored. It is hypothesized that classification accuracy of humeral rotation movements will be lower at higher levels of abduction and adduction effort due to increased synergy presentation.

## A.3 Methods

### *A.3.1 Participants*

Four moderately to severely impaired chronic stroke survivors, as determined by the upper-extremity portion of the Fugl-Meyer assessment (10 < FMA-UE score < 45), have been recruited to participate with a sample goal of n=8. This population exhibits the flexion synergy at levels of effort less than limb weight (approximately 50% shoulder abduction strength) and constitute the population that a powered device would benefit most. The experimental procedures involving human subjects described in this paper were approved by Northwestern University's Institutional Review Board.

### *A.3.2 Equipment and Instrumentation*

This study used the Arm Coordination Training 3-D ($ACT^{3D}$) device (Fig. 2) developed at Northwestern University that has been used in prior studies exploring abnormal synergies after stroke [127]. The end effector integrates a 6-DOF load cell to measure forces and torques and an instrumented gimbal to measure joint angles and enables control of pure abduction/ adduction (vertical) loads while simultaneously enabling control of horizontal plane parameters. Data from the $ACT^{3D}$ was recorded at 50Hz. 12 channels of surface EMG (anterior, intermediate, and posterior deltoid, upper-trapezius, supraspinatus, infraspinatus, teres complex, latissimus dorsi, pectoralis major, biceps brachii, triceps lateral head, and brachioradialis) were recorded at 1000 Hz using a Delsys Bagnoli-16 (Delsys, Cambridge, MA).

Figure 19. Participant in setup. Robot arm extends toward bottom right. Entire arm is able to abduct (up) and adduct (down) 2 inches in either direction. Forearm is held via rigid cast.

### *A.3.3 Protocol*

Subjects were required to dynamically abduct/adduct at 5 different levels of effort (0%, ±25%, and ±50% max abduction(+) and adduction(-)) based on maximum isometric voluntary torque measured at the beginning of the experiment. Horizontal haptic surfaces (actuator-emulated physical constraints) were positioned 5cm above and below 90 degrees of abduction. This allowed the subject to remain safe while actively manipulating the loads within a defined range of motion. Loads were applied and subjects were required to raise (abduct) or lower (adduct) the load off the surfaces. While maintaining the required abduction/adduction effort, the participant attempted to elicit their maximal isometric external or internal rotation torque. This paradigm is labeled "dual-task." For each 10-second trial, the first 5 seconds consisted of one abduction/adduction effort followed by the addition of isometric internal/external rotation for the last 5s of the trial. Fig. 3 depicts the vertical position, abduction torque, and external rotation torque during a sample trial at 25% max abduction. A minimum of three trials of each condition were completed. Additional trials were added as necessary to obtain three correctly performed trials with maximum rotation torques within 10% of each other. These trials were used in the subsequent analysis.

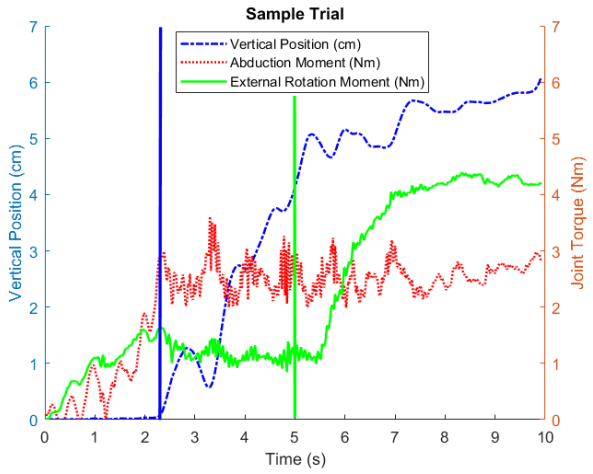


Figure 20. Raw data from ACT$^{3D}$. Vertical position of robot in blue, lifting off haptic surface at 2.2s (marked with blue vertical line). Abduction joint torque in red during 25% abduction max trial. Visual and auditory cue to externally rotate provided at green vertical line. External rotation torque in green.

### *A.3.4. Signal Processing*

Force, moment, and EMG data for each trial was segmented and labeled into the appropriate class as follows. Data within the first 5 seconds of the trial in which the subject had their arm off both haptic surfaces (abducting or adducting at the appropriate load) was segmented and labeled either abduction or adduction with corresponding load level as appropriate. Data between 6.5 to 9.5 seconds in each trial was segmented and labeled as external or internal rotation with corresponding load level as applicable. Forces and moments were not able to be used independently to delineate proper class or data cutoff due to the natural coupling of these degrees of freedom. Rotation torque commonly occurred during the pure abduction and adduction portion of the trial and at higher load levels subjects were less able to produce torque outside of this coupling (e.g. produced minimal change towards external rotation during 50% maximal adduction).

EMG data were band pass filtered between 20Hz and 400Hz and notch filtered around applicable multiples of 60 ± 3Hz using a $6^{th}$ order Butterworth filter. Four time-domain features were extracted for each 200ms window of EMG data, stepping through by 25ms, including mean-absolute value, number of zero-crossings, number of slope-sign changes, and the length of the waveform. For force and moment data, only mean values were used for each 200ms window.

### *A.3.5 Classification*

Labeled data sets were provided to a linear discriminant analysis (LDA) classifier. A three-way trial-wise cross-validation was utilized to average the effects of possible poor trials. Classification accuracies for all 15 classes (5 single-task abduction/adduction and 10 dual-task abduction/adduction plus maximal external or internal rotation) were calculated for three data sets: forces and moments (FM), EMG only, and combined forces (Comb), moments and EMG.

An alternative method of classification in which two classifiers run parallel was also evaluated [131]. One classifier for abduction, adduction or neither and a separate one for external rotation, internal rotation, or neither. Although as described, this method eliminates the ability to classify between different load levels it may offer increased classification accuracies of each movement type and could allow for the intensity of movement to be estimated using a different method. Data were relabeled to accommodate this simpler structure. All data with abduction or adduction were labeled as such and likewise for all data with internal or external rotation. Dual-task data were thus used as part of the abduction/adduction train and test sets as well as part of the internal and external rotation classifier train and test sets. A three-way trial-wise cross-validation was again used.

## A.4 Results and Discussion

### *A.4.1 15-Class Classifier*

Table I shows the confusion matrix identifying classifier accuracy and error using the combined data set (forces, moments, and sEMG). 14 of the 15 classes were classified above 90 percent accuracy, indicating a usable and functional control signal [28]. Although this does not characterize the independence of these movements within the stroke population, it does indicate that there is enough difference between these movements to make control of a device possible as accuracies are at or above 90% [28]. Not shown are the confusion matrices for the other data sets. Table II shows the summary of all data sets including within movement averages. Force and moment data provided an average 94.3% accuracy, EMG 79%, and data sets combined, 94.9% accuracy.

Table XIII. Confusion Matrix 15-Class Classifier

| Confusion Matrix | | Predicted Class using LDA of combined data | | | | | | | | | | | | | | |
|---|---|---|---|---|---|---|---|---|---|---|---|---|---|---|---|---|
| | | AB/AD | | | | | ER | | | | | IR | | | | |
| | | 50% AB | 25% AB | 0% | 25% AD | 50% AD | 50% AB | 25% AB | 0% | 25% AD | 50% AD | 50% AB | 25% AB | 0% | 25% AD | 50% AD |
| AB/AD | 50% AB | 99.58 | | | | | 0.42 | | | | | | | | | |
| | 25% AB | | 99.43 | | | | | 0.57 | | | | | | | | |
| | 0% | | | 98.54 | | | | | 1.46 | | | | | | | |
| | 25% AD | | | | 96.80 | | | | | 0.17 | | | | | 3.03 | |
| | 50% AD | | | | | 94.73 | | | | | 5.27 | | | | | |
| ER | 50% AB | 1.34 | | | | | 97.47 | | | | | 1.19 | | | | |
| | 25% AB | | 1.51 | | | | | 98.49 | | | | | | | | |
| | 0% | | | 5.26 | | | | | 94.21 | | | | | 0.53 | | |
| | 25% AD | | | | | | | | | 87.61 | | | | | 12.39 | |
| | 50% AD | | | | | 3.08 | | | | | 93.62 | | | | | 3.30 |
| IR | 50% AB | 1.05 | | | | | 2.25 | | | | | 96.71 | | | | |
| | 25% AB | | | | | | | 6.96 | | | | | 93.04 | | | |
| | 0% | | | 4.71 | | | | | 2.17 | | | | | 93.13 | | |
| | 25% AD | | | | 1.50 | | | | | 8.48 | | | | | 90.02 | |
| | 50% AD | | | | | 3.01 | | | | | 6.93 | | | | | 90.05 |

Green = accuracy > 90%, Orange = 65% < accuracy < 90% Yellow > 5% error.

Classification errors using the forces and moments data set generally occurred along the diagonals of other movement types (e.g. misclassify ER as AB). This indicates that there may be internal or external rotation occurring during the first component where only abduction or adduction is being attempted. Future work is needed to determine if this is particular to the abnormal synergy post-stroke or if this is a normal physiologic limitation. In other words, individuals may not be able to completely isolate these movements in this device. Alternatively, it may indicate impaired ability to generate patterns out-of-synergy (e.g. internal rotation during abduction) thus resulting in misclassification. The classifier using EMG had much lower accuracies in general but the errors were within movement type (e.g. ER at 25% AB misclassified as ER at 50% and 0% AB). These findings indicate that this LDA-based classifier is not able to adequately discriminate between activation levels.

It is interesting to note that within the combined classifier, EMG generally has a negative effect during adduction (AD)

Table XIV. Summary of Confusion Matrices

| 15-Class Accuracies | | Data Sets | | |
|---|---|---|---|---|
| | | FM | EMG | Comb |
| AB/AD | 50% AB | 99.21 | 96.27 | 99.58 |
| | 25% AB | 99.53 | 92.44 | 99.43 |
| | 0% | 99.62 | 72.77 | 98.54 |
| | 25% AD | 98.11 | 77.60 | 96.80 |
| | 50% AD | 97.17 | 79.40 | 94.73 |
| AB/AD Avg | | 98.73 | 83.70 | 97.82 |
| ER | **50% AB** | **94.55** | 81.09 | **97.47** |
| | **25% AB** | **89.34** | 79.28 | **98.49** |
| | 0% | 94.38 | 65.06 | 94.21 |
| | **25% AD** | **94.99** | 77.76 | **87.61** |
| | **50% AD** | **98.74** | 69.39 | **93.62** |
| ER Avg | | 94.40 | 74.52 | 94.28 |
| IR | **50% AB** | **93.50** | 73.13 | **96.71** |
| | **25% AB** | **85.71** | 77.53 | **93.04** |
| | 0% | 89.64 | 80.13 | 93.13 |
| | 25% AD | 92.46 | 75.54 | 90.02 |
| | 50% AD | 87.72 | 87.64 | 90.05 |
| IR Avg | | 89.81 | 78.80 | 92.59 |

loads as opposed to a positive effect during abduction (AB) loads. It is hypothesized that since the muscles that are primary adductors are also primary internal rotators that the classifier has a difficult time making distinctions between the two.

### *A.4.2 Parallel Classifier*

Parallel classification is an alternate classification method and, as trained, eliminates the need or ability to discriminate between different levels of effort. The output of each classifier would then control its own respective DOF, one for abduction/adduction and one for external/internal rotation. Classification accuracies were generally higher compared to the 15-class classifier as shown in Table III, especially for external and internal rotation. The combined data set may provide adequate control in both degrees of freedom whereas the load cell data may be best for abduction and adduction and the EMG data best for internal and external rotation. The limitation of this simpler classification strategy is the loss of discrimination between levels of abduction and adduction effort, which may be especially useful in rehabilitation and to prevent the loss of strength over time. This loss of strength could result from reliance on an assistive device but could be minimized or eliminated by requiring the user to produce effortful contractions of a certain level. Future work may explore the possibility of expanding this classifier to include different abduction/adduction levels.

Table XV. Summary Parallel Classifier

| Parallel Accuracies | Data Sets | | |
|---|---|---|---|
| | FM | EMG | Comb |
| No AB/AD | 99.39 | 81.53 | 99.66 |
| ABD | 96.66 | 92.71 | 96.86 |
| ADD | 98.21 | 89.83 | 96.95 |
| **Avg AB/AD** | **98.09** | **88.02** | **97.82** |
| No ER/IR | 97.20 | 98.07 | 98.20 |
| ER | 94.14 | 95.93 | 95.71 |
| IR | 86.86 | 97.74 | 96.65 |
| **Avg ER/IR** | **92.73** | **97.25** | **96.85** |

## A.5 Conclusion

This work is a good and necessary first step in determining a useable control strategy for a wearable shoulder exoskeleton post-stroke. These two classification methods show promise in

being able to control a device supporting or controlling shoulder abduction and adduction simultaneously with external and internal rotation. Future work will attempt to minimize required number of inputs, maximize accuracy, and test these strategies real-time on a robotic device.

# Appendix B. Feasibility of Myoelectric Control of Robot after Stroke – Case Study

Kopke JV, Ellis MD, Hargrove LJ. Feasibility of Two Different EMG-Based Pattern Recognition Control Paradigms to Control a Robot After Stroke – Case Study. Paper presented at: 2020 8th IEEE RAS/EMBS International Conference for Biomedical Robotics and Biomechatronics (BioRob); 29 Nov.-1 Dec. 2020, 2020.

## B.1 Abstract

Stroke often results in chronic motor impairment of the upper-extremity yet neither traditional- nor robotics-based therapy has been able to affect this in a profound way. Supporting the weak affected shoulder against gravity improves reaching distance and minimizes abnormal co-contraction of the elbow, wrist, and fingers after stroke. However, it is necessary to assess the feasibility and efficacy of real-time controllers for this population as technology advances and a wearable shoulder device comes closer to reality. The aim of this study is to test two EMG-based controllers in this regard.

A linear discriminant analysis based classifier was trained using extracted time domain and auto-regressive features from electromyographic data acquired during muscle effort required to move a load equivalent to 50 and 100% limb weight (abduction) and 150 and 200% limb weight (adduction). While rigidly connected to a custom lab-based robot, the participant was required to complete a series of lift and reach tasks under two different control paradigms: position-based control and force-based control.

The participant successfully controlled the robot under both paradigms as indicated by first moving the robot arm into the proper vertical window and then reaching out as far as possible while remaining within the vertical window.

This case study begins to assess the feasibility of using electromyographic data to classify the intended shoulder movement of a participant with stroke during a functional lift and reach type task. Next steps will assess how this type of support affects reaching function.

**B.2 Introduction**

Stroke is the leading cause of long-term disability in the U.S. and the second leading cause worldwide [41]. Fifteen million strokes occur annually around the world [41], up to two- thirds of which result in permanent disability of the upper-extremity [42]. Unfortunately, traditional physical therapy and robotics based therapies result in little functional improvement (less than the clinically important difference) in chronic stroke, leaving many stroke survivors impaired for life [42]. Common upper-extremity motor impairments include weakness, abnormalities of muscle tone, and motor discoordination [16,107].

Several robotics groups have worked on lab-based devices, targeting rehabilitation through neuroplasticity using intensive, long-duration, repetitive and task oriented therapy. Those devices have proven to be as effective as dose matched conventional therapy but neither mode of therapy has resulted in long term clinically relevant improvements in motor control [132-135].

Conversely, many groups have shown significant positive effects during force- or position-based support of the paretic shoulder. Specifically, the abnormal co-contraction of elbow, wrist, and finger flexors that often occurs during shoulder abduction is minimized or avoided, enabling

greater reaching distance and less unintentional and undesired movement of the wrist and fingers [13,14,76,107]. Thus, a novel solution may be to extend the concept of humeral elevation support to a wearable exoskeleton for continuous assistance. Prior to design and development of such a device, it is essential to determine control feasibility and efficacy and to determine how the sequelae of stroke might affect control of the wearable device. This work used a lab-based robot to test the feasibility of two real-time user-in-the-loop control paradigms; force-control and position-control.

Based on our prior work, it is feasible to discriminate between 8 different isometric shoulder and elbow tasks using electromyographic (EMG)-based linear discriminant analysis pattern recognition [63,64]. Further work successfully extended this concept to a dual-task and slightly less constrained environment requiring dynamic adduction or abduction against prescribed loads simultaneously with isometric external or internal rotation [120].

An EMG based time-delayed artificial neural network has been used to predict assistive forces for the paretic arm within the sagittal plane during target based reaching [113]. It was concluded that EMG from residual effort can produce an effective command signal for post-stroke assistive devices and that "residual movement coupled with assistive forces could enable functional movements following stroke", but also noted some general issues with respect to stability. We hypothesize that our control scheme will be

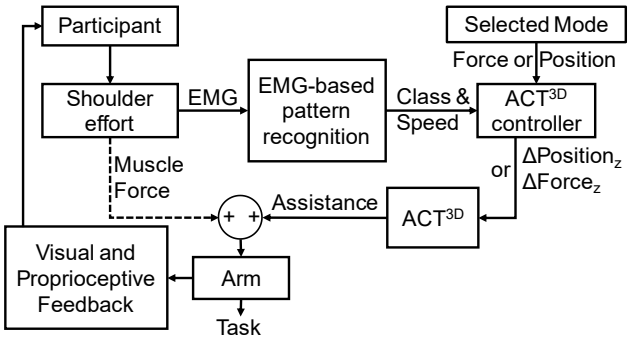


Figure 21. Real-time, user in the loop, EMG-based pattern recognition control scheme which modifies the vertical position or vertical force supporting the arm. Dashed line applicable to Force support condition as force generated from muscle contributes to task completion but reduces over time as controller continues to adjust force based on EMG. Note that Δ signifies an incremental change in either the vertical position or vertical support force as determined by the output of the controller and the mode.

more successful because it operates in only 1 degree of freedom - the vertical direction. Furthermore, as opposed to continuously predicting force, our control scheme induces incremental changes to force or position based on the output of an EMG-based pattern recognition system every 25ms (Fig. 1).

The purpose of this case study is to demonstrate control feasibility and efficacy of such a paradigm and enable the next steps in design of a powered upper extremity orthosis to aid stroke survivors in ADLs. This study will generate knowledge of how real-time control of humeral elevation support affects reaching function. Determining how distal limb effort affects active control of a device will also help determine if control of a device is feasible and advantageous.

## B.3 Methods

For this feasibility case-study, one participant with moderate chronic motor impairments after stroke has been consented per Northwestern University IRB STU00210805. Moderate motor impairment was determined through use of the upper extremity portion of the Fugl-Meyer Assessment with a score within the range of 10 and 45. Data were collected over one session.

### *B.3.1 Experimental Setup*

The participant was seated and secured in a Biodex chair (Biodex Medical Systems, Inc., Shirley, NY) with nylon belts to constrain movement of the upper body and positioned with her shoulder abducted 85º with 0° horizontal adduction and with neutral internal and external rotation. The elbow center of rotation was positioned over a freely rotating mount with a rotational potentiometer (acting as a digital goniometer) to measure elbow rotation. The medial and lateral epicondyles were clamped with foam in the custom mount. A lightweight fiberglass cast was

applied to her forearm (not crossing the elbow or wrist joints) to facilitate a comfortable rigid attachment of the arm to the robot at the forearm (Fig. 2).

Eight pairs of Ag/Ag-Cl gel electrodes were placed over the following muscle sites as prescribed in the guidelines set forth in Anatomical Guide for the Electromyographer: anterior, middle, and posterior deltoid, pectoralis major, teres complex, latissimus dorsi, biceps, and triceps [136]. A custom amplifier system based on the Texas Instruments ADS1299 was used to sample EMG at a frequency of 1 kHz and with a gain of 1k.

*B.3.2 Robot Description*

The ACT$^{3D}$ consists of the admittance controlled HapticMaster robot (Moog Inc., The Netherlands) with a six degree of freedom load cell end effector (JR3, Woodland, CA) (Fig. 2). Similar equipment configurations have been used in prior studies; however, in this work the control of vertical position or vertical force provided by the robot comes from information acquired from an embedded real-time EMG-based pattern recognition controller. The robot was configured to be unconstrained in the transverse (horizontal) plane and allowed horizontal shoulder abduction/adduction and elbow flexion/extension movement while controlling either the force or the position in the vertical direction. Horizontal surfaces were programmed to limit the amount of vertical movement to +5/-

Figure 22. Participant set up in the ACT$^{3D}$ robot. Humeral abduction angle reduced for visual appreciation. Robot is controlled via force or position but only in the vertical direction (denoted by arrows) via online classifier. Shoulder internal and external rotation are fixed at anatomical neutral. All other motions at the shoulder and elbow are free and controlled solely by the participant.

10 cm (ceiling/floor) from the 85° abduction position described above. The target vertical window during lift and reach trials is ±5 cm from the 85° initial condition equating to approximately ±11° of humeral elevation.

### *B.3.3 Control System Training*

The participant's arm was weighed, and force support was provided so that the participant lifted 50% and 100% of the weight of their arm. Additionally, a positive vertical force equivalent to 150% and 200% of her limb weight was applied, forcing her arm into the "ceiling". Within each of these conditions, 3 trials of 3 seconds each were collected in which the participant either lifted (abducted) or depressed (adducted) her arm between the starting surface and the opposite one. Three trials of 3 seconds of rest as well as gentle movement with the limb weight fully supported were also recorded. The EMG data (Fig. 3) from these initial trials were used to train the abduction/adduction/no-movement classifier (Fig. 4) which was used to control the robot during a lift and reach task (*Section F*).

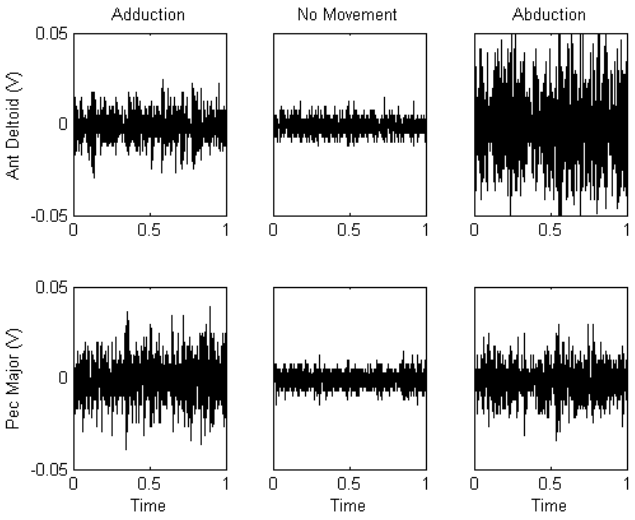


Figure 23. One second of representative raw EMG data from 2 channels (Anterior Deltoid and Pectoralis Major) during 3 movement classes (Adduction, No Movement, and Abduction).

### *B.3.4 Data Segmentation and Feature Extraction*

Data were segmented into 200ms windows and steps of 25ms (175ms overlap) were taken through the data. Four time-domain features (mean relative value, waveform vertical length,

number of zero crossings, and number of slope sign changes) and autoregressive features from a 6th order model were extracted from each channel of EMG and concatenated to form a 80-element (8 channels x 10 features) feature vector [137]. The mean relative value is the absolute value of the signal amplitude around a reference point that is the mean of all values in the data window (200ms). The waveform vertical length is the sum of the absolute values of the difference in signal amplitude between adjacent points. No data normalization or standardization was performed. This type of pattern recognition classifier has been successfully used to control prosthetic limbs and showed promise in our preliminary offline studies [34,63,120,122,123].

### *B.3.5 Position- and Force- Controller*

The 200ms windows of EMG feature data are classified by the classifier every 25ms, and the decision resulted in both a class prediction (abduction, adduction, or no-movement) and a proportional movement speed prediction [124]. The direction and speed were then input to the robot controller and applied to the robot over the next 25ms window (Fig. 1 and Fig. 4). Thus, when the position-based controller detects a person is attempting to lift (abduct) or depress (adduct) their arm it will incrementally change the robots position accordingly, proportional to the amount of

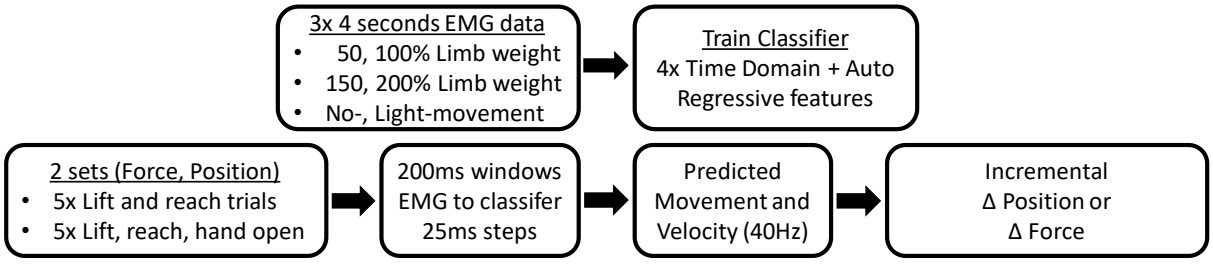


Figure 24. Data flow: classifier training, and classifier output to control the ACT$^{3D}$. Top line: Training data collected under different loading conditions followed by data segmentation, feature extraction, and determination of class discriminator. Bottom: use of real-time controller feeding output to low-level controller at 40Hz to induce incremental changes in the vertical position or the vertical force supplied by the ACT$^{3D}$ depending on the mode. Note that Δ signifies an incremental change in either the vertical position or vertical support force as determined by the output of the controller and the selected mode.

EMG activity. The force controller worked similarly but instead of changing the position each frame, the force support was incrementally changed each frame in proportion to the amount of EMG activity. For example, if a participant is trying to lift their arm, the controller will detect this and continually add increments of vertical support force each 25ms until the participant is no longer using their shoulder abduction muscles.

### *B.3.6 Lift and Reach Task*

To test the usability and efficacy of the classifier we implemented a lift and reach task in which the participant would lift their arm from the "floor" into the target window and extend their elbow as far as possible. The arm is supported by changing the vertical position or force via EMG input to the proportional on-off based controller and subsequent output to the robot. This online controller portion included 10 lift and reaches in each support condition (position support and force support). Five of the reaches in each condition were followed by maximal hand opening. The participant lifted her arm up off of a horizontal plane (located 10cm below 85° of abduction), to a vertical window ±5cm from 85° and then reached out as far as possible and then lowered her arm. Each trial lasted a maximum of 15 seconds.

## B.4 Results

The participant successfully controlled the robot under both paradigms as indicated by first moving the robot arm into the proper vertical window and then reaching out at far as possible while remaining within the vertical target window. These results support the idea that these modes of control are feasible and warrant completion of this study.

Results from a representative lift and reach trial from each control paradigm are presented in Fig. 5. The left column presents the position control and the right column presents the force control. Each vertical stack represents the same trial under the prescribed condition. The top plots depict both what the robot experienced (black line) as well as a reconstruction of the output of the controller (cumulative sum of velocity*time increment) (gray line). The middle plots depict the shoulder abduction angle (black line) with the target abduction window outlined between the gray

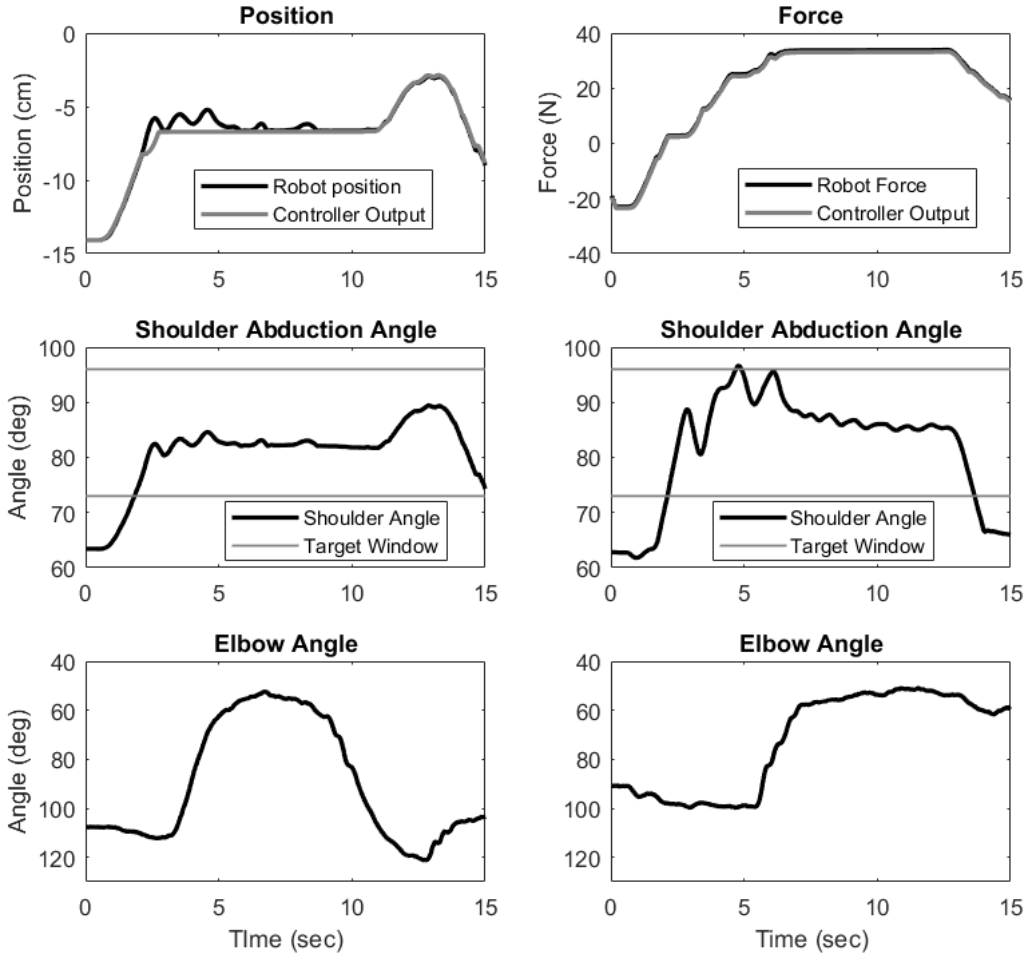


Figure 25. Real-time Position-control (Left) and Force-control (Right) during lift and reach task. Top) Black line: the actual position (left) and force (right) of the robot; gray line: the calculated position and force using the output from the classifier (both class and velocity). Middle) Shoulder Abduction angle in black, with target window for task completion marked in gray. "Ceiling" and "floor" safety boundaries not depicted. Bottom) Elbow angle during the lift and reach task with 0° equal to arm fully extended.

lines. The bottom plot simply shows the elbow angle with a change towards elbow extension (0°) during the reach in both control paradigms.

**B.5 Discussion**

This case study examines the feasibility of using EMG-based pattern recognition control to control vertical support of a lab-based robot after stroke. We intend to extend this study to compare the efficacy of these two control paradigms on improving reaching ability to expand the user's workspace. Additionally, we hope to demonstrate different control schemes on lab-based robots to emulate a wearable device to determine design requirements (e.g. most important degrees of freedom to actuate/control) and efficacy of different proposed control schemes on functional tasks.

As seen in Fig 5. this participant was able to effectively control the vertical position (left) and force (right) of the robot during a lift and reach task. She lifted her arm into and maintained it within a target range while reaching out. The force controller shows marked increase in oscillation in shoulder abduction angle induced by the interplay between the force produced by the participants muscle effort and the controller/robot response to the EMG associated with that effort. More participants must complete the protocol to examine and comment on the generalizability of this effect.

The discrepancy between the controller and the robot in the top left plot is because only the floor (negative vertical) was constrained. Thus a misclassification of abduction for no-movement did not change the position of the robot but the participant was still able to lift their arm up off the supportive surface. We plan to impose both floor and ceiling constraints moving forward to better

simulate a humerus being rigidly attached to a wearable device. These preliminary results hint that real-time and closed-loop EMG-based pattern recognition after stroke is possible.

This work is primarily limited by having only one participant. However the uncertainty surrounding successful implementation warrants this initial "proof-of-concept." Additionally, training data were limited in depth (9-18 seconds of each class) and breadth as it did not include any muscle activity of other shoulder-based motions. Future work will address these concerns to fully evaluate these two real-time control paradigms as compared to preset or prescribed position or force support.

### B.6 Conclusion

This participant was able to control the robot under the prescribed conditions. This study will continue and be complete when 14 participants complete the protocol. Future work will focus on optimizing and minimizing EMG channels and necessary training data as well as identifying ways to implement therapeutic training using the force based controller, possibly by gradually reducing the maximal force support over time.